2009

Structural Investigation of the Complex of Filamin A Repeat 21 with Integrin αIIb and β3 Cytoplasmic Tails – A Potential "Transmission" to Regulate Cell Migration

Jianmin Liu
Cleveland State University

STRUCTURAL INVESTIGATION OF THE COMPLEX OF FILAMIN A REPEAT 21 WITH INTEGRIN α_{IIb} & β_3 CYTOPLASMIC TAILS —A POTENTIAL "TRANSMISSION" TO REGULATE CELL MIGRATION

JIANMIN LIU

Bachelor of Science in Chemical Engineering

Changchu University of Technology

July, 1999

Master of Science in Chemistry

Changchu University of Technology

July, 2002

submitted in partial fulfillment of requirements for the degree

DOCTOR OF PHILOSOPHY IN CLINICAL-BIOANALYTICAL CHEMISTRY

at the

CLEVELAND STATE UNIVERSITY

August, 2009

This dissertation has been approved

for the Department of CHEMISTRY

and the College of Graduate Studies by

Dissertation Chairman, Edward Plow Ph.D.

Department & Date

Jun Qin Ph.D.

Department & Date

Yan Xu Ph.D.

Department & Date

John Masnovi Ph.D.

Department & Date

Aimin Zhou Ph.D.

Department & Date

STRUCTURAL INVESTIGATION OF THE COMPLEX OF FILAMIN A REPEAT 21 WITH INTEGRIN α_{IIb} & β_3 CYTOPLASMIC TAILS —A POTENTIAL "TRANSMISSION" TO REGULATE CELL MIGRATION

JIANMIN LIU

ABSTRACT

Cell functions in multi-cellular organisms are strongly depend on the dynamic cooperation between cell adhesion and cytoskeleton reorganization. Integrins, the major cell adhesion receptors, bind to extracellular matrix (ECM) and soluble ligands on the cell surface and link to the actin cytoskeleton inside the cell membrane. In this manner, integrins integrate cell adhesion and cytoskeleton reorganization by acting as a mechanical force transducer and a biochemical signaling hub (Zamir and Geiger 2001). Consequently, integrins are vital for development, immune responses, leukocyte traffic and hemostasis, and a variety of other cellular and physiological processes. Integrins are also are the focal point of many human diseases, including genetic, autoimmune, cardiovascular and others. In terms of the cell-ECM adhesion, integrins can exist in two major states, active, where it binds to appropriate extracellular ligands, and inactive, where it disassociates from extracellular ligands. The cellular pathways that modify the integrin extracellular ligand binding states have been called inside-out integrin signaling while the pathways that are mediated by the extracellular binding have

been called outside-in integrin signaling. Although the directions of outside-in and inside-out signaling point to each other, they often happen reciprocally. Rather than just integrins alone accomplishing integrin signaling, numerous proteins are recruited around integrins and are limited to the clearly defined range of focal adhesion that are large molecular complexes containing >100 proteins which link integrins to cytoskeleton (Figure 1) (Zaidel-Bar et al. 2004). Proteins that directly interact with integrins are crucial for understanding integrin signaling. More importantly, proteins that link integrins to the cytoskeleton are responsible for both mechanical forces and biochemical signal transduction, as well as reorganizing the cytoskeleton. Moreover, the modification of integrin ligand binding states is dependent on the linkage to the cytoskeleton. Filamin is one of the main proteins that link integrins to the cytoskeleton and it has profound significance in integrin-mediated cell functions. Human filamin is a dimeric actin-binding protein, consisting of an actin-binding domain followed by 24 immunoglobulin repeats with the last repeat being the dimerization motif. Of the 24 immunoglobulin repeats of filamin, repeat 21(FLN21) has been characterized as a major integrin binding partner. The results in this dissertation provide a molecular level understanding of integrin-filamin interaction. A mechanism of how the integrin-filamin complex integrates cell adhesion mediation and cytoskeleton reorganization was proposed based on the determined structure and other biophysical and biochemical studies. Nuclear magnetic resonance (NMR) is a powerful method for studying protein

structure and protein-protein interactions, provided by advances in the high resolution and accuracy of NMR. Since the structural nature of protein is the foundation of understanding all biological and physiologic processes, I believe the results presented here shape the integrin field.

TABLE OF CONTENTS

Page

LIST OF TABLE

Page

LIST OF FIGURES

ABBREVIATIONS

I nuclear spin quantum number

$\mathbf{I}$ nuclear spin angular momentum

I_z Z-component of nuclear spin angular momentum

M magnetic quantum number

$\boldsymbol{\mu}$ nuclear magnetic moment

μ_z z-component of nuclear magnetic moment

γ gyromagnetic ratio

$\hbar$ reduced Planck's constant (Planck's constant divided by 2π)

E Energy

$\mathbf{B_0}$ the static external magnetic field

ω_o Larmar frequency

σ cross-relaxation rate

τ_c rotational correlation time

CHAPTER I

INTEGRIN AND FILAMIN

1.1 Integrin — a bi-directional mechanical force and signaling transduction machinery

Cells must reside in the extracellular matrix (ECM) not only for physical support but also for exchange of biochemical signals and mechanical forces. These tasks are mainly mediated and accomplished by a large family of cell surface receptors, the integrins (Hynes 1987; Ruoslahti and Pierschbacher 1987). Mechanochemical signals originating from one side of cell membrane can be sensed on the other side by integrins and feedback can be transmitted back again in the form of mechanochemical signals. This has been called bi-directional integrin signaling. These signals can mediate cytoplasmic kinases, growth factors, ion channels, and the assembly and reorganization of ECM and cytoskeleton, etc. Many integrin signals congregate around cell cycle regulation, directing cells to

live or die, to proliferate, or to exit the cell cycle and differentiate (Williams et al. 1994; Clark and Brugge 1995; Clark and Hynes 1997; Schlaepfer and Hunter 1998).

Integrins have been identified in numerous animal species from sponges to mammals and they are ubiquitously expressed on the cell surface. Each Integrin consists of two sub-units, β and α. In humans, eight β and eighteen α subunits have so far been identified, assembling into twenty-four different integrins,. Each α and each β subunit form a noncovalent heterodimer and each subunit crosses the membrane once. Most of the polypeptide (>1600 amino acids in total) comprises the extracellular domains while the two short cytoplasmic tails are typically 20-50 amino acids long. β and α combinations distinguish different integrins, for example $\alpha_{IIb}\beta_3$ and $\alpha_v\beta_3$, and each integrin has its own specific functions (Hynes 1987; Ruoslahti and Pierschbacher 1987).

Integrins' extracellular domains can associate with extracellular matrix proteins such as fibronectin, laminins, collagens and vitronectin. Most integrins can recognize several ECM ligands and conversely, some extracellular ligands can bind to several different integrins (Calderwood 2004; Arnaout et al. 2005). Appropriate interactions between extracellular ligands and integrins are necessary for normal cell functions. Binding of the integrin's extracellular domains by different ligands can send different signals to cells (outside-in signaling). For

example, depending on the signals from extracellular ligand binding, cells may either proliferate or exit the cell cycle and differentiate.

Upon binding to ECM, integrins become clustered in the plane of the cell membrane and recruit cytoskeletal proteins, which promotes the assembly of actin filaments. The reorganization of actin filaments, in turn, leads to more integrin clustering, consequently boosting the ECM binding. Accordingly, ECM, integrins and cytoskeletal proteins assemble into aggregates on each side of the cell membrane. In this reciprocal manner, the inside and outside of the cell is physically connected, which allows a cooperative regulation of cell function (Burridge and Chrzanowska-Wodnicka 1996) (Figure 1).

Integrin-mediated attachment to ECM plays a central role in cell migration. Cyclic forming and breaking of the attachment generates the directional forces to move cells toward needed locations. It was hypothesized that the process of cell migration relies on the integrin-cytoskeleton connections and that the generation of force be driven through the cytoskeleton (Horwitz 1997; Sheetz et al. 1998) (Figure 1).

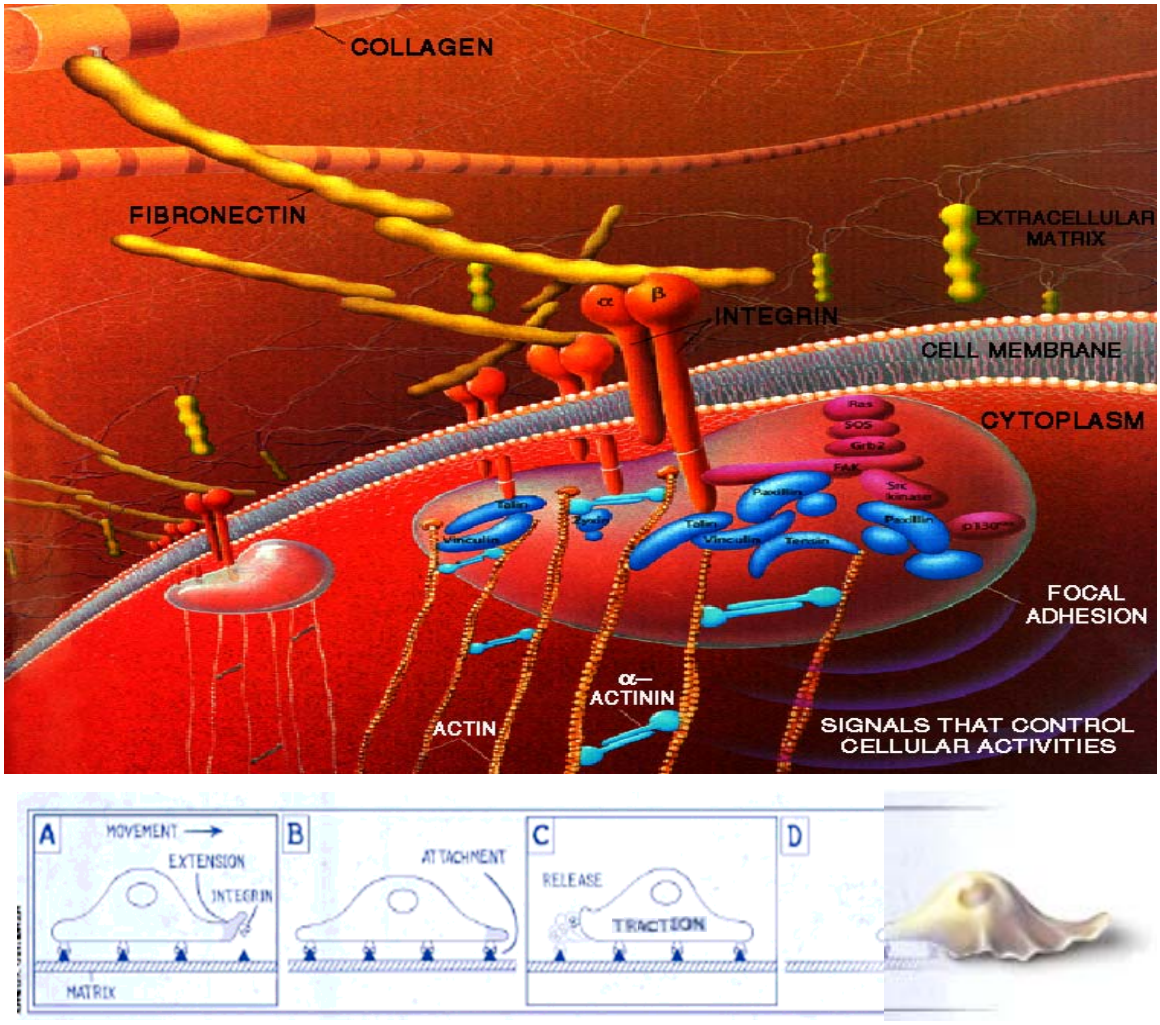

Figure 1 Integrin-mediated cell adhesion.

In the upper figure, integrins (orange) span cell membranes, holding a cell in place by attaching at one end to molecules of the extracellular matrix (or to molecules on other cells) and at the other end to the cell's cytoskeleton. Using their cytoplasmic domains, integrins connect to this cytoskeleton through a highly organized aggregate of molecules – a focal adhesion – that includes such cytoskeletal components as actin, talin, α-actin and filamin. Integrins transduce signals from both inside (inside-out signaling, see text) and outside (outside-in signaling, see text) of the cells. (Modified from (Horwitz 1997))

In the lower figure, cells "walk" on the matrix by cyclically forming and breaking integrin-mediated attachments to the matrix. They create foot-like extensions to reach the farther attaching point (A) and then form new attachments (B). Next they release the attachment at the rear (C), which causes the back end to move forward, then the cycle starts anew (D).

Very unique to integrins, a huge number of cellular proteins are dynamically organized around integrin cytoplasmic tails to form the large macromolecular assembly that has been called a focal adhesion. Continually and in an orderly manner, focal adhesion proteins sense mechanochemical signals from integrins and convey them to other parts of the cell. Vice versa, feedback in the form of mechanochemical signals can be transmitted through integrins back to the cell surface by re-assembling the focal adhesion proteins. All these bi-directional activities of integrins start or end with the proteins interacting with integrin cytoplasmic tails. Thus, during the last decade, integrin research has specifically focused on the integrin-binding proteins as well as the mechanochemical signals those integrin-protein complexes convey.

1.2 Integrin-mediated cell functions

Due to their special position in the cell signaling system, integrins regulate many critical cell activities. Integrin-mediated ECM anchorage itself is required for normal cell function: loss of anchorage causes apoptosis in many cell types. This may help in maintaining tissue integrity by preventing cells that have lost their attachment to their appropriate surroundings from launching themselves to other locations. Specific ECM-integrin recognition is required for cell survival and cell cycle progression (Meredith et al. 1993; Frisch and Francis 1994). To migrate, the cell must cyclically establish new ECM-integrin adhesions at its leading edge

(front) and release adhesions at the trailing edge (rear). Integrins are also desired for optimal functioning of growth factor receptors as well as other membrane receptors (Cybulsky et al. 1994; Vuori and Ruoslahti 1994; Jones et al. 1997). Other integrin-regulated cell functions include the activation of a range of protein tyrosine kinases (Wary et al. 1996; Wary et al. 1998), regulation of ion channels (Haussinger et al. 2003; Kawasaki et al. 2004), etc.

Among integrins, $\alpha_{IIb}\beta_3$ (also known as GPIIb/IIIa), which is present with high density on the surface of blood platelets, has been the most characterized and is the central integrin in this dissertation. $\alpha_{IIb}\beta_3$, when activated and bound to fibrinogen and fibrin, is responsible for crosslinking platelets within a developing blood clot. This $\alpha_{IIb}\beta_3$ activation, which results in platelet aggregation, is controlled precisely. Failure of sensible platelet aggregation leads to the bleeding disorder Glanzmann thrombasthenia (George et al. 1990), whereas pathological formation of platelet aggregates results in thrombosis (Lefkovits et al. 1995). Platelet aggregation must be strictly confined to the precise region of damage, be it a couple of square micrometers. This $\alpha_{IIb}\beta_3$-mediated activation is also remarkably fast. It switches all $\alpha_{IIb}\beta_3$ integrins on a single platelet (some 50,000 molecules) from their non-adhesive state when circulating in blood vessels to being intensely sticky (where the affinity is increased over several orders of magnitude) within 5 seconds. The trigger of activation is from within the cell in response to extracellular chemical (Lollo et al. 1993; Constantin et al. 2000) and/or

mechanical stress (Zwartz et al. 2004). As it has an indispensable role in thrombosis and hemostasis, $\alpha_{IIb}\beta_3$ is the most intensively studied integrin and it provides a thought-model for how many integrins are believed to be regulated.

1.3 Mechanical forces and integrin

Mechanical forces are vital to the mediation of cell morphology and organism physiology. Control by physical forces is most noticeable in blood pressure regulation, remodeling of bone, maintenance of muscle and perception of touch and sound (Davies 1995; Ernstrom and Chalfie 2002; Lehoux and Tedgui 2003). At the cellular level, mechanical forces impact cytoskeletal organization, gene expression, cell migration, proliferation and survival (Huang and Ingber 1999). Additionally, forces can be conveyed to the cytoskeleton network to alter cell shape and motility, even to the nucleus to regulate nuclear events without cytoplasmic chemical intermediates (Maniotis et al. 1997). Integrins, as the major cell surface receptor that connects ECM and the cytoskeleton, have been widely accepted as the mechanical force sensor and transducer. However, unlike biochemical signal transduction, mechanical aspects of integrin-mediated adhesion are very poorly understood. Generally speaking, traction forces generated form the cytoskeleton are passed to the ECM through integrins, as are the tensions applied to cells from the ECM. The influences of mechanical force on integrin-mediated adhesion include an increase in the density of integrins, the

recruitment of adhesion proteins and the elongation of the adhesion site in the direction of force (Harris et al. 1980; Pelham and Wang 1999; Balaban et al. 2001; Ballestrem et al. 2001; Riveline et al. 2001). Since integrins also regulate cell signaling, they may transform physical forces into biochemical signals as well (Schwartz and Assoian 2001). Conversely, focal adhesion sites may generate forces on the surrounding substratum and require surfaces to be sufficiently stiff to support tension (Pelham and Wang 1997; Schoenwaelder and Burridge 1999). Focal adhesions are normally connected to actin filaments, and in stationary state tensions pull focal adhesions toward the center of cell. But during migrating, the front of the migration direction stays fixed, whereas adhesions of the rear relieved (Figure 1), indicating that mechanical forces from focal adhesions and the cytoskeleton can modify integrin-ligand binding affinity. Mechanical force has been proposed to change the conformation of integrins but has not been tested directly (Schwartz and Ingber 1994). This evidence all points to the strong relationship between mechanical forces and integrin-mediated adhesion.

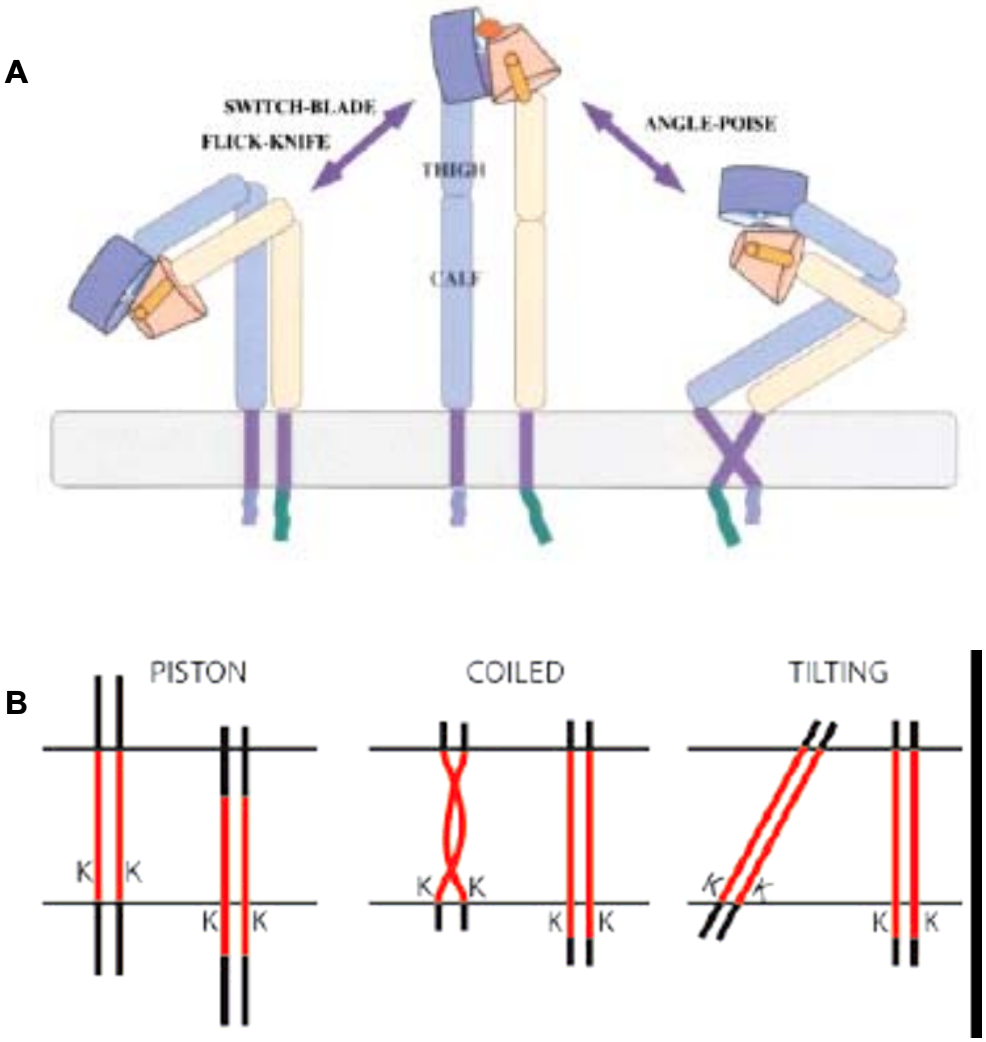

Figure 2 Integrin extracellular domain and transmembrane domain signaling.
(A). Two proposed models for the straightening up of integrin extracellular domains during activation. The main difference between the switch-blade and flick-knife model is the relative orientation between the C-termini of the legs and transmembrane domains. The angle-poise model incorporates the possibility that the transmembrane domains may move in and out of the membrane during activation (Hynes 2002).
(B). Three proposed models of transmembrane (TM) domains during integrin activation. In the piston model the TMs move as a rigid piston. In the coiled model the two TMs are coiled around each other as a coiled coil. In the tilting model the TMs adapt to the bilayer by tilting. Change in tilt angles may push a few residues into the cytosol. A feature in the piston model distinct from the other two is that the membrane proximal sections of the extracellular domains also move in and out of the membrane (Stefansson et al. 2004).

1.4 integrin signaling regulation

Integrin signaling is a super complicated process not only because integrins play diverse roles in many biological processes but also because the nature of the conformational changes leading to integrin activation remains controversial (Hynes 2002; Liddington and Ginsberg 2002; Shimaoka et al. 2002; Humphries et al. 2003).

Publication of high-resolution structures and *in vivo* EM images have represented the major advances in the integrin filed. However, only separate structures of extracellular domains, transmembrane domains and cytoplasmic tails are available up to now and the lack of high-resolution structure of intact integrin has hindered a full understanding of integrin signaling. Crystal structure of $\alpha_v\beta_3$ extracellular domains showed that $\alpha_v\beta_3$ was bent over at a 135° angle (Xiong et al. 2001). Although this bent form was suggested to be the inactive state in the beginning, it has been mostly accepted lately to be the active state since EM images of ligand-bound integrins show an extended structure (Weisel et al. 1992; Du et al. 1993). Thus, in this dissertation it will be presumed that the once bent-over extracellular domains are straightened up in order to bind ligands, the process being called integrin activation. The proposed mechanisms of transmembrane domains include that upon activation the transmembrane helices may move in and out of the membrane. Detailed review of the structure of extracellular domains and transmembrane domains is beyond this dissertation.

Strong evidence has established that integrin cytoplasmic tails play a vital role in integrin signaling although they are much smaller than their extracellular domains. The cytoplasmic tails interact with many cytoskeletal and signaling proteins to closely regulate various cellular events (outside-in signaling). More importantly, integrin cytoplasmic tails can modulate the activation state of integrin (inside-out signaling) by altering the structure and function of the extracellular domains. Intensive research has shown that separation of the cytoplasmic tails is a key step in integrin activation whereas interaction between the tails keeps integrins inactive. Deletion of entire α or β subunit's cytoplasmic tails produces a constitutively active $\alpha_{IIb}\beta_3$ integrin. Additionally, deletion of the highly conserved membrane-proximal region of either α_{IIb} or β_3 gives the same result, indicating the membrane-proximal region be the binding interface between α_{IIb} and β_3 (O'Toole et al. 1991; O'Toole et al. 1994; Hughes et al. 1995; Hughes et al. 1996; Peter and Bode 1996). From mutagenesis studies a salt bridge between residues R995 of α_{IIb} and D723 of β_3 was proposed to stabilize the $\alpha_{IIb}\beta_3$ interaction. Mutation of either one to alanine produces a constitutively active integrin (Hughes et al. 1996). Moreover, the engineered tail clasp of $\alpha_L\beta_2$ or $\alpha_M\beta_2$ blocks integrin activation, whereas release of these constraints activates ligand binding (Lu et al. 2001; Kim et al. 2003). However, the binding affinity between the tails is very weak, the main reason to obstruct the co-crystallization of the two molecules. The α_{IIb}/β_3 complex structure demonstrated by NMR is suitable for showing the weak interaction

although different opinions exist within NMR studies regarding the structural details (Vinogradova et al. 2002; Weljie et al. 2002) (Figure 2). Furthermore, talin, a well-known integrin activator, ablated the interaction between the $\alpha_{IIb}\beta_3$ cytoplasmic tails (Vinogradova et al. 2002) with its much higher binding affinity for the β_3 tail (Calderwood et al. 1999; Calderwood et al. 2002). The binding site on β_3 for talin was mapped to K716-N744, completely overlapping the α_{IIb}/β_3 interface, suggesting a competition mechanism for talin's separation of the α_{IIb}/β_3 clasp (Vinogradova et al. 2002). Thus, the interaction between integrin α and β cytoplasmic tails by their membrane-proximal regions keeps integrins in their inactive state. Any effect that can disrupt this interaction may activate integrins. The major question to this mechanism is that, if activation involves separation of tails and straightening up of once bent extracellular domains, how does separation of tails straighten up the extracellular domains? After all, it is about 10-20 nm from the tails to the far end of the extracellular domains. Besides, it is hard to explain how the structural changes resulting from separating the weak interacting small tails cause such dramatic conformational changes of much bigger extracellular domains. Several models of long-range allosteric changes were proposed, but no experiments support any of them.

The membrane-distal regions of cytoplasmic tails are also important. Deletions of the membrane-distal region in β tails are found to block activation in several integrins (Hibbs, Jakes et al. 1991; Hibbs, Xu et al. 1991; Chen et al. 1994;

O'Toole et al. 1994; Hughes et al. 1995; O'Toole et al. 1995; Wang et al. 1997). Tyrosine to alanine mutations in the first conserved NPxY motif strongly inhibit integrin activation and perturb the native structure at the NPxY sites and areas within the membrane-proximal region as well (Ulmer et al. 2001). Mutations in NPxY can disrupt the binding of β tails with many cytoskeletal and signaling proteins (Liu et al. 2000), and $\alpha_{IIb}\beta_3$ activation by talin requires the intact NPxY (Calderwood et al. 1999; Calderwood et al. 2000). Moreover, the membrane-distal region of β tail has been mapped to the binding sites for numerous cytoskeletal and signaling proteins, including filamin (Kiema et al. 2006). Thus it was believed that the β membrane-distal region can bind to integrin activation regulators and disturb the αβ clasp by changing the conformation of the membrane-proximal region of β tails. Modification of the membrane-distal region of the α subunit also can change the integrin activation state but this is more cell-type-specific (O'Toole et al. 1994). Furthermore, in $\alpha_{IIb}\beta_3$ the absence of the portion immediately after GFFKR in α_{IIb} may ablate the inactive conformation of β_3 (Ginsberg et al. 2001) and a P998A, P999A mutation within this region perturbs the conformation of the α_{IIb} tail (Vinogradova et al. 2000) and activates $\alpha_{IIb}\beta_3$ (Leisner et al. 1999). Thus, the membrane-distal region of the α subunit may regulate integrin activity by affecting integrin structural conformation.

1.5 integrin-binding proteins in focal adhesions

Because cytoplasmic tails have no intrinsic enzymatic activity, they are believed to dynamically recruit signaling molecules to transmit mechanochemical signals, either inward to the cell to regulate cellular events or outward from the cell to modify ligand binding states. Solution NMR found that both integrin α and β subunits alone are less structural unless they bind each other or other molecules to stabilize their structure. Moreover, they may adopt distinct structures upon interacting with different binding partners. Thus the proteins that directly interact with integrins and have been called integrin activity regulators or regulatory proteins are very important. They not only transmit mechanochemical signals but also mediate ligand binding activity. At least 21 proteins have been identified that bind to integrin tails (Zhao et al. 2004). It is unclear how the small integrin tails (mostly 20-50 residues) would accommodate so many binding proteins. In any case, integrin tails must recognize different regulators, in distinct manners, which lead to specific downstream events. Exactly how these specific recognitions occur and what mechanochemical signals they transmit warrant individual analysis. But most of them are not clear at the molecular level since few 3D structures of integrin-regulator complexes have been determined.

Since many signaling pathways have to send or receive signals, integrins have the prominent ability to swiftly (from subsecond to minute) and reversibly change their adhesive functions. Thus, no single protein, *i.e.* pathway can occupy

integrin tails for more than several milliseconds or serious dysfunction could occur. In another words, in order to avoid exaggerated signaling, these transient events have to be shut off immediately after their missions are achieved. On the other hand, $\alpha_{IIb}\beta_3$ molecules on platelets are very special since their activation is irreversible and they are maintained in their inactive state all the time while circulating in blood.

In a recent investigation on talin-mediated integrin signaling, it was found that talin can be dissociated from integrin β tail by a talin-binding protein, Iγ phosphatidylinositol phosphate kinase (PIPKIγ) (Barsukov et al. 2003; Ling et al. 2003). Structural analysis disclosed that PIPKIγ has an overlapping integrin β tail binding site with talin. Thus the PIPKIγ-talin complex was formed to released integrins for other activity. These findings have led an interesting mechanism where a downstream target acts as a molecular switch to regulate the integrin-regulator complex (Ling et al. 2003). Such regulation of the highly trafficked integrin-regulator interactions, albeit not clearly understood, may be critical for the cyclic linkage/breakage of the ECM-integrin-cytoskeleton connection during cell spreading and migration.

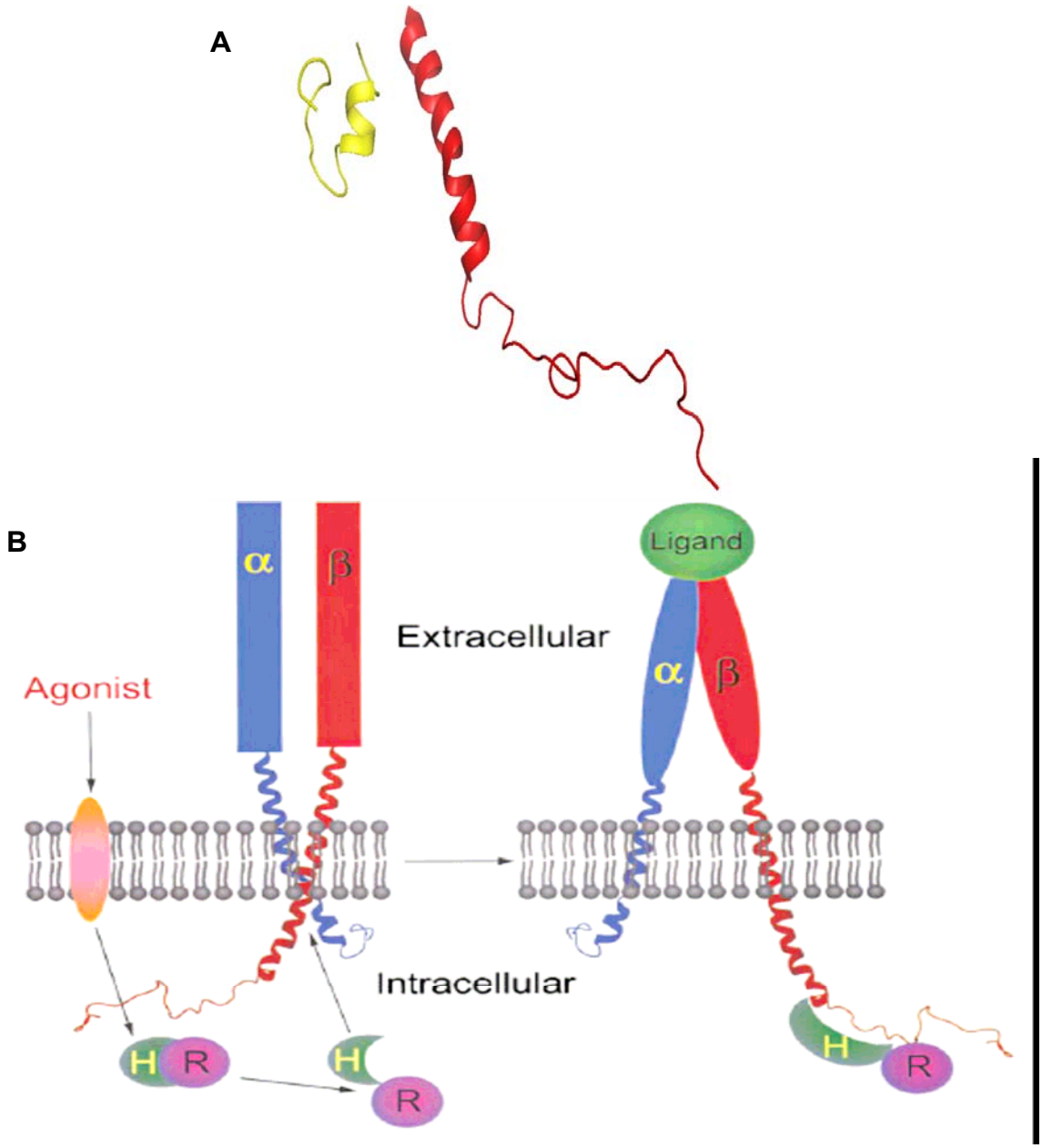

Figure 3 Integrin α_{IIb}/β_3 cytoplasmic tail signaling.
(A). NMR structure of integrin α_{IIb}/β_3 cytoplasmic tails in aqueous solution. The structure of α_{IIb} in yellow exhibits a helical secondary structure in its N-terminal part that terminates at P998. The β_3 tail also has a helix between K716 and K738 in its N-terminus. The β_3 C-terminus does not have well-defined structure. The primary interface of α_{IIb}/β_3 complex is between their N-terminal helices (Vinogradova et al. 2002).
(B). The proposed mechanism of talin regulation of integrin ligand binding affinity by disruption of α_{IIb}/β_3 interaction. Talin is composed of head (H) and rod (R) domains (Vinogradova et al. 2002).

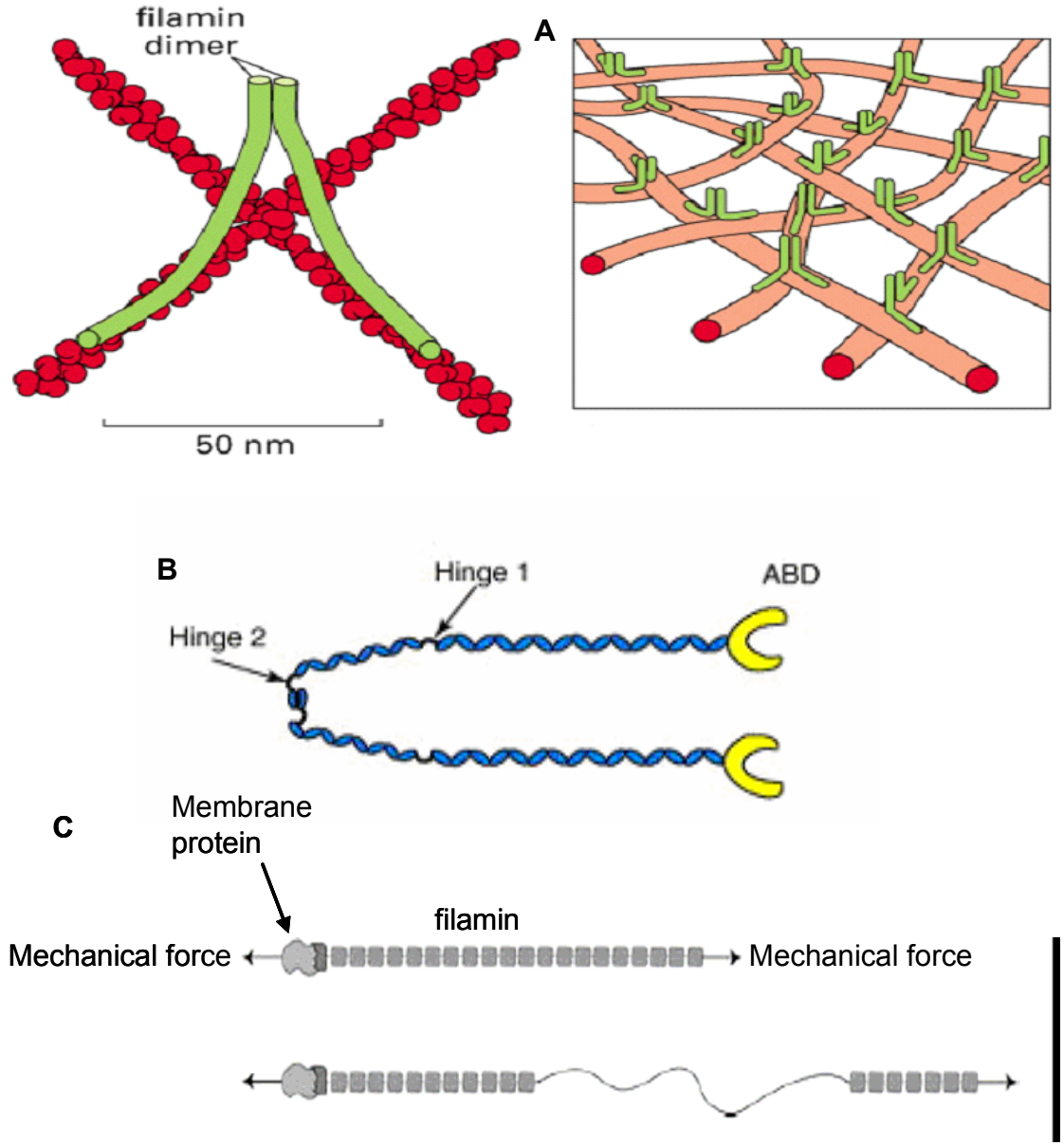

Figure 4 Filamin.
Filamin crosslinking actin filament (A) and filamin's molecular architecture (B) (Grzegorz M. Popowicz, 2006).
(C). Schematic model of the pulling of the complex of filamin denoted by a rod-like protein composed of 20 tandem repeats bound to another protein (at left like an integrin). The arrow shows the direction of mechanistic force. The external forces exerted on the filamin-protein complex can stretch filamin a long distance without disrupting the binding between filamin and its binding partner (Yamazaki et al. 2002).

1.6 Filamin-mediated integrin activity

The association of integrins with the actin cytoskeleton is indispensable for many cell functions such as migration, fibronectin matrix assembly and focal adhesion formation (Ali and Hynes 1977; Reszka et al. 1992; Wu et al. 1995; Huttenlocher et al. 1996), mainly because this association provides a physical bridge across the cell membrane to facilitate the mechanical force and the biochemical signals (Huttenlocher, 1996). Instead of directly binding to the cytoskeleton, integrins' cytoplasmic tails anchor to the cytoskeleton via actin-binding proteins. Three actin-binding proteins, filamin, talin and α–actinin, have been found to connect integrins to the actin cytoskeleton. It is very likely that integrin's distinct linkage to the cytoskeleton may account for its diverse functions; for instance talin has been the recognized activator whereas filamin has been suggested as an inhibitor of integrin ECM ligand binding affinity. Integrin β subunits have been believed to associate with actin-binding proteins with characteristic specificity (Liu et al. 2000). For example, the muscle-specific β_{1D} integrin binds to talin more strongly than either the widely expressed β_{1A} or the leukocyte-specific integrin β_7 (Belkin et al. 1997; Pfaff et al. 1998). By contrast the β_7 tail binds more tightly to filamin than those of the other integrins (Pfaff et al. 1998). Moreover, static light scattering experiments indicate that both filamin and α-actinin bind less tightly to integrin $\alpha_{IIb}\beta_3$ than talin (Goldmann 2000). The differences in the strength of β tail binding to different cytoskeleton proteins may

contribute to integrin functional specificity in different cell types (Calderwood et al. 2001). The structural mechanism of filamin's effect on integrin function is the center of attention of this dissertation.

1.6.1 Filamin introduction

Filamin is a large actin-binding protein that integrates cellular architectural and signaling functions and is fundamental for fetal development and cell locomotion. In humans there exist three highly homologous isoforms, A, B and C. Filamin A and filamin B are widely expressed whereas filamin C shows more restricted expression in skeletal and cardiac muscle (Stossel et al. 2001; van der Flier and Sonnenberg 2001; Feng and Walsh 2004). Filamin contains an N-terminal actin binding domain (ABD) followed by an array of 24 immunoglobulin-like repeats (filamin 1-24) interrupted by two hinges (Figure 3 B)(Calderwood et al. 2000). It exists as a V-shaped parallel homodimer with repeat 24 as the dimerization domain (Figure 3) (Pudas et al. 2005). Filamin's main function is to cross-link actin cytoskeleton networks into an orthogonal matrix and facilitate the dynamic reorganization of the cytoskeleton by acting as a versatile scaffold. Distinct from other actin-binding proteins, filamin promotes the high-angle branching of actin filaments and stabilizes loose microfilament architecture, as found in the cortical actin network. In addition, as a good example of its multifunctionality, filamin's dimeric array has evolved into a scaffold for

mechanical force transmission and signal transduction (Calderwood et al. 2000). Recent genetic studies have shown significant roles for filamin in diseases affecting brain (Fox et al. 1998; Sheen et al. 2001; Feng and Walsh 2004), bone and the cardiovascular system (Robertson et al. 2003; Stefanova et al. 2005).

1.6.2 Integrin-filamin interaction mediates cell functions

It has been found that filamin binding to integrin modulates cell migration (Calderwood et al. 2001; Kiema et al. 2006). Artificially tightened integrin-filamin interaction blocks cell polarization and transient membrane protrusion which are the earliest steps in cell migration. In this way increased integrin-filamin interaction may act as a brake in cell migration in response to cell signals. This phenomenon was recently explained as follows: the increased recruitment of filamin to integrin may lead to increased stability of the actin microfilament network and restrict membrane protrusion, or filamin tethers may limit the mobility of integrins to form clusters, thus subsequently suppressing integrin signaling (Calderwood et al. 2001). Moreover, filamin A bound to integrin transduces stress signals to the actin cytoskeleton and the subsequently stiffened cytoskeleton enables cells to resist the strain. Cells lacking filamin A do not show the same stiffening response (Glogauer et al. 1998). When bound to integrin, filamin is well placed to influence integrin signaling and reorganization of the actin cytoskeleton. Such ECM-integrin-filamin-cytoskeleton linkage promotes cell generation of

mechanical traction force during migration and also exerts tension during ECM-cytoskeleton remodeling in response to ligand-adhesion (outside-in signaling). The possibility that the complex of filamin and membrane protein can endure the external force has been investigated using atomic force microscopy. The tandem repeats of filamin are proposed to undergo cyclic unfolding and refolding to endure either external or internal forces without disruption of the complex of filamin and membrane protein, rather than go through the disassociation and association of the complex. The latter process would require a much longer time and much more energy. During the reversible unfolding of the Ig repeats, filamin can be stretched to several times the length of its native state (Yamazaki et al. 2002).

It also was shown that filamin can crosscompete with talin to bind integrins (Figure 4) (Kiema et al. 2006) which further links filamin to integrin inside-out signaling as a negative regulator of integrin activity. However, there is no evidence to date that filamin can maintain integrins in their inactivated state. Since integrins α & β are less structural in solution and the interaction between them is very much weaker than the interaction between membrane bound α/β and any other integrin-associated protein, it may be sensible that there are proteins like filamin that can stabilize the integrin α/β clasp by acting as a clasp holder, preventing non-specific interactions. Yeast two-hybrid studies and GST-FLN pull down assays have mapped integrin-binding to repeat 21 (FLN21) (Figure 4 A)

(Calderwood et al. 2001; Travis et al. 2004). Although filamin's other repeats exhibit binding to integrin β tail, repeat 21 has been identified as the major binding site since it has a much higher binding affinity than other repeats. Furthermore, most of studies suggest that the major binding site on integrin for FLN21 is the β C-terminus (Figure 4)(Kiema et al. 2006). A few structures of filamin 21 and the C-terminus of integrin β tails have been published. In those structures, filamin binds to the same region on integrin β tail as talin does, which has provided the structural enlightenment for filamin's competition against talin to occupy integrins. However, it can not exclude the interaction between FLN21 and either integrin β-membrane proximal or α subunit because these interactions may not be detectable by pull-down assays or co-crystallization.

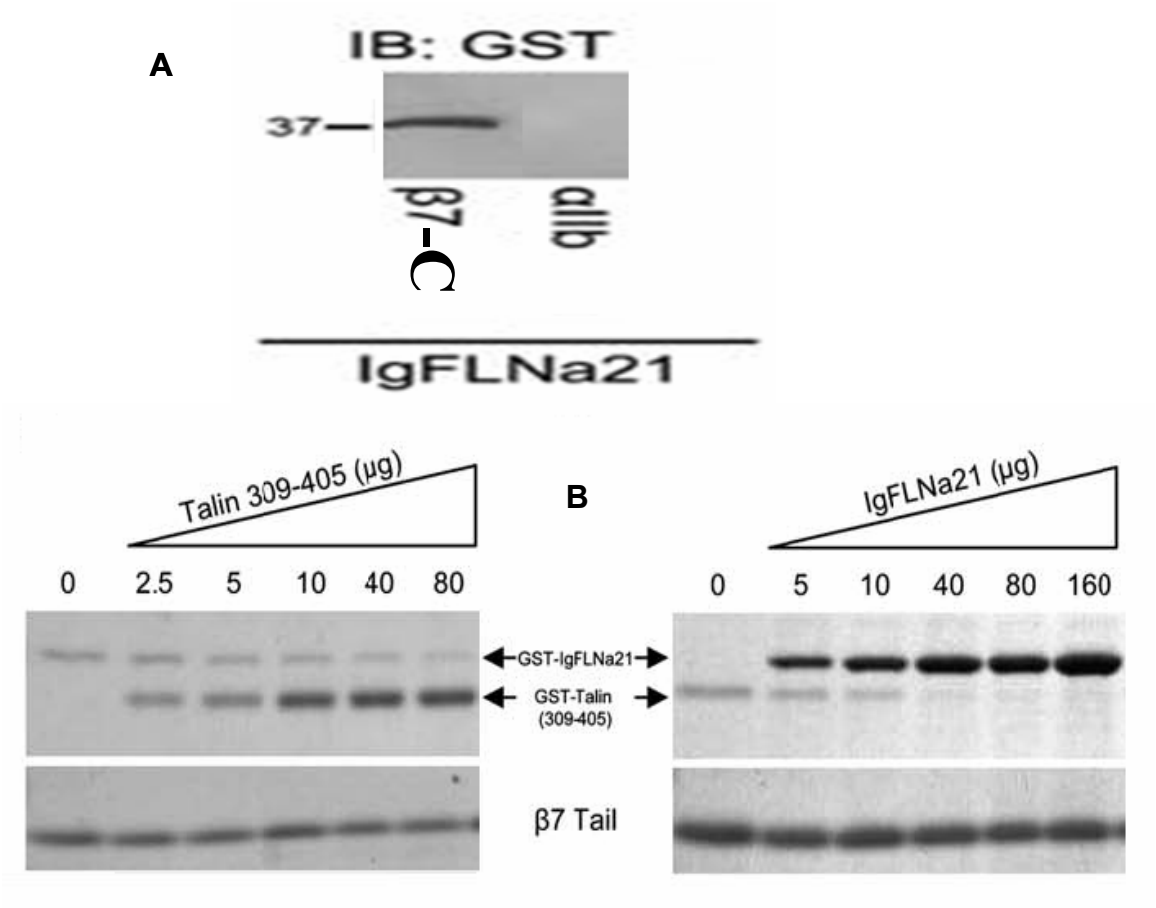

Figure 5 FLN21a cross-competing with talin.

(A). Affinity pull down assay shows that GST-FLN21 is able to pull down β_7 C-terminus but not α_{IIb}.

(B). FLN21 cross-competes with talin to bind β_7 C-terminus (Tiila Kiema, 2006).

(β_7 C-terminus: LNWKQDSNPLYKSAITTTINPRFQEADSPTL)

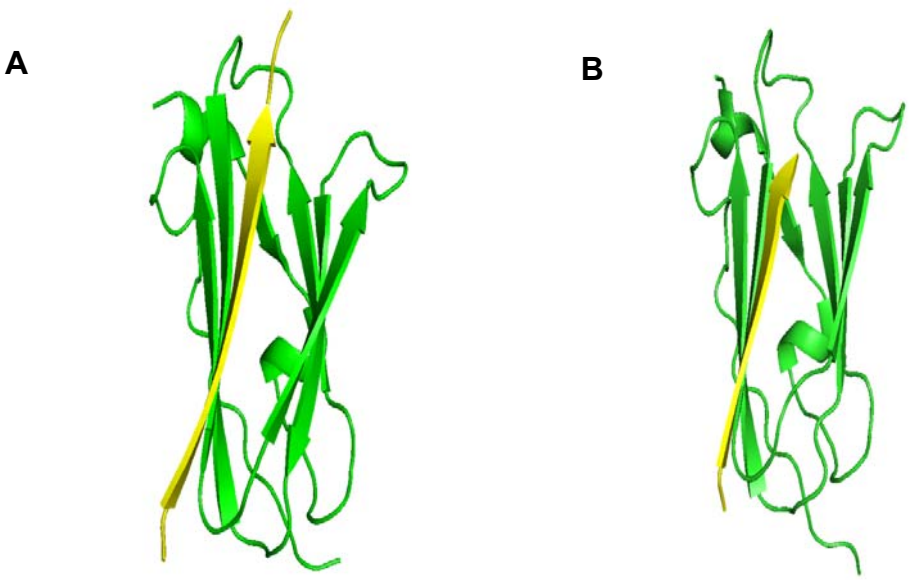

Figure 6 Filamin complexed with different partners.
(A). X-ray structure of FLN21a complexed with β7 C-terminus (Kiema et al. 2006).
(B). X-ray structure of FLN21a complexed with migfilin peptide (Lad et al. 2008).

1.6.3 A filamin-downstream protein-migfilin may regulate filamin-integrin interaction

Migfilin, also named filamin-binding LIM protein-1, is a recently discovered, widely expressed protein that is emerging as a key regulator of a host of major cellular activities such as shape modulation, motility and differentiation (Tu et al. 2003). With a mass of about 50 kDa, migfilin consists of three C-terminal LIM domains, a central proline-rich region, and an N-terminal portion which has been identified to bind to filamin. Very similar to integrin, migfilin's N-terminal portion binds to several filamin repeats with repeat 21 showing the strongest binding affinity. Recently the crystal structural of filamin and migfilin N-terminal peptide was published and the binding manner is roughly the same as the interaction between filamin and integrin β C-terminus, indicating migfilin and integrin may compete for binding filamin (Lad et al. 2008)(Figure 5). Thus, migfilin has been suggested to be a regulator of filamin-integrin interaction (Tu et al. 2003).

1.7 Research aims and significance

The research aims of this dissertation are to demonstrate a ternary complex structure of FLN21a, integrin α_{IIb} and β_3 cytoplasmic tails and the biological and physiological significance this structure can represent. Firstly, this dissertation will present a field-shaping idea that filamin can maintain the integrin $\alpha_{IIb}\beta_3$ clasp and thereby lock integrins in their inactive ligand binding state. The

idea presented here may elucidate the mechanism by which, on circulating platelets, $\alpha_{IIb}\beta_3$ integrins tightly maintain their “off” state, whereas in response to signals they can switch to the active ligand binding state and form a blood clot within seconds. Secondly, this dissertation will propose a mechanism of how integrin-filamin interactions bi-directionally transmit the mechanochemical signals. For the outside-in pathway, integrin-filamin interaction can sense mechanochemical signals and convey them to other parts of cell. For the inside-out pathway, through this interaction biochemical signals can be transduced by modulating the integrin ligand binding state while mechanical forces from the cytoskeletal contraction can be directly transmitted the cell surface to generate forces for cell spreading and migration.

CHAPTER II

Solution protein NMR methods

2.1 NMR overview

NMR stands for Nuclear Magnetic Resonance. In the definition, the first word “Nuclear” denotes that it is the atomic nucleus that is analyzed in NMR spectroscopy, distinct from other magnetic resonance techniques such as the electron in Electron Spin Resonance (ESP). All nuclei, composed of neutrons and protons, have the intrinsic quantum property of spin. The property of spin manifested by NMR is the nuclear spin angular momentum $\mathbf{I}$ which is characterized by nuclear spin quantum number I.

$$|\mathbf{I}| = [\mathbf{I}\cdot\mathbf{I}]^{1/2} = \hbar[I(I+1)]^{1/2}$$

in which $\hbar$ is the reduced Planck’s constant (Planck’s constant divided by 2π). If in a given isotope the nuclear mass number is odd then I is equal to a half-integer. If in a given isotope the nuclear mass number is even and its atomic number is odd

then I equals an integer larger than zero. If the nuclear mass number of a given isotope is even and its atomic number is even too then $I=0$ and $\mathbf{I}=0$, *i.e.*, there is no spin. Because the NMR phenomenon relies on the existence of nuclear spin, the nuclei with zero spin quantum number is NMR inactive. The $I=½$ isotopes, often called spin half, are the most studied. For protein NMR, the most important nuclei with $I=½$ are ^{1}H, ^{15}N, and ^{13}C. Nuclei with spin a quantum number greater than ½ possess quadrupolar moments arising from nonspherical nuclear charge distribution. The quadrupolar coupling causes spectra very complicated to interpret. Moreover, the lifetimes of the magnetic state for quadrupolar nuclei in solution are much shorter than are the lifetimes for spin half nuclei, which make NMR signals decrease too fast to observe. Deuterium with $I=1$ is used to lock the magnetic field. Besides, since the resonance frequency of deuterium is very different from a proton, it is not observable when the acquisition frequency is set on proton. In addition, because the deuteron gyromagnetic ratio is 6.5-fold smaller than the proton gyromagnetic ratio, deuterium is much less effective than protons at causing dipolar relation with the directly attached heteronucleus and surrounding protons. These properties of deuterium are made good use of in protein NMR.

The spin angular momentum is quantized. This means that both magnitude and orientation of the spin angular momentum are quantized. The orientation of the spin angular momentum is referred to by the magnetic quantum

number m. m can take values from + I to − I, in integer steps. Hence for any given nucleus, there is a total of $2I + 1$ angular momentum states. In the absence of external fields, the $2I + 1$ angular momentum states all have the same energy, and the spin angular momentum vector does not have a preferred orientation. By convention, the value of the z-component is

$$I_z = \hbar m$$

Nuclei that have nonzero spin angular momentum is always associated with a non-zero magnetic moment ($\boldsymbol{\mu}$) via the relation

$$\boldsymbol{\mu} = \gamma \mathbf{I}$$

It is this magnetic moment that allows the observation of NMR absorption spectra caused by transitions between nuclear spin levels. That is why we have the word “magnetic” in the definition of NMR. As a consequence of the Wigner-Eckart theorem, the nuclear magnetic moment is colinear with the spin angular momentum, thus

$$\mu_z = \gamma I_z = \gamma \hbar m$$

in which the gyromagnetic ratio is a characteristic constant for a given nucleus. The magnitude of the gyromagnetic ratio, in part, determines how much nuclear spin angular momentum can be received as the magnetic moment in NMR spectroscopy. Because angular momentum is a quantized property, so is the nuclear magnetic moment. Consider nuclei that have a spin of one-half (which is the only nuclear type discussed in this dissertation), like ^{1}H, ^{13}C or ^{15}N. The

nucleus has two possible spin states: m = 1/2 or m = −1/2 (also referred to as spin-up and spin-down, or α and β spin states, respectively). These states are degenerate, *i.e.*, they have the same energy. Hence, the number of atoms in these two states are approximately equal at thermal equilibrium. If a nucleus is placed in a magnetic field, however, the interaction between the nuclear magnetic moment and the external magnetic field means the two states no longer have the same energy. The energy of a magnetic moment $\boldsymbol{\mu}$ when in a static external magnetic field $\mathbf{B_0}$ (in units of Tesla or T) is given by:

$$E = -\boldsymbol{\mu} \cdot \mathbf{B_0} = -\mu_z \cdot \mathbf{B_0} \cos\theta$$

Usually $\mathbf{B_0}$ is chosen to be aligned along the z axis, therefore cosθ=1:

$$E_m = -\mu_z \cdot B_0 = -\gamma I_z B_0 = -\gamma m \hbar B_0$$

As a result the different nuclear spin states have different energies in a non-zero magnetic field, resulting in 2I + 1 equally spaced energy levels which are known as the Zeeman levels. Moreover, the spin-half nuclei have two energy states. In hand-waving terms, we can talk about the two spin states of a spin 1/2 as being aligned either with or against the magnetic field. If γ is positive for ^{1}H and ^{13}C (or negative for ^{15}N) then m = 1/2 energy state is lower (or higher). The energy difference between the two states is:

$$\Delta E = \gamma \hbar B_0$$

and this difference results in a small population bias toward the lower energy state. (Figure 7) The sensitivity of NMR spectroscopy depends on the population

differences between Zeeman states. This simply explains much of the incentive to build more powerful magnets for use in NMR spectroscopy.

The last word “resonance” in NMR signifies that resonant absorption by nuclear spins will occur only when electromagnetic radiation of the correct frequency is being applied to match the energy difference between the nuclear spin levels in a constant magnetic field of the appropriate strength. By Planck’s Law, the frequency of the required electromagnetic radiation is given by

$$\omega = \Delta E/\hbar = \gamma B_0,\ \nu = \omega/2\pi = \gamma B_0/2\pi$$

in units of s^{-1} or Hertz, respectively. The resonant absorption stimulates the transitions between Zeeman levels. Analogous to other areas of spectroscopy, the selection rule governing magnetic transition is $\Delta m = \pm 1$. For an isolated spin-half nucleus, only two nuclear spin states exist and two energy levels separated by $\Delta E = \gamma \hbar B_0$ are obtained by application of an external magnetic field. Thus a single Zeeman transition between the energy levels exists, which corresponds to (speaking to the excitation of nuclei in the thermal equilibrium states) the transition from the α state to β state (positive γ) or from the β state to the α state (negative γ). The magnetic resonance frequencies typically correspond to the radio frequency (or RF) range of the electromagnetic spectrum for magnetic fields up to ~20 T. A unique advantage of NMR is that the resonant frequencies of different nuclides are so well apart that they can be manipulated and measured separately. For example, in the external magnetic field of 11.7 T, the ^1H frequency is 500 MHz,

^{13}C's is 125 MHz, and ^{15}N's is 50 MHz. After a period of illumination, the RF is turned off and the excited nuclei tend to return to their thermal equilibrium state by emitting photons having the same frequency as the resonant frequency. It is this frequency which is detected in NMR.

2.1.1 Chemical shift

The most important feature of NMR is that instead of all nuclei of the same nuclide resonating at the same frequency predicted by $\omega = \gamma B_0$, the observed resonance frequencies are slightly different, depending on the local chemical environments of individual nuclei. The differences in resonance frequencies are referred to as chemical shifts and it is the chemical shifts that allow NMR to probe the structure of molecules. The chemical shift arises due to the secondary fields induced by the orbiting of electrons around the nucleus. Thus the actual net magnetic field “felt” by a specific nucleus depends upon the sum of the static magnetic field and the local secondary fields. The effect of the secondary fields is called nuclear shielding which can add to or weaken the effect of the static field. Accordingly, the energy gap between Zeeman levels and the frequency required to achieve resonance are also modified. It is usual in spectroscopy to quote the frequency or wavelength of the observed absorption. But, NMR spectroscopy use “ppm” for the position of the chemical shift. The reason for using ppm is that the frequencies of NMR are directly proportional to the strength of the external field.

Therefore, applying the different strength of the external field will change the frequency, which makes it difficult to compare spectra between spectrometers which operate at different field strengths. Introducing ppm is done to get round this problem and make NMR spectra independent of the field strength.

Like most of spectroscopy, NMR spectra plot the intensity of absorption (or emission) against frequency (Figure 8 A). In conventional one-dimensional NMR (1D), intensity is straightforwardly displayed in spectrum. But in multiple dimensional NMR intensity is plotted against two or three or even more frequencies, and usually is not directly displayed in spectrum because mostly frequencies are concerned (Figure 8 B). So, each peak has an intensity and two frequency coordinates in 2D NMR, three frequency coordinates in 3D, etc. What these coordinates represent depends on the experiment in question. For example, in the 2D NOESY experiment the frequency coordinates of the peaks give the chemical shifts of dipolar coupled spins. Another example is the NH-HSQC experiment, in which one frequency coordinate gives the ^{15}N chemical shift, while the other gives the chemical shift of the attached proton. In protein NMR, chemical shift assignment is the primary step and it is very important because it is the foundation for subsequent steps. Moreover, chemical shift perturbation in NH-HSQC is a convenient method to probe protein-protein interactions.

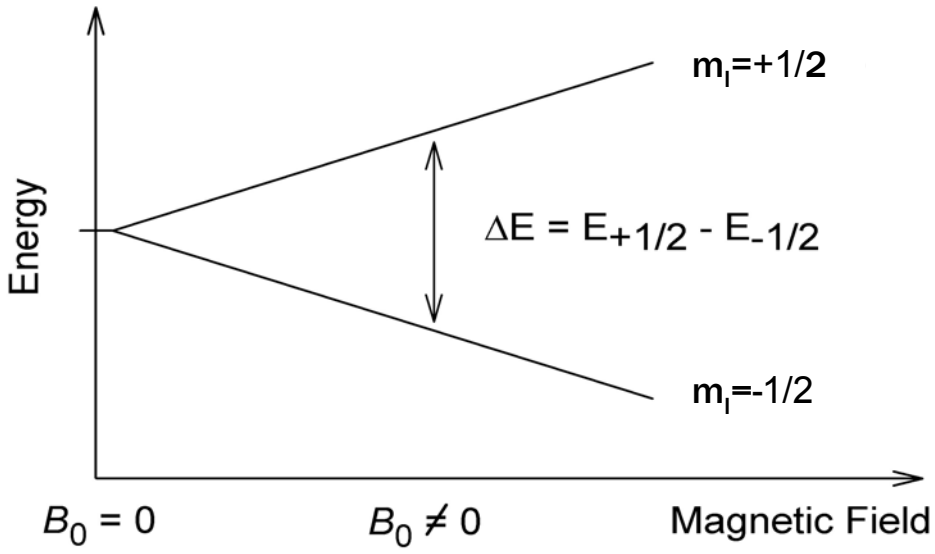

Figure 7 The energy difference between two spin states for spin-half nuclide.

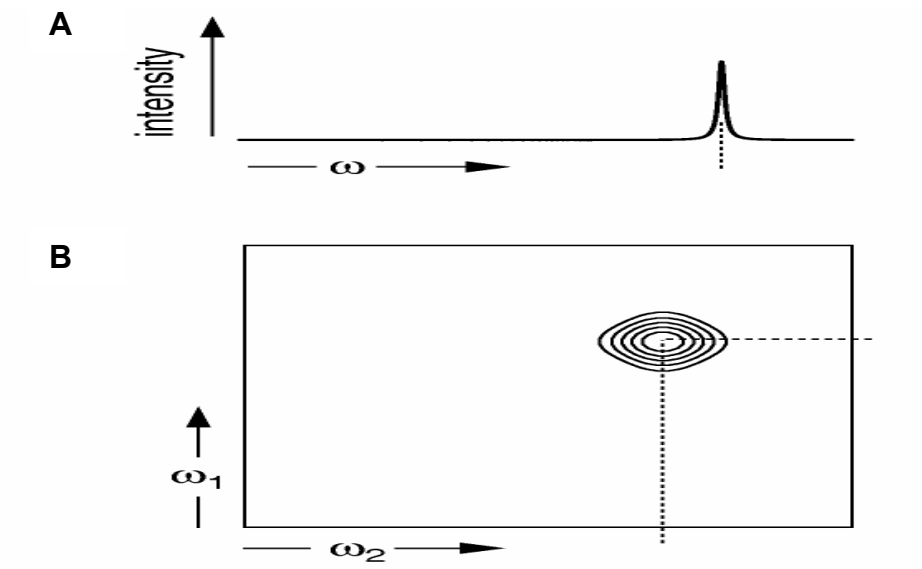

Figure 8 NMR spectrum.
(A). In a conventional 1D spectrum, each peak has a single frequency coordinate. (B). In a 2D spectrum, each peak has two frequency coordinates. The details of how to construct multidimensional experiments are presented in this dissertation due to space limits. Briefly, in 2D NMR experiments the pulse sequence may be divided in general into the following blocks: preparation—evolution (t1) and mixing—detection (t2). The evolution time t1 is incremented stepwise. For each t1 increment a separate FID is detected in t2. Thus a signal is obtained which is a function of the two time variables t1 and t2: S(t1, t2). The Fourier transformation over both t1 and t2 results in a spectrum as a function of two frequencies (ω2 horizontal, ω1 vertical).

2.1.2 J-coupling

J-coupling (also called indirect dipolar coupling, scalar coupling or spin-spin coupling) is the coupling between two nuclei that share chemical bonds. J-coupling arises due to the influence of bonding electrons on the magnetic field running between the two nuclei. The strength of J-coupling is measured by the J-coupling constant, $^{n}J_{ab}$, in which n designates the number of covalent bonds separating the two nuclei, a and b. the magnitude of $^{n}J_{ab}$ is usually expressed in Hertz. In contrast to the resonant frequency, J-coupling is independent of the field strength. The presence of J-coupling causes the splitting of NMR lines or peaks and J-coupling is mediated by chemical bonds and therefore is very useful in establish the fine structure of molecules. In protein NMR, since the global conformation is more concerned, and the splitting of NMR peaks further reduces the signal to noise ratio, J-coupling is less useful and often eliminated by the technique called de-coupling in acquisition. However, the roles of J-coupling underlie NMR experiments but are just behind the scenes because J-coupling modulated magnetization transfer is the fundamental method for correlating nuclei in multiple dimensional NMR experiments (Figure 9).

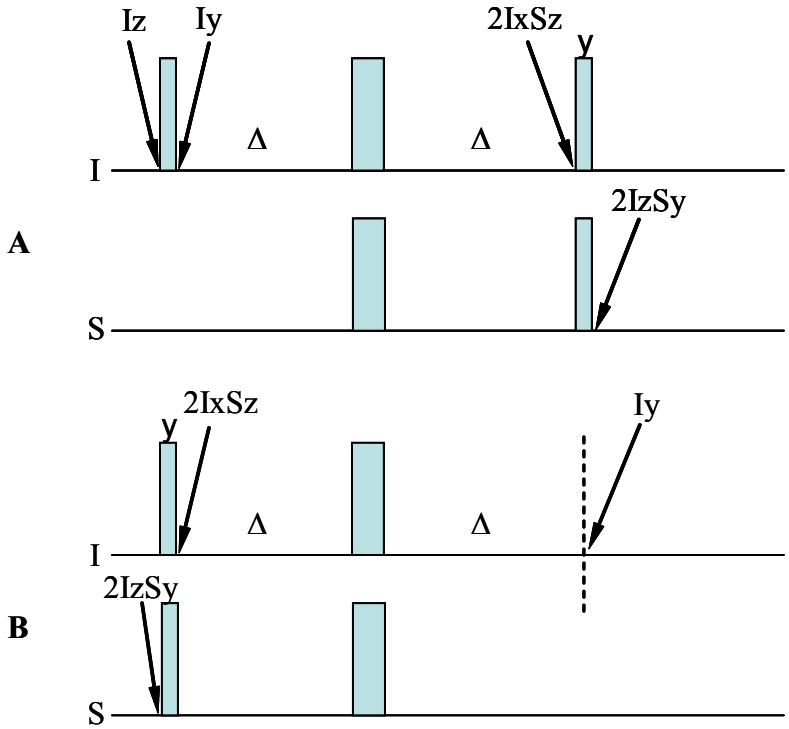

Figure 9 J-coupling modulated heteronuclear magnetization transfer.
Thinner rectangles indicate a 90° pulse, whereas wider rectangles indicate a 180° pulse. The characters above the pulse indicate the pulse phase and the phase for pulse without indication is x. Δ is the delay for evolution and is optimal at $1/4J_{IS}$ in the pulse sequences shown here. I and S denote the product operators of two nuclides. They can be considered as the magnetization. Only the magnetization on x and y are observable, like Ix, Iy, Sx, and Sy. The idea of magnetization transfer can be understood such that when the pulse sequence starts from the nuclide I's observable magnetization and ends up the nuclide S's observable magnetization, we say magnetization is transferred from nuclide I to nuclide S.
(A). The magnetization is transferred from I nuclide to S nuclide.
(B). The magnetization is transferred from S nuclide to I nuclide.

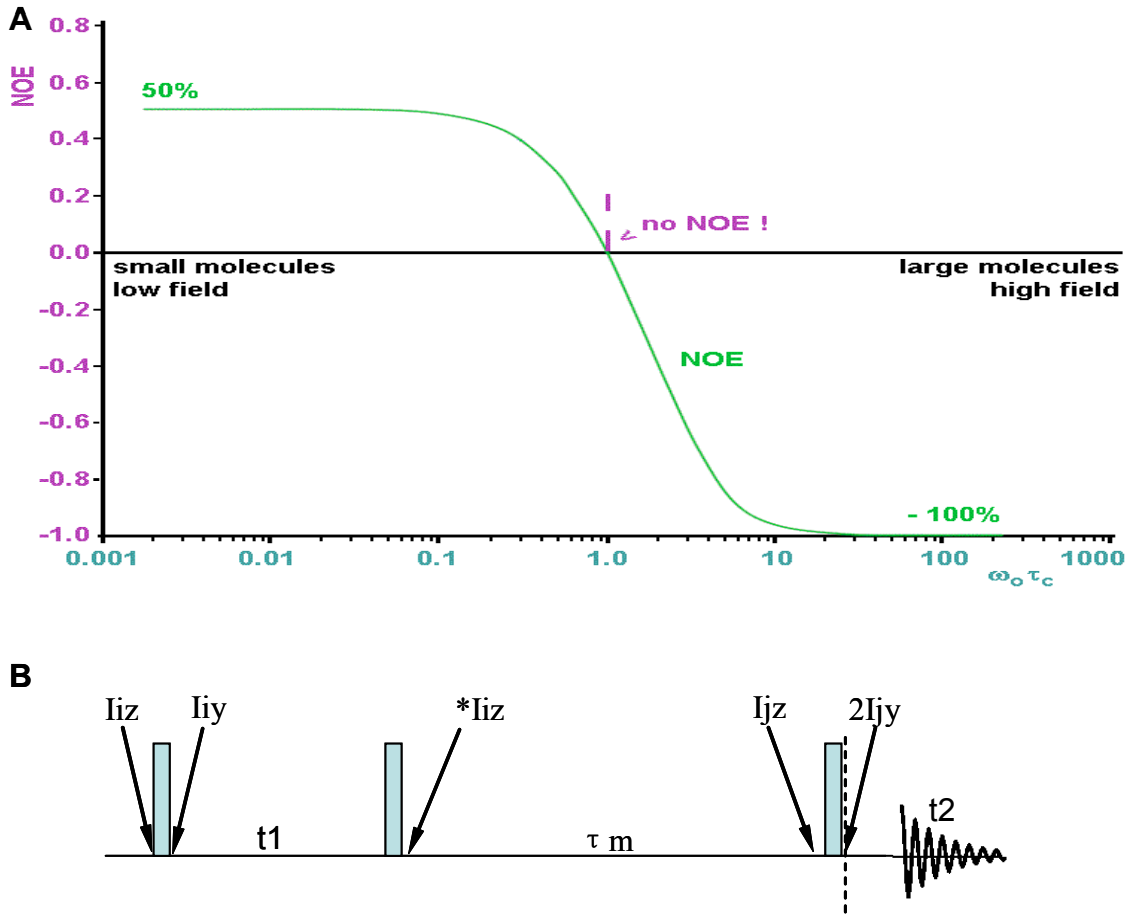

Figure 10 NOE.

(A). Illustration of how the NOE changes sign from positive to negative as the $\omega_o\tau_c$ increases. The cross-over occurs when $\omega_o\tau_c$ is just over 1. For protons at a ω_o frequency of 600 MHz, the cross-over point is at $\tau_c \approx 300$ ps.

(B). Basic 2D NOESY pulse sequence. The magnetizations other than longitudinal Iiz at (*) can be suppressed by phase cycling and gradient pulse which are not shown here and are not the topic in this dissertation.

(C). Magnetization transfer pathway.

2.1.3 dipolar coupling

The direct dipole-dipole coupling is very useful for molecular structural studies, since it depends only on known physical constants and the inverse cube of internuclear distance. Estimation of this coupling provides a direct spectroscopic route to the distance between nuclei and hence the geometrical form of the molecule. Although internuclear magnetic dipolar couplings contain a great deal of structural information, in isotropic solution they average to zero as a result of rotational diffusion. However, their effect on nuclear spin relaxation results in measurable nuclear Overhauser effects (NOEs). Compared to J-modulated magnetization transfer, which is often called through bond magnetization transfer, dipolar coupling modulated magnetization transfer is called through space magnetization transfer.

The magnetization transfer efficiency is determined by the dipolar cross-relaxation rate constant (σ). The value of the dipolar cross-relaxation rate constant (σ) is defined by

$\sigma = b^2 \frac{1}{2} \tau_c$ in fast motion ($\omega_o \tau_c << 1$)

$\sigma = - b^2 \frac{1}{2} \tau_c = b^2 \frac{3}{10} j(2\omega_o) - b^2 \frac{1}{20} j(0)$ in slow motion ($\omega_o \tau_c >> 1$)

in which j(ω) is the spectral density; size term b is proportional to the inverse three power of the distance between two interacting ^{1}H spins, which make the dipolar cross-relaxation rate constant (σ) proportional to the inverse sixth power of the

distance between two interacting ^1H spins; τ_c is the rotational correlation time which is the average time it takes for a molecule to rotate one radian (360°/2π). The larger the molecule the slower it moves and the bigger τ_c; ω_o is the Larmor frequency of the spins and can be considered to be the acquisition frequency. The dependence of NOE value on ω_o and τ_c is illustrated in Figure 10 A. At the cross-over point, where σ = 0, NOEs vanish! For protons at a ω_o frequency of 600 MHz, the cross-over point is at $\tau_c \approx 300$ ps. Moreover, after crossing the cross-over point, NOE absolute value increases steeply as the value $\omega_o\tau_c$ increases. τ_c can be estimated for a spherical protein by,

$$\tau_c \approx MW/2400 \text{ (ns)}$$

For α_{IIb} (2.5 KDa), GST-FLN21a (36.9 KDa) and MBP-β_3, their τ_c (estimated) are 1 ns, 15 ns and 20 ns, respectively (α_{IIb} is not spherical). These big differences in the rotational correlation time and the correspondent NOE between α_{IIb} and GST-FLN21a/MBP-β_3 are taken advantage of in transferred NOE experiments.

The experiment used to measure NOEs is the NOESY (Nuclear Overhauser Effect Spectroscopy) and the pulse sequence is shown in Figure 10 B. Initially, a 90°-t1-90° element is used to frequency label the spins and return the magnetization to the z-axis (or longitudinal magnetization). Magnetization transfer occurs via dipolar coupling for a period τ_m before observable transverse magnetization is created and acquired. In the initial rate approximation (very small mixing time τ_m), cross-peak intensities in NOESY are proportional to the

cross-relaxation rate constants, which make NOE cross-peaks proportional to the inverse sixth power of the distance between two proximal spins. However, NOESY mixing times short enough to satisfy the initial rate approximation usually are impractical because the cross-peak intensities then have low signal-to-noise ratios. Thus, because by using longer mixing times NOESY cross-peaks are no longer directly proportional to cross-relaxation rate constants, precise ^{1}H-^{1}H separations cannot be determined from the NOE cross-peak intensities. The method to translate NOE cross-peaks to the distance constraints will be discussed in 2.5.1.1.

2.2 HSQC

HSQC experiment has very important roles in protein NMR and is the basic heteronuclear experiment. The idea of HSQC is the root of all other heteronuclear experiments and its pulse sequence itself has become the building block for multidimensional experiments as well. Moreover, HSQC chemical shift perturbation mapping is a popular method for studying protein-protein interactions. HSQC stands for Heteronuclear Single Quantum Correlation. “Heteronuclear” indicates this experiment has the frequency coordinates from different nuclides, often proton-carbon or proton-nitrogen. The concept “quantum” has not been discussed due space limitations. But simply, “Single Quantum” can be understood as the HSQC experiment having only single observable magnetization ($2I_zS_y$)

during the t1 chemical shift evolution period (Figure 9 A). The advantage of having single quantum is to simplify the spectrum and as a result have good resolution. “Correlation” means that HSQC peaks correlate the two heteronuclear nuclei. Correlation is actually the common feature for all multidimensional heteronuclear NMR experiments, which is that through appropriate magnetization transfer steps (Figure 9) and tuning the delay “Δ” to the J-coupling constant between interested nuclei (2-4 B), specific nuclei can be selected and correlated. ^{1}H-^{15}N HSQC correlates the nitrogen and the directly attached proton that make the amide bond within each amino acid residue.

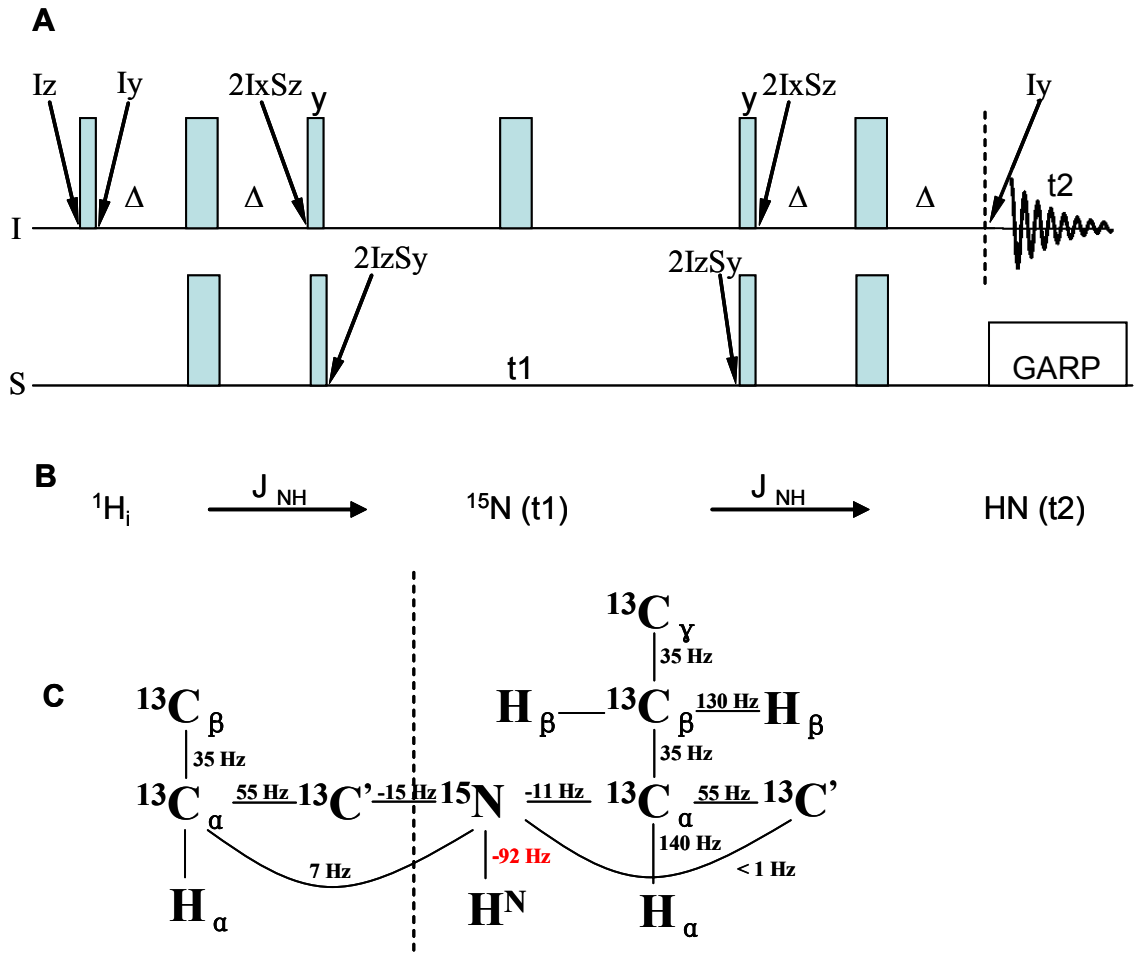

Figure 11 HSQC.

(A). Basic HSQC pulse sequence. It can be seen that it is just pulse sequences in Figure 9 A and B having a ^{15}N chemical shift evolution. “GARP” is the decoupling pulse during acquisition time to decouple the proton and nitrogen.

(B). The magnetization transfer steps are illustrated. The delays Δ are optimized to the J_{NH} shown in C. The pulse sequence in A, the idea of magnetization in B, and the J-coupling constants in C are generally applied in multidimensional protein NMR experiments.

Due to the special constitution of proteins (Figure 10 C), that each residue has one amide (except that proline does not have an amide proton, and tryptophan, asparagine, glutamine, lysine and arginine have sidechains with amides), ^{1}H-^{15}N HSQC presents the chemical shifts from backbone amides and perturbation of these chemical shift strongly recommends the conformation changes which may be induced by interaction with an added binding partner. So, generally the ^{1}H-^{15}N HSQC is run twice under the same conditions, except that one is on ^{15}N labeled protein alone, and the other one is on ^{15}N labeled protein with the desired unlabeled binding partner added. Since the natural abundance of ^{15}N in unlabeled protein is not enough to be observed in the short acquisition time of the experiment, the addition of unlabeled protein will not affect the labeled protein's spectrum except to perturb the chemical shifts of the labeled protein's resides by either direct interaction or allosteric effect. The overlay of the two resulting spectra can clearly show the perturbed residues, and the perturbation ($\Delta\delta_{(HN,N)}$) can be evaluated by

$$\Delta \delta_{(HN,N)} = \sqrt{(\Delta \delta_{HN})^2 + (0.154 \times \Delta \delta_{N})^2}$$

in which $\Delta\delta_{HN}$ and $\Delta\delta_{N}$ are the chemical shift perturbation induced in the proton and nitrogen coordinates, respectively. The identity and location of peaks that undergo binding-dependent chemical shift perturbations are mapped onto the three-dimensional structure of the protein to yield the putative binding site for the partner protein.

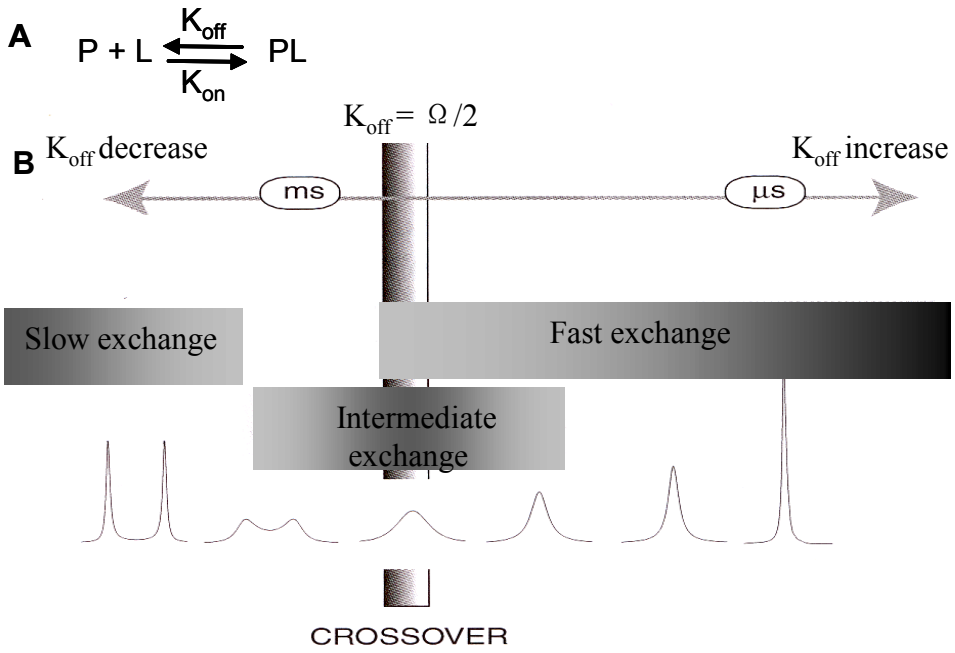

K_D	K_{off}	Lifetime of complex
1 nM	0.1 S^{-1}	10 S
1 uM	100 S^{-1}	10 mS
1 mM	10^5 S^{-1}	10 uS

Figure 12 Chemical exchange regions.

Considering a 1:1 protein-ligand interaction as a chemical reaction A. We assume that protein is labeled in HSQC. The disassociation constant (binding affinity constant) of this interaction can be defined by $K_D = K_{off}/K_{on}$. The value of Koff can be estimated from $K_{off} \sim 10^8 \times K_D$ when assuming k_{on} to be diffusion limited in the protein concentration used by NMR. Motional time scales of chemical exchange are defined by comparing K_{off} with chemical shift difference $\Omega = \delta_f - \delta_b$ in which δ_f and δ_b are the chemical shifts for free and bound states of protein, respectively. Thus, fast: $k_{off} >> \Omega$; intermediate: $k_{off} \sim \Omega$; slow: $k_{off} << \Omega$, as shown in B. The lifetime of the complex = $1/k_{off}$ and If chemical shift differences between free and bound state are 100-1000 Hz, which make lifetimes at intermediate exchange 1-10 mS. To the right of the crossover point, the resonant frequency is dependent on the binding affinity and protein-ligand ratio. To the left of the crossover point the resonant frequencies just represent the free and bound states. But, apparently HSQC is still able to tell the existence of interactions even beyond the fast exchange region.

Although this approach is very useful for studying protein interactions in solution the result has to be analyzed carefully and this approach also has limitations. First of all, the binding site cannot be concluded because perturbation may come from direct interaction or allosteric effects, although the greater perturbed residues are more likely to be the binding site. Second of all, this approach is limited to relatively low-affinity interactions because these are in the motional region of fast exchange (Figure 11). Motional regions have distinct effects on the NMR line and resonant frequency. In fast exchange, the NMR line is narrowed by fast exchange motion and the resonant frequency is the average over frequencies of free and bound states, depending on the binding affinity and the protein-ligand concentration ratio. It is this dependence that allows HSQC to study the interaction. As can be seen from the table in Figure 12, fast exchange usually corresponds to the interaction with affinity bigger than 1 uM. Intermediate exchange severely reduces the signal to noise ratio by line-broadening whereas the chemical shift changes in slow exchange region are not dependent on interaction. However, the appearance of line-broadening can still indicate the formation of the protein-ligand complex.

2.3 Transferred NOE

Beside HSQC, transferred NOE (or exchange-transferred Nuclear Overhauser Effect SpectroscopY, *i.e.* et-NOESY or et-NOE) is another important

method to probe the protein-ligand interaction. et-NOE has the particular advantage of allowing detailed structural analysis of high-molecular-weight complexes that are not amenable to direct study by other NMR methods, due to large line widths or other intractable properties such as low solubility. The et-NOE method uses excess ligand (typical ligand : protein ratios range from 10 to 50, *i.e.* protein : ligand percentages range from 2% to 10%), so that the resonance line shapes resemble those of the unbound ligand in solution, but the cross-relaxation measured from the NOE spectrum is predominantly determined by internuclear distances within the ligand in the bound state. Like HSQC, et-NOE is also limited to the fast exchange interaction in order to observe a single resonance peak averaged over the free and bound states. The size of the ligand is set by the condition that the dipolar interaction is insignificant for the free ligand, in order that no NOESY cross-peak intensity (or very little) is observed. In practice, the ligand rotational correlation time is near the value for the NOE null condition (*i.e.* $\omega_o\tau_c$ = 1.12) or shorter, which corresponds to a molecular weight of ≤ 5 kDa. (2.1.3) The absence of a NOE signal for the unbound state is easily confirmed by measuring the NOESY spectrum of the free ligand under conditions identical to those used to measure the et-NOESY spectrum of the complex. The macromolecule should be high molecular weight, approximately ≥ 35 kDa, and with no upper limit.

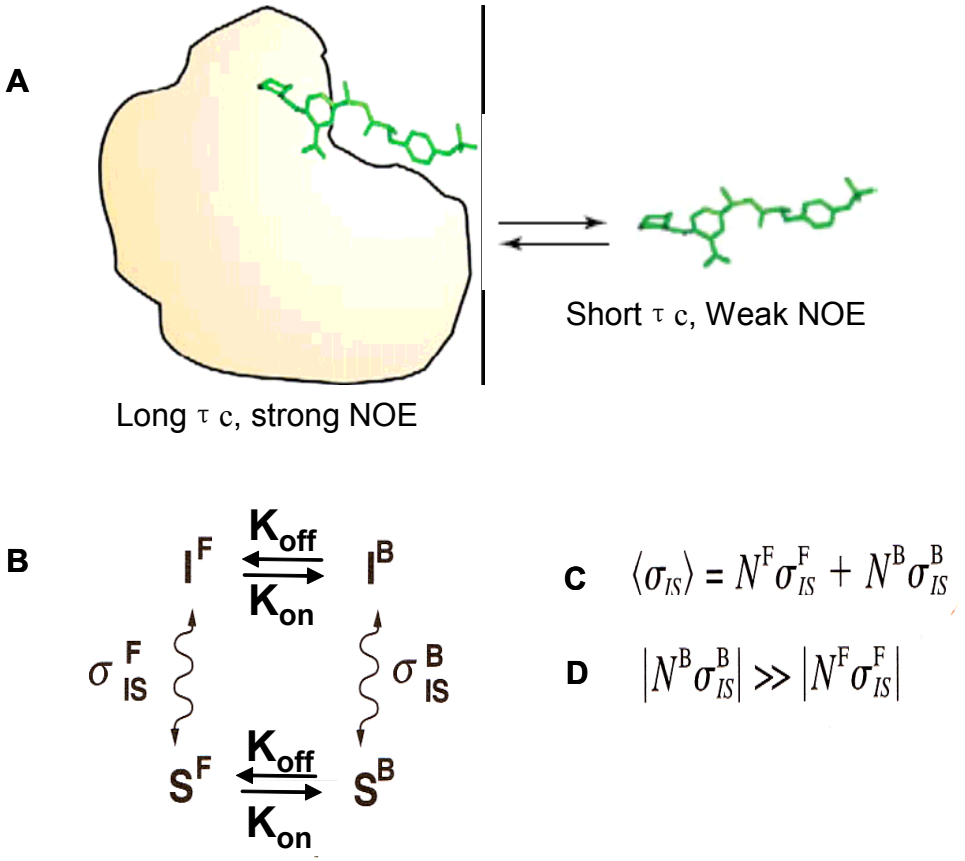

Figure 13 Transferred NOE.

(A). A small molecular ligand, present in molar excess of a macromolecular receptor. A strong NOE developed in the complex is transferred to the free ligand state and measured from free ligand resonances.

(B). I and S are two protons within the ligand. is The cross-correlation rate is σ, which is directly proportional to the initial build-up of cross-peak intensity. F and B denote free and bond state, respectively. K_{off} and K_{on} have the same definition as in Figure 11. N is the molar concentration. The overall cross-correlation rate is described in C. To observe the transferred NOE, the condition in D must be satisfied. The value of σ is determined by τ_c. (2.1.3) Thus, the larger the population of bound form and greater the value of σ^B, the more intense the cross-peaks.

2.4 Resonance assignment

In the opening step of any investigation by NMR spectroscopy, each resonance (or peak) in the NMR spectrum must be assign to a specific nucleus in the molecule under analysis. Resonance assignment must be sequence specific, *i.e.*, each resonance must be assigned to a spin (or atom) in a particular amino acid residue in the protein sequence. The main strategies for the resonance assignment include homonuclear ^{1}H NMR spectra (which only need unlabeled proteins) and ^{13}C and ^{15}N heteronuclear correlation spectra (which require isotopically labeled proteins). Which one is utilized depends upon whether labeled proteins are available and the protein molecular weight (it is difficult to fully assign proteins >15 kDa with homonuclear spectra). Within these two main strategies, the variant subsets of experiments may be used in the real case, often depending on the protein complexity and researcher's preference. In this dissertation, integrin α_{IIb} tail was assigned using homonuclear experiments TOCSY (TOtal Correlation SpectroscopY) and NOESY due to its small molecular weight of 2.5 kDa. Integrin β_3 and FLN21a use heteronuclear J-correlation spectra: CBCANH and CBCACONH for $^{1}H^{N}$, ^{15}N, $^{13}C\alpha$ and $^{13}C\beta$, HNCO and HNCACO for ^{13}CO. CBCANH and HNCACO provide sequential assignment. HCCH-TOCSY assigns $^{1}H\alpha$, and sidechain ^{13}C and ^{1}H. Due to space limitations, other subsets of assignment experiments will not be discussed.

2.4.1 Homonuclear 1H assignment for unlabeled proteins

The basic principle for homonuclear ^{1}H assignment is to use TOCSY to identify and categorize resonance positions within each amino acid spin system and to use NOESY to sequentially connect the amino acid spin systems (Wuthrich 1986) (Figure 13). Random coil ^{1}H chemical shifts have been determined for unstructured peptides (Arno Bundi 1979; Schwarzinger et al. 2000; Schwarzinger et al. 2001) and the distribution of ^{1}H chemical shifts (averaged over all observed conformations) for proteins are in a database compiled by BioMagResBank (Beverly R. Seavey 1991). The backbone amide $^{1}H^{N}$ signals are usually the best resolved set of resonances within a protein ^{1}H NMR spectrum. Thus, the $^{1}H\alpha$ and side chain resonance positions are most readily determined by the observation of direct and relayed crosspeaks to the backbone amide spins. Besides, theoretically ^{1}H 2D spectra are symmetric about the diagonal. However, in real spectra this symmetry often is broken due to experimental artifacts, such as a streak of noise at the frequency of the water resonance which arises from incomplete solvent suppression. For these reasons, initial analyses of TOCSY and NOESY focus on the sidechain to amide proton crosspeaks occurring above the diagonal.

At the first step, ^{1}H resonances in TOCSY are categorized on the basis of their chemical shifts to establish sets of $^{1}H^{N}$, $^{1}H\alpha$, and aliphatic sidechain resonances that belong to the same amino acid residue spin systems. A protein of

N residues has N distinct backbone-based spin systems (Wuthrich 1986). Aromatic ^{1}H spins of tyrosine, phenylalanine, tryptophan, and histidine residues, sidechain amide protons of glutamine and asparagines residues, the sidechain guanidinium group of arginine residues, and the methyl group of methionine residues are not scalar coupled to the remainder of the sidechain and consequently comprise distinct spin systems. Association of the sidechain and backbone resonances of these amino acid residues has to be made on the basis of intraresidue NOR correlations.

At the second step of the assignment process, every spin system is assigned to a particular residue within the polypeptide chain by using NOESY to sequentially connect the spin systems identified from TOCSY. Statistical analysis of hydrogen atom locations has shown that a majority of the short distances between $^{1}H^{N}$, $^{1}H\alpha$ and $^{1}H\beta$ are between residues adjacent in the primary sequence. Thus, identification of intense NOEs from $^{1}H^{N}$, $^{1}H\alpha$ and/or $^{1}H\beta$ of one spin system to $^{1}H^{N}$ of a second spin system suggests that the two spin systems are adjacent in the primary sequence, with the first spin system nearer to the C-terminus of the protein. Identification of a series of sequential NOE interactions placing several spin systems in the order i, i+1, i+2, …, i+n, eventually will match a unique section of the primary amino acid sequence of the protein (Wuthrich 1986). During this process, distinguishing sequential NOEs from intraresidue and non-sequential long-distance ones are critical to avoid misassignment.

Intraresidue NOEs that can be recognized by comparing TOCSY are much easier to identify than long-distance NOEs. The explicit identification of sequential $1H^N$-$^1H^N$, $^1H\alpha$-$^1H^N$, and $^1H\beta$-$^1H^N$ can reduce the ambiguity resulting from non-sequential NOEs. Additionally, the sequential ordering of spin systems must match the primary sequence. However, with the molecular weight increased, the amplification of the complexity and resonance overlap in NOESY make it difficult to explicitly identify and distinguish the intraresidue, sequential and non-sequential long-distance NOEs, which is the intrinsic reason that NOE-based assignment strategy has the size limit <15 kDa.

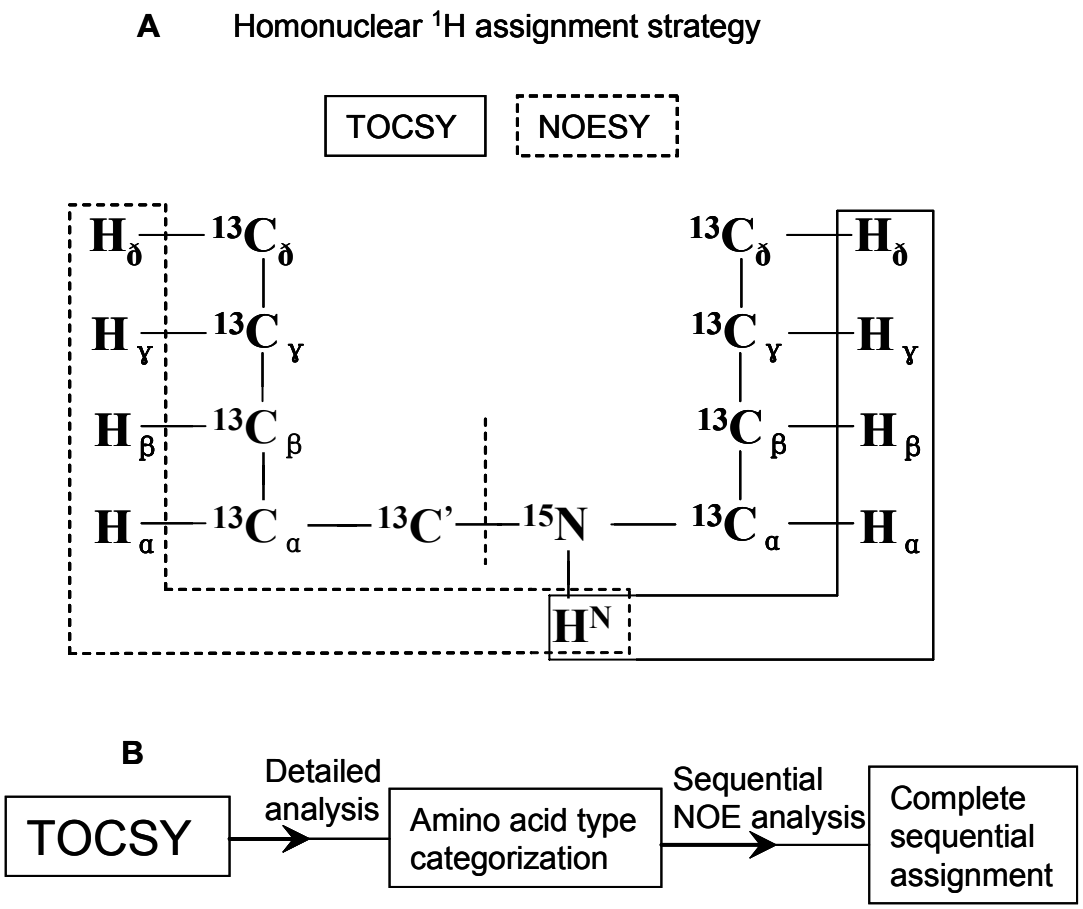

Figure 14 Homonuclear assignment.
(A). The correlations between aliphatic sidechain and amide protons for TOCSY and NOESY experiments. The correlations for residues with long sidechain can be observed by increasing the mixing time in TOCSY. The long correlations are not usually observed in NOESY. But for transferred NOEs I used, they can be observed due to cross-correlation rate transferred from the larger binding partner. (B) The scheme of the homonuclear ^{1}H NMR assignment strategy.

2.4.2 Heteronuclear J-correlation assignment for isotopically labeled proteins

Employing the relatively uniform and well-resolved heteronuclear one-bond and two-bond couplings (Figures 10 and 14), a bank of triple-resonance experiments were introduced to facilitate heteronuclear J-correlation assignment. Only the experiments performed in this dissertation are discussed here. A combination of CBCANH (Figure 14) and CBCACONH experiments provide a complete backbone resonance assignment (Grzesiek 1992; Grzesiek 1992). In the CBCANH experiment, the amide $^{1}H^{N}$ and ^{15}N resonances of each amino acid are correlated with both the intraresidue α and β carbons of the preceding residue. In the complementary CBCA(CO)NH, each backbone amide is correlated with the α and β carbons of the preceding residue only (Grzesiek 1992b). Using the information from the CBCA(CO)NH experiment, it is simple to distinguish intraresidue from interresidue correlations in the CBCANH. Additionally, in the CBCANH, the Cα resonances of all residues are opposite in sign to the Cβ resonances (Grzesiek 1992a), which makes it easy to distinguish Cα from Cβ resonances. Also, Thr, Ser, and Ala can be easily identified based on their unique pairs of Cα/Cβ chemical shifts. This information is used to assign each stretch of amino acids to a unique section of the protein sequence. These assignments can be confirmed by checking the amino acid type probabilities (Grzesiek 1993a) for the other residues in each stretch. These assigned stretches

will then be aligned in sequential order, and the alignment can be confirmed by matching the interresidue Cα and Cβ signals of the last residue in the preceding sequence. In practice, a few interresidue sequential connections may be lost in the less sensitive CBCANH experiment (smaller 1JCαN and 2JCαN couplings) due to the short lifetime of nuclei such as Cα or fast exchanging NHs in the loop region. This problem can be circumvented by combining CBCA(CO)NH and other experiments such as NOESY experiments. Breaks in the sequential alignment will also occur at proline residues for both CBCANH and CBCA(CO)NH but it wouldn't affect assignment and their resonance frequencies can be obtained from their following residues. Furthermore, HNCO and HNCACO that correlate the amide $^{1}H^{N}$ and ^{15}N with both the intraresidue and the preceding ^{13}CO signals (rather than the $^{13}C\alpha$ spins) provide alternative correlation to solve the ambiguity and they are very helpful due to less overlap in the ^{13}CO dimension. The resonance frequencies obtained from HNCACO and HNCO can be used later to generate dihedral angle constraints for structural determination. Using HCCH-TOCSY, sidechain ^{1}H and ^{13}C resonance can be obtained by going though each carbon plane according to the Cα and Cβ chemical shifts acquired from CBCANH and CBCA(CO)NH. Thus, to this point, a fully assigned chemical shift table is supposed to be generated for NOE resonance assignment in the next step of NMR structural investigation. The advantage of using 3D-heteronuclear-edited experiments for assignment, rather than homonuclear 2D experiments, is the

significant reduction in crosspeak overlap. Additionally, potential errors that arise from misassignment of sequential and long-distance connectivity in the NOE-based assignment are avoided because assignment are based solely on predictable through-bond scalar correlations.

Sequence-specific assignment of NMR resonances typically requires many different experiments and a substantial effort. However, it usually does not reveal much information about the protein under investigation. Assignment is a necessary prerequisite to achieving further biochemical goals such as structural determination.

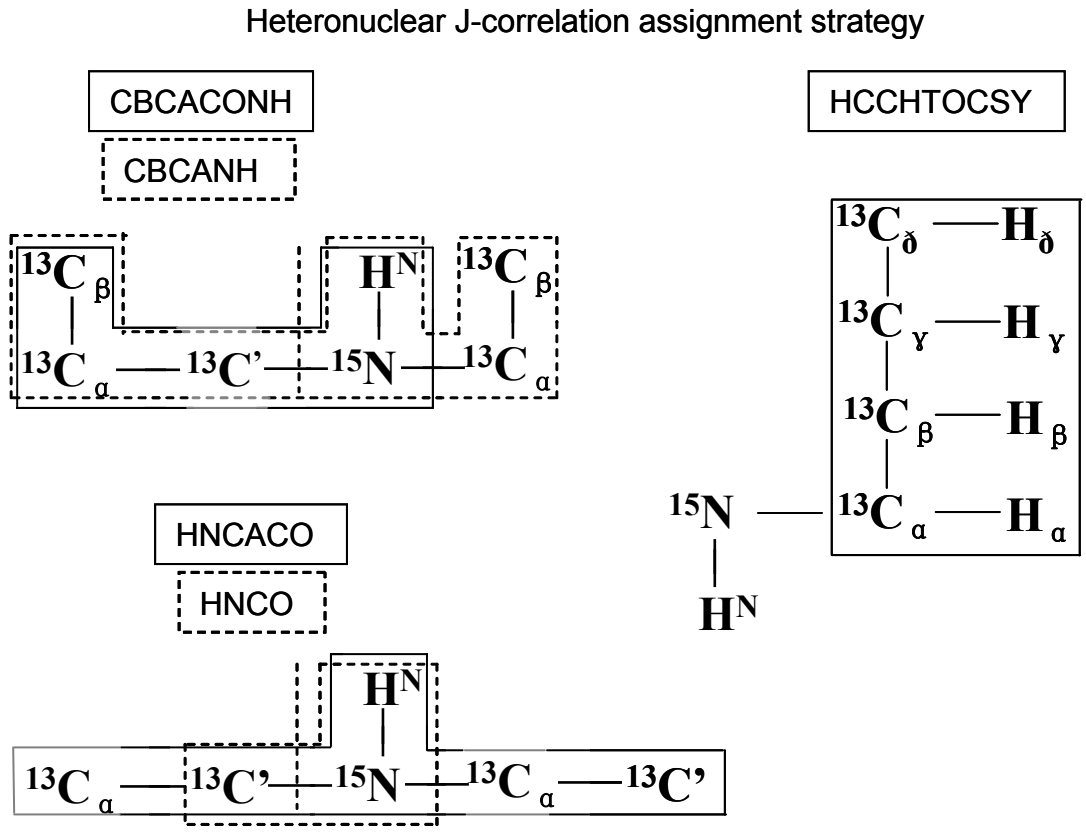

Figure 15 The triple-resonance experiments.

The triple-resonance experiments used in this dissertation for backbone assignment and HCCH-TOCSY for sidechain assignment. The correlated spins are indicated by box. The spins in grey boxes are indirect.

2.5 Structural determination

2.5.1 Conformational constraints

2.5.1.1 NOE distance constraints

The interproton distance constraints derived from NOE interactions have formed the basis of protein structure determination by NMR spectroscopy. A majority of the constraints used to calculate the three-dimensional structural of a protein come from many hundreds of NOE crosspeaks picked and assigned from NOESY experiments. The intraresidue and sequential NOE crosspeaks that are used for the homonuclear ^{1}H assignments are also NOE constraints too, although they help the structural folding much less than long-distance ones. Structural misfolding may be caused if the intraresidue or sequential NOE crosspeaks were misassigned to the long-distance. Moreover, because the intensity of the intraresidue and sequential NOE crosspeaks are often stronger than long distance ones, the important long distance NOE crosspeaks may be lost due to resonance degeneracy. 3D ^{13}C- or ^{15}N-edited NOESY experiments were developed for solving those problems because diversifying the NOE crosspeaks to ^{13}C and ^{15}N can largely improve the spectral resolution. For saving machine time, a simultaneous $^{13}C/^{15}N$ acquisition was often applied in a single pulse sequence named $^{15}N/^{13}C$-edited NOESY, which is used in this dissertation for

FLN21a and integrin β_3 tail. In order to solve protein-ligand complex structure, a half-filter pulse can be combined in NOESY experiments to generate subspectra containing different types of crosspeaks. The subspectra included the isotope-edited NOESY which provides intramolecular NOE constraints for protein in the protein-ligand complex, and isotope-filtered NOESY which provides intermolecular NOE constraints for determining the protein interface. The filter depends on the perfect match to the $^1J_{CH}$ coupling constants, which is never perfect due to small variations in the scalar coupling constant. The small variations in the scalar coupling constant reduce the intensity of NOE crosspeaks in isotope-edited NOESY whereas in isotope-filtered NOESY they result in breakthrough errors, *i.e.*, the appearance of intramolecular NOE crosspeaks from isotope labeled protein. The breakthrough peaks in isotope-filtered NOESY are exceptionally problematic because they cause ambiguity in spectral interpretation. Various schemes are available to increase the degree of suppression of the breakthrough peaks but at the price of sensitivity, which is not favorable for the weak protein-ligand interaction. The alternative method for the isotope-edited/filtered experiment is to use perdeuterated sample in the complex. This method is used in this dissertation for determining the interface between FLN21a and β_3, FLN21a and α_{IIb}. The sidechain to amide ^{1}H NOE interactions between ^{15}N/2D-FLN21a and β_3, and between ^{15}N/2D-FLN21a and α_{IIb} were observed in ^{15}N NOESY experiments.

The precise ^{1}H-^{1}H separations cannot be determined from the NOE crosspeak intensities due to the failure to satisfy the initial rate approximation. (2.1.3) Instead, NOE crosspeaks are classified into strong, medium, weak, and very weak categories, corresponding to interproton distance constraints of 1.8-2.7 Å (1.8-2.9 Å for NOEs involving $^{1}H^{N}$ protons), 1.8-3.3 Å (1.8-3.5 Å for NOEs involving $^{1}H^{N}$ protons), and 1.8-5.0 Å, and 1.8-6.0Å, respectively (Williamson et al. 1985). The lower bound of 1.8 Å (approximately van der Waals contact) is the same in all restraint classes. This is because atoms that are very close can nonetheless have very weak NOE interactions, or even no visible crosspeak at all. The upper bounds for distances involving methyl protons and non-stereospecifically assigned methylene protons can be corrected appropriately for center averaging (Wuthrich et al. 1983), and an additional 0.5Å can be added to the upper distance limits for NOEs involving methyl protons (Clore et al. 1987; Wagner et al. 1987). The non-stereospecifically assigned restraint is included but is expressed ambiguously in the restraint file, e.g. 6 HA → 8 HB#, where the # wildcard indicates that the beta protons of residue 8 are not stereo specifically assigned. Only structurally useful intra-residue NOEs are included in the intra-residue interproton distance constraints. Thus, NOEs between protons separated by two bonds or between non-stereospecifically assigned protons separated by three bonds will not be incorporated in the constraints. The initial structure calculations are iteratively performed with NOE analysis since many

NOEs are ambiguous and can only be assigned based on looking at the initial structures.

2.5.1.2 Dihedral angle constraints

Dihedral angle constraints are important for high resolution NMR structure determination. Φ and Ψ dihedral angle constraints can be derived from a database analysis of backbone chemical shifts using the program TALOS (Cornilescu et al. 1999). TALOS compares observed chemical shifts to a database of proteins with N, $^{1}H^{N}$, Cα, Cβ, CO, ^{1}Hα assignments and high resolution structures to obtain Φ and Ψ angles for incorporation into structure calculations.

2.5.1.3 Hydrogen-bonding constraints

Experimentally derived hydrogen bonding information is also valuable for determining the protein structure. Generally, after dissolving a protein into D_2O solution a series of 2D ^{1}H-^{15}N HSQC spectra are repeatedly acquired to observe the decrease in amide proton resonance intensities. The hydrogen bonding constraints are deduced on the basis of slowly exchanging amide protons (Wagner 1982). The hydrogen-bonding constraints have a large impact on the nature and precision of the resulting structures and they need to be used carefully because the observation of the slow exchange may result from steric effects

rather than hydrogen bonding. Thus hydrogen bonding constraints are usually only enforced in well-defined regions of regular secondary structure.

2.5.2 Structural calculation

2.5.2.1 Calculation procedure

Procedures for NMR structural calculations are designed to find the coordinates for the atoms within the protein by exploring all regions of conformational space to satisfy the input constraints in an unbiased fashion. Although a variety of procedures to calculate atomic resolution protein structures using constraints derived from experimental NMR data have been developed and new ones can be expected to appear in the future, the procedures share some characteristics due to the intrinsic nature of NMR structural determinations: i, the constraints derived from NMR experiments are ranges of allowed distances, angles, etc. rather than single values, reflecting the fact that the experimental data contain uncertainties both in measurement and interpretation. As a result, NMR structural determinations do not calculate a unique structure, but rather repeat a structural calculation many times to generate an ensemble of structures. ii, Only a small number of the possible constraints are observable experimentally due to peak overlap/chemical shift degeneracy, lack of stereospecific assignments, etc. As a result, constraints that aim to enhance some physical reasonableness, such

as bond angles, bond lengths and proper stereochemistry (chirality and the planarity of aromatic rings) on the system are normally included in the calculation to supplement the experimentally derived constraints in order to increase the efficiency and accuracy of structural calculation. iii, Because multiple protons have the same chemical shift, it is often not possible to tell which atoms are involved in a NOESY crosspeak. As a result, calculations generally start with a set of unambiguous constraints and use the resulting structure as a template to resolve the ambiguous constraints. Multiple calculation cycles are conducted to resolve as many ambiguous NOE crosspeaks as possible. From the discussion above, a good ensemble of structures should minimize violations of the input constraints and at the same time accurately represent the full permissible conformational space under the constraints (Havel 1991; Hyberts et al. 1992; Rieping et al. 2005)(Figure 15).

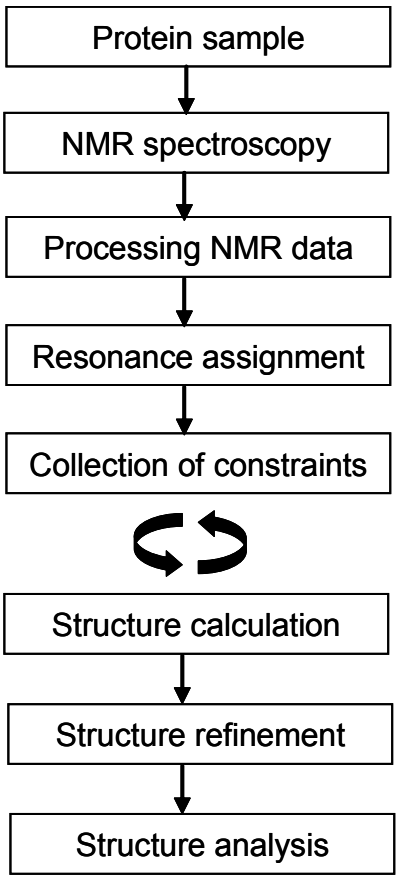

Figure 16 Outline of the procedure for NMR protein structure determination.

A

$$E_{NOE} = \begin{cases} K_{NOE}(r_{ij}-r_{ij}^{u})^2 & \text{if } r_{ij} > r_{ij}^{u} \\ 0 & \text{if } r_{ij}^{l} < r_{ij} < r_{ij}^{u} \\ K_{NOE}(r_{ij}-r_{ij}^{1})^2 & \text{if } r_{ij} < r_{ij}^{l} \end{cases}$$

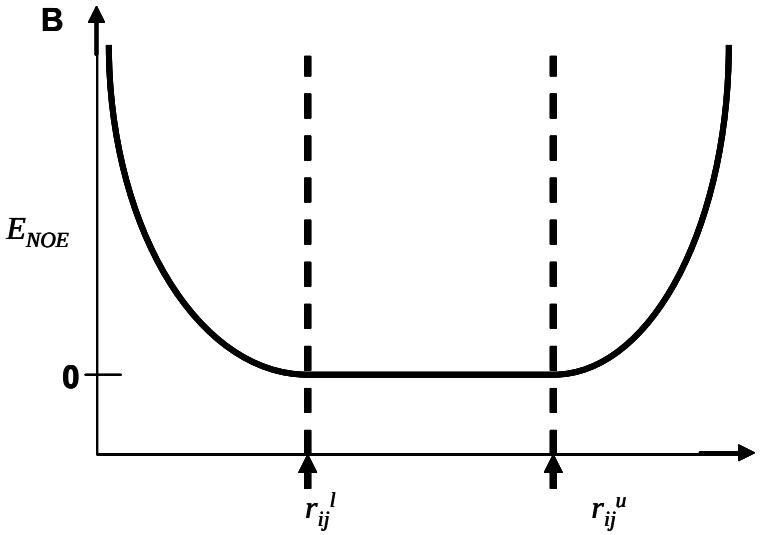

Figure 17 NOE energy term.
A. r_{ij}^{l} and r_{ij}^{u} are the lower and upper bounds of the NOE distance constraint, and K_{NOE} is the chosen force constant, typically ~ 250 kcal•mol^{-1}•nm^{-2}.
It is somewhat permissible to violate constraints but it raises energy.
B. Example of NOE pseudo-energy term.

The method used in this dissertation to calculate the complex structure of FLN21a-α_{IIb}-β_3 is simulated annealing (SA). SA is a spectral implementation of restrained molecular dynamics algorithms (rMD) using a simplified force field (Nilges et al. 1988). The objective of a molecular dynamics calculation in an NMR structural calculation is basically to search the conformation space of the protein for structures that minimize a target function, which is taken as potential energy of the system. Hence, simulated annealing is conducted using a target function that includes the simplified potential energy function plus pseudo-energy terms based on the NMR-derived constraints. These potentials drive the structure toward a conformation that will reduce the violation of the constraints during a forced heat-up and cool-down annealing cycle. In practice, the program that best adapted SA and was used in this dissertation is X-PLOR (Brunger 1992). The target function in X-PLOR is defined by:

$$E\,(\text{total}) = E\,(\text{bonds}) + E\,(\text{angles}) + E\,(\text{dihedrals}) + E(\text{impropers}) + E\,(\text{nonbonded pairs}) + E\,(\text{NMR})$$

In which the first five terms are “real” energy terms corresponding to bond length and bond angle potentials, torsion angle potentials, terms to enforce the proper chiralities and planarities, and nonbonded energy terms including the van der Waals and electrostatic energy terms, respectively. The NMR constraints are incorporated into the last term, which is a pseudo-energy term included to

represent the cost of violating the constraints (Brunger 1992)(Figure 16). X-PLOR consists of solving Newton's equations of motion

$$m_i \frac{d^2 x_i}{dt^2}(t) = -\nabla_{xi} E(\text{total})$$

In which m is the atomic mass and the index i runs through all free atoms. The equation can be solved in Cartesian coordinate space.

2.5.2.2 Structure analysis and structure refinement

Although in Figure 15 structure refinement and structure analysis follow the steps of structure calculation they normally are incorporated into the structure calculation. Especially, structure analysis is critical to uncover if the previous calculation cycle is successful, *i.e.*, if the input restraints are fully satisfied and the resultant structures are physically reasonable. Structure analysis works as a touchstone for resolving the ambiguous NOE crosspeaks and structure refinement. Additionally, the structure analysis generates indicators of the quality of the calculated structure to be reported.

The differences among the members in a given ensemble of structures are measured using the root-mean-square deviation (RMSD) (Schlueter et al. 2007). This parameter has be used often to indicate the quality of the structure determination and it is assumed that the lower the RMSD values, the better the results. However, what the RMSD measures is the precision, *i.e.*, the consistency

within the ensemble of the structures, instead of the accuracy, *i.e.*, how the ensemble of structures represents the true molecular conformations and the variance therein. Thus an RMSD value that is too low may not be real and the corresponding ensemble of structures may fail to reflect the internal dynamics of the molecule (Metzler et al. 1989).

The overall energies of the structures are often reported. Again, the lower the energy, the better. But the value of energy is only meaningful in a relative fashion because it depends on the potential energy function used, the size of the dataset and the force field.

Another important aspect of NMR structure analysis is checking the geometric quality of structure models. Bond lengths and angles in proteins are accurately known from analyses of structures of small molecules (Musil et al. 1991). Deviation from those idealized values are measured to uncover the abnormalities or errors in the geometry. Since bond lengths and angles are often tightly constrained in NMR structure calculation algorithms, outliers in bond lengths and angles can strongly indicate structural distortion due to erroneous NMR constraints. The dihedral angles Φ, Ψ and ω of each residue determine the backbone conformation of a protein. The combination of Φ and Ψ of amino acids were found to be restricted to certain ranges due to the steric effect (Ramachandran et al. 1963). Aside from the steric restrictions, Φ and Ψ exhibit preferences that depend on residue type and secondary structure elements,

resulting in more narrow residue-specific Φ and Ψ ranges. A so-called Ramachandran plot can visualize Φ and Ψ by classifying Φ and Ψ combinations into four regions: favored, additionally allowed, generously allowed and disallowed, as implemented in the PROCHECK program (Laskowski et al. 1993). A shortcoming of statistics based on divisions in different regions of the Ramachandran plots is that these regions are generalized for all residues (except glycines and prolines). As mentioned above, different amino acids exhibit different Φ and Ψ preferences. Thus, neglecting residue-specific preferences can result in the wrong classification. Therefore the outliers need to be checked carefully to question whether they are truly abnormal conformations or are errors. Typical examples of non-erroneous outliers include active-site residues and D-amino acids.

The accordance of structure models with the experimental data can be measured using the root-mean-square deviation of the inter-atomic distances from their experimentally derived upper and lower bounds. In case of a bi-harmonic potential used in simulated annealing, all deviations from the target distance are included (Brunger et al. 1998). RMSD for NOE constraints are calculated by

$$RMSD_{NOE} = \sqrt{\frac{1}{NrNm}\sum_{k=1}^{Nr}\sum_{l=1}^{Nm}(\Delta kl)^2}$$

$$\begin{cases} d_{kl} > r_k^{upper} & \Delta kl = (d_{kl} - r_k^{upper}) \\ r_k^{lower} < d_{kl} \leq r_k^{upper} & \Delta kl = 0 \\ d_{kl} < r_k^{lower} & \Delta kl = (r_k^{lower} - d_{kl}) \end{cases}$$

in which d_{kl} is the actual distance for constraint k in model l, r_k^{upper} is the upper bond of constraints k and r_k^{lower} is the lower bond of constraints k. The sum is calculated over all Nr distance constraints and Nm structural models. In general, the lower the RMSD, the better the fit of the structure to the experimental data.

In contrast to structure calculation, which starts from nothing, structure refinement starts with well-define structures. The refinement by restrained energy minimization can result in a better structural ensemble. The structure calculation algorithms for NMR structures usually use a simplified force field that contains only the most dominant parts of the conformational energy. Therefore, the resulting structures may be unfavorable with respect to a full, 'physical' energy function (Brooks et al. 2009). The conformational energy of a conformation obtained from a structure calculation program can be reduced significantly by restrained energy minimization, *i.e.*, by locating a local minimum of the conformational energy function in the near vicinity of the input structure. Because the energy of the structures is correlated with the number and size of the constraint violations the energy can be reduced by constraint relaxation, *i.e.*,

choosing the constraints steeper than in the preceding structure calculation cycle. Repeated relaxation of a given constraint can result in the removal of it. Constraint removal needs to be rationalized based on reinterpretation of the experimental data, which does not necessarily pose a problem. Besides, hydrogen bonds show a marked improvement upon energy minimization because the geometric force fields used for the structure calculations normally do not contain a driving force for hydrogen bond formation (Luginbuhl et al. 1996).

CHAPTER III

RESULTS AND DISCUSSION

3.1 Expression and purification of proteins and NMR sample preparation

Integrin α_{IIb} cytoplasmic tail (CT) preparation (W^{988}-E^{1008}): the cDNA of the peptide was inserted into a pET31b vector (Novagen, Inc.) that fuses small peptides to an insoluble protein ketosteroid isomerase (KSI). The fused α_{IIb} CT was then expressed as an inclusion body with KSI. The peptide was labeled by inducing the T7 promoter of pET31b vector with isopropyl-β-D-thiogalactopyranoside (IPTG) in E. coli BL21 (DE3/pLYS) cells where $^{15}NH_4Cl$ (1.1 g/L) and/or ^{13}C glucose (3 g/L) were used as the sole nitrogen and carbon sources. Purification of the peptide including the cleavage of KSI by CNBr was performed according to the manufacturer's instructions. The peptide was further purified by HPLC. Unlabeled, ^{15}N labeled and $^{15}N/^{13}C$ labeled α_{IIb} CT samples were prepared.

Integrin β CT preparation (K^{716}-T^{762}):

1, β_3 CT were subcloned into pET15b (Novagen, Inc) that contains an N-terminal His-tag. Expression and purification of the β CTs fused to the His-tag were performed according to the protocols from Novagen, Inc. The β CTs were largely expressed in inclusion bodies and hence a denaturation-renaturation protocol (Novagen, Inc.) was used. Both His-tag-β CTs were further purified by reverse phase HPLC and the final yields were 4-5 mg/liter culture. Due to unpleasant line-broadening and low solubility, modification of β3 CT was conducted using a QuikChange Site-Directed Mutagenesis Kit from Stratagene. The strategy of expression and purification is the same as above. In addition, MBP-β_3 was prepared following the protocols in our lab's previous study [8].

2, Since the β_3 membrane proximal region (β_3 MP) is important for integrin activity regulation, β_3 K716-W739 was cloned into pET31b vector and express in E. coli BL21 (DE3/pLYS) cells. The purification is the same as α_{IIb} CT. Unlabeled and ^{15}N labeled samples were prepared as well.

FLN21 preparation: Filamin C repeat 21 (FLN21c) (F^{2302}-S^{2415}) which was subcloned in the E. coli expression vector pGEX-5X-1 was obtained from our collaborator Cary Wu at University of Pittsburgh. FLN21c expression was induced in E. coli BL21(DE3) with 1mM IPTG at 37°C and growth was continues for 10-12 hours at room temperature. Protein was purified by affinity purification using Glutathione Sepharose 4B as per the manufacturer's instructions (GE

Lifesciences). The purified protein was cleaved with Factor Xa (Novagen) to separate the GST fusion tag from the FLN-21c. After the cleavage reaction was complete, the protein was passed through glutathione beads to remove GST from the cleaved FLN-21c. A final step of gel filtration on a Superdex 75 column (GE Lifesciences) was performed to remove traces of GST and other minor contaminants. Filamin A repeat 21 (FLN21a) (G^{2236}-G^{2330}) subcloned into pGST parallel (Sheffield 1999) was induced in E. coli BL21(DE3) with 0.6mM IPTG at room temperature for 20 hours. Protein was purified by Glutathione Sepharose 4B and cleaved with TEV. Protein was passed through glutathione beads again and further purified by Superdex 75.

The α_{IIb} CT and N-terminal 24 amino acids fragment of migfilin (M^{1}ASKPEKRVASSVFITLAPPRRDV^{24}) was synthesized by our biotechnology core and purified by HPLC and verified by mass spectroscopy.

NMR sample preparation: the appropriate amount of proteins were dissolved in 25 mM phosphate buffer, 5 mM NaCl, 1 mM DTT (pH 6.4). For the samples with α_{IIb} and β_3, 1 mM $CaCl_2$ was added since the previous study demonstrate that divalent cations can stabilize the integrin α/β complex (Haas and Plow 1996; Vallar et al. 1999). For samples needing to be acquired for more than 12 hours, 0.02% NaN_3 was added to suppress bacteria growth.

3.2 Verification of filamin binding α_{IIb} and β_3 membrane-proximal region

2D ^{1}H-^{15}N heteronuclear single quantum correlation spectrum (HSQC) of ^{15}N labeled FLN21a in the presence and absence of unlabeled α_{IIb} and β_3-MP were examined separately. Addition of α_{IIb} and β_3-MP, respectively, induce very decent chemical shift perturbations on FLN21a HSQC spectra, indicating the interaction (Figure 18). Also, α_{IIb} in higher concentration ratios or β_3-MP can cause severe line-broadening on FLN21a HSQC spectra, indicating that the interactions are in the intermediate exchange region. The inverse experiments, *i.e.*, with ^{15}N labeled α_{IIb} and β_3-MP titrated separately by unlabeled FLN21a, were also performed and confirm the interaction (Figure 18, A and B). More importantly, in the inverse experiments, N-terminal migfilin peptide was further added to the mixture. Due to its stronger binding affinity to FLN21a, migfilin detached FLN21a from integrin and the HSQC spectra of α_{IIb} and β_3-MP were shifted back to their free forms. These results exclude the possibility of non-specific interaction causing the spectral changes. Additionally, a β_3 tail with the first five residues truncated was perturbed much less than full length β_3 tail, which further illustrates the critical role of β_3 membrane-proximal region in the interaction with FLN21a (Figure 18 C). For the interaction of FLN21a and α_{IIb}, another NMR experiment, transferred NOE, was performed, which is shown in the following section (Figure 20 B).

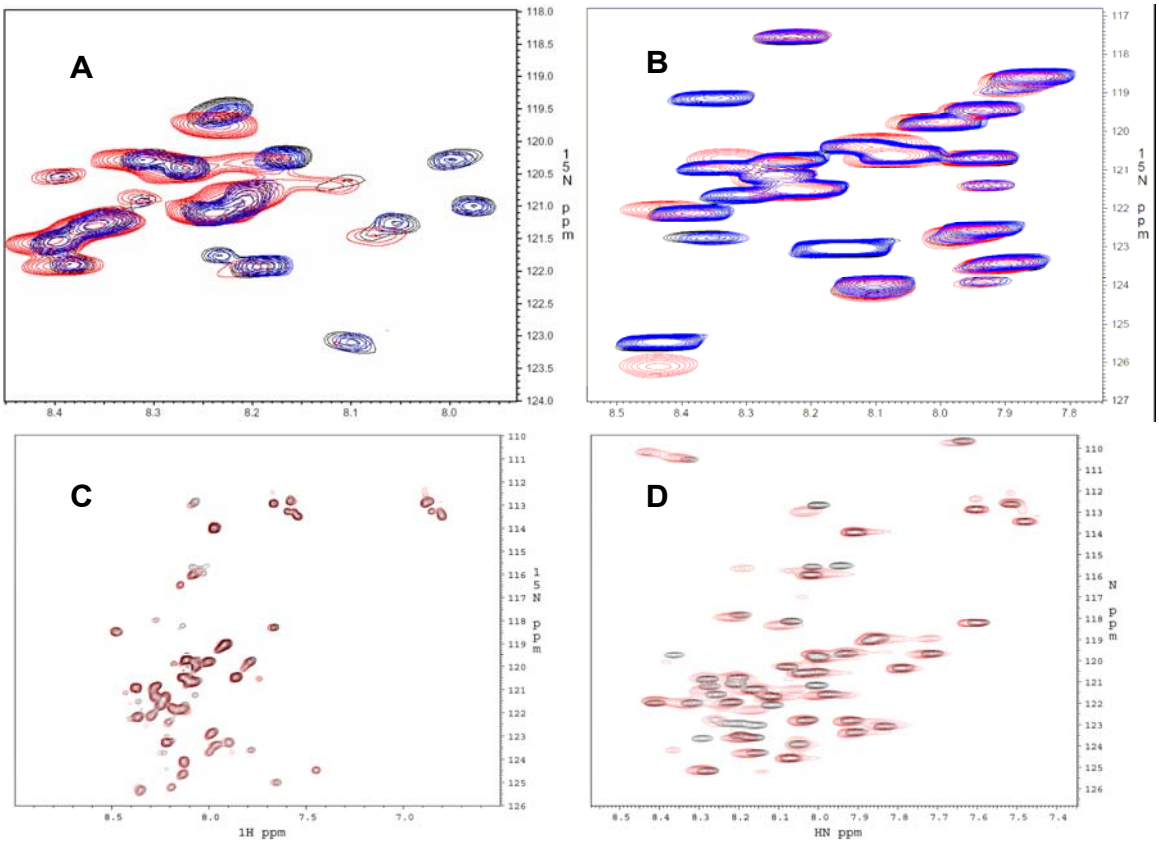

E

β_3-MP: —K[716]LLITIHDRKEFAKFEEERARAKW[739]

Trun-β_3: —I[721]HDRKEFAKFEEERARAKWDTANNPLYKEATSTFTNITYRGT[762]

KK-β_3: —K[716]KKITIHDRKEFAKFEEERARAKWDTANNPLYKEATSTFTNITYRGT[762]

Migfilin N-terminal peptide: —M[1]ASKPEKRVASSVFITLAPPRRDV[24]

Figure 18 Integrin and filamin interactions studied by HSQC spectra.
Expanded region of HSQC spectra of
(A). ^{15}N-labeled α_{IIb} in the absence (black), and presence (red) of unlabeled FLN21a, and presence (blue) of the unlabeled FLN21a and migfilin;
(B). ^{15}N-labeled β_3-MP in the absence (black), and presence (red) of unlabeled FLN21a, and presence (blue) of the unlabeled FLN21a and migfilin;
(C). ^{15}N-labeled trun-β_3 in the absence (black), and presence (red) of unlabeled FLN21a;
(D). ^{15}N-labeled KK-β_3 in the absence (black), and presence (red) of unlabeled FLN21a.
(E). Residue sequences of β_3-MP, trun-β_3, KK-β_3, and migfilin peptide. The residues underlined on β_3-MP are truncated in trun-β_3. The residue in red are LL to KK mutations. The residues underlined on migfilin are the peptide used in the crystal of FLN21a-migfilin.

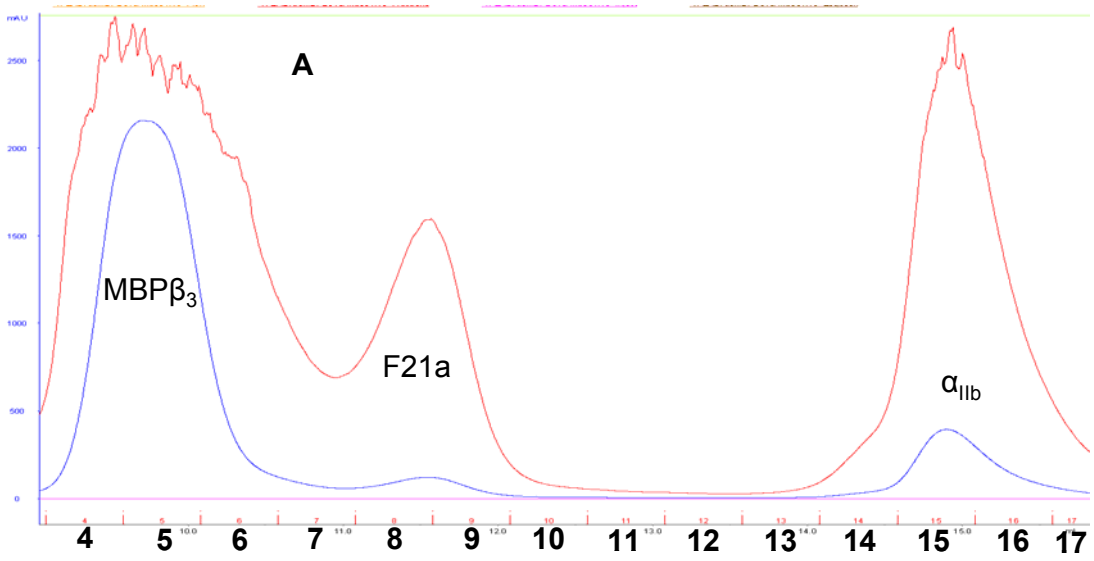

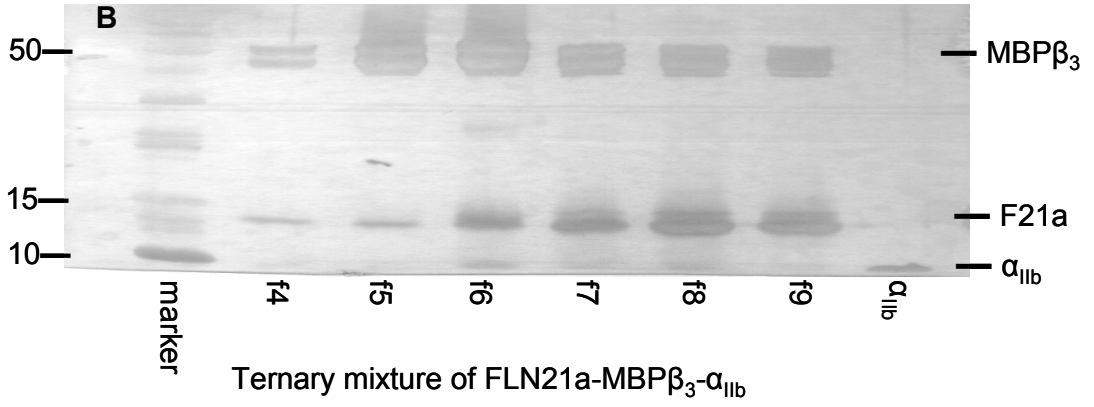

Ternary mixture of FLN21a-MBPβ3-αIIb

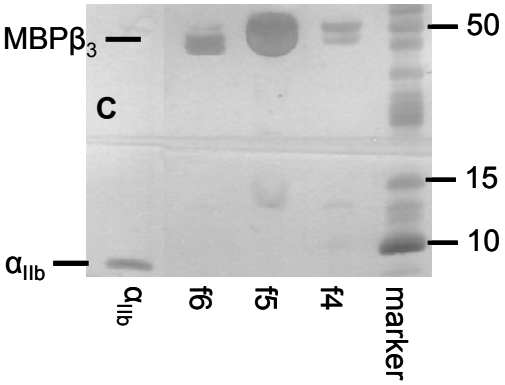

Binary mixture of MBPβ3-αIIb

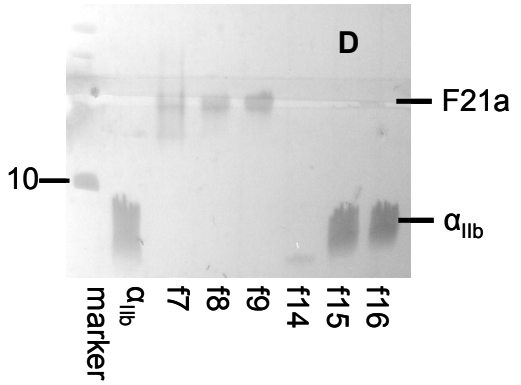

Binary mixture of FLN21a-αIIb

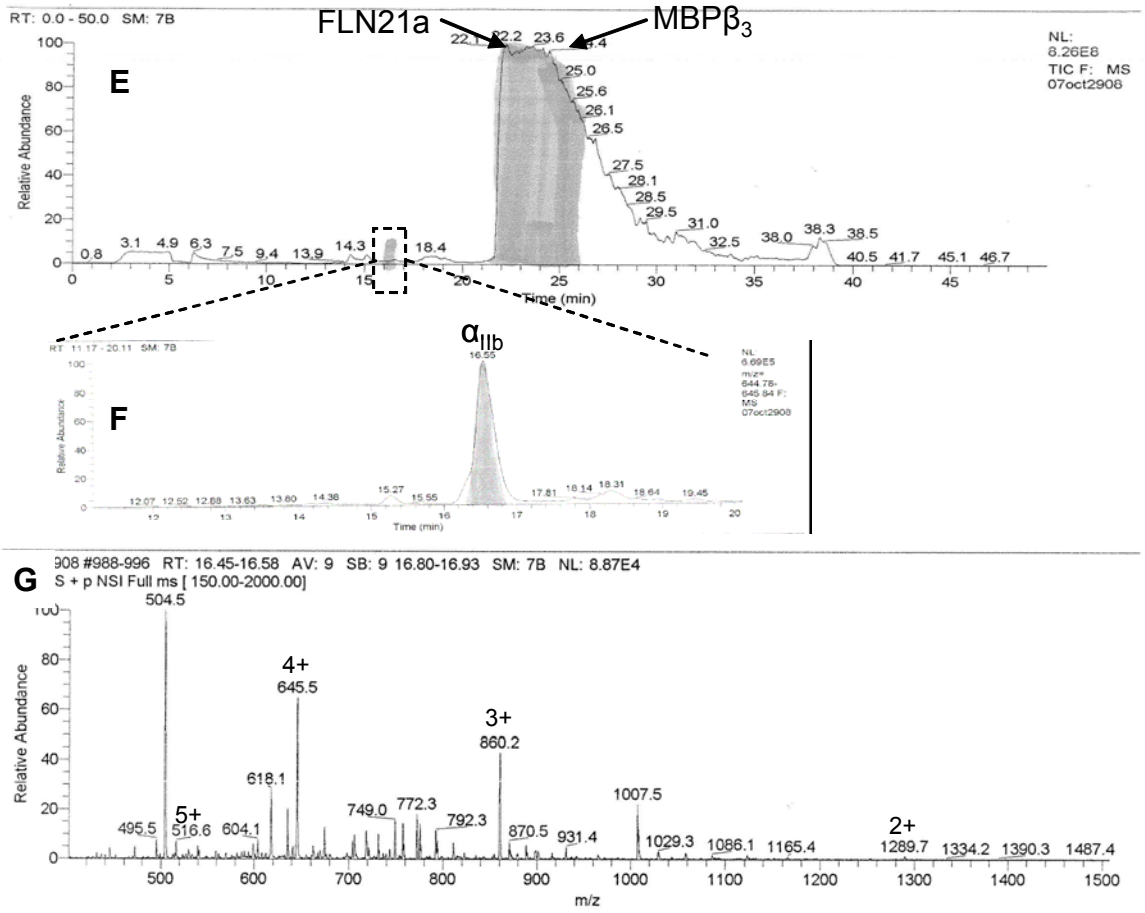

Figure 19 Gel filtration co-elution of integrin and filamin.

(A). Gel filtration chromatograph of the ternary mixture: MBP-β_3 (fraction (f) f4, f5, f6), FLN21a (f8, f9) and α_{IIb} (f15, f16);

(B). Gel filtration fractions of the ternary mixture are visualized by SDS-PAGE using silver stain;

(C). Gel filtration fractions of the binary mixture of MBP-β_3 and α_{IIb} (Gel filtration chromatograph not shown) are visualized by SDS-PAGE using silver stain;

(D). Gel filtration fractions of the binary mixture of FLN21a and α_{IIb} (Gel filtration chromatograph not shown) are visualized by SDS-PAGE using silver stain.

(E). LCMS chromatograph of gel filtration fraction f6 of ternary mixture (A). Peaks eluting at 22.20 minute and 23.61 minute are FLN21a and MBP-β_3 respectively. (their corresponding MS spectra not shown here). Peak shown in an extended chromatograph (F) elutes at 16.60 minute, which is α_{IIb} pulled down in the ternary complex FLN21a-MBPβ3-α_{IIb}. Mass spectrum under 16.6 minute, *i.e.*, α_{IIb}, is shown in (G). Mass and charge value are shown on each fragment of the α_{IIb} molecule. The mass value multiplied by charge value is equal to the molecular weight of α_{IIb} molecule.

3.3 Verification of the ternary complex

With knowledge of filamin binding to α_{IIb} and β_3, a big question would naturally be whether a filamin molecule binds to α_{IIb} and β_3 resulting in a ternary complex, or whether two filamin molecules bind to α_{IIb} and β_3 separately, resulting in two binary complexes. Addressing this question is difficult with NMR techniques alone. Thus, I turned to the method of gel filtration co-elution. In order to obtain the best separation on gel filtration and also avoid the insolubility of β_3 tails, MBP (maltose binding protein) fusion full-length cytoplasmic tail of β_3 (MBP-β_3) was used to form the ternary mixture of FLN21a (10 kDa), α_{IIb} (2.5 kDa) and MBP-β_3 (48 kDa) (Figure 19). For the best binding saturation, excess amounts of α_{IIb} and MBP-β_3 were used. Elution fractions were analyzed by SDS-PAGE and visualized with silver stain to detect the presence of α_{IIb} (Figure 19 B) and by LCMS for accurate molecular weight determination (Figure 19 E, F, G) The results demonstrate that α_{IIb} is co-eluted with FLN21a and MBP-β_3 in the ternary mixture but not in the binary mixtures of α_{IIb}/FLN21a and α_{IIb}/MBP-β3 used as controls. Thus, the relationship among the three molecules is that each binary interaction is enhanced by the third party, which is the reason that α_{IIb} is not co-eluted in the binary mixtures. This also suggests an interesting possibility that filamin enhances the α_{IIb}/β_3 interaction that is the inactive state of the integrin.

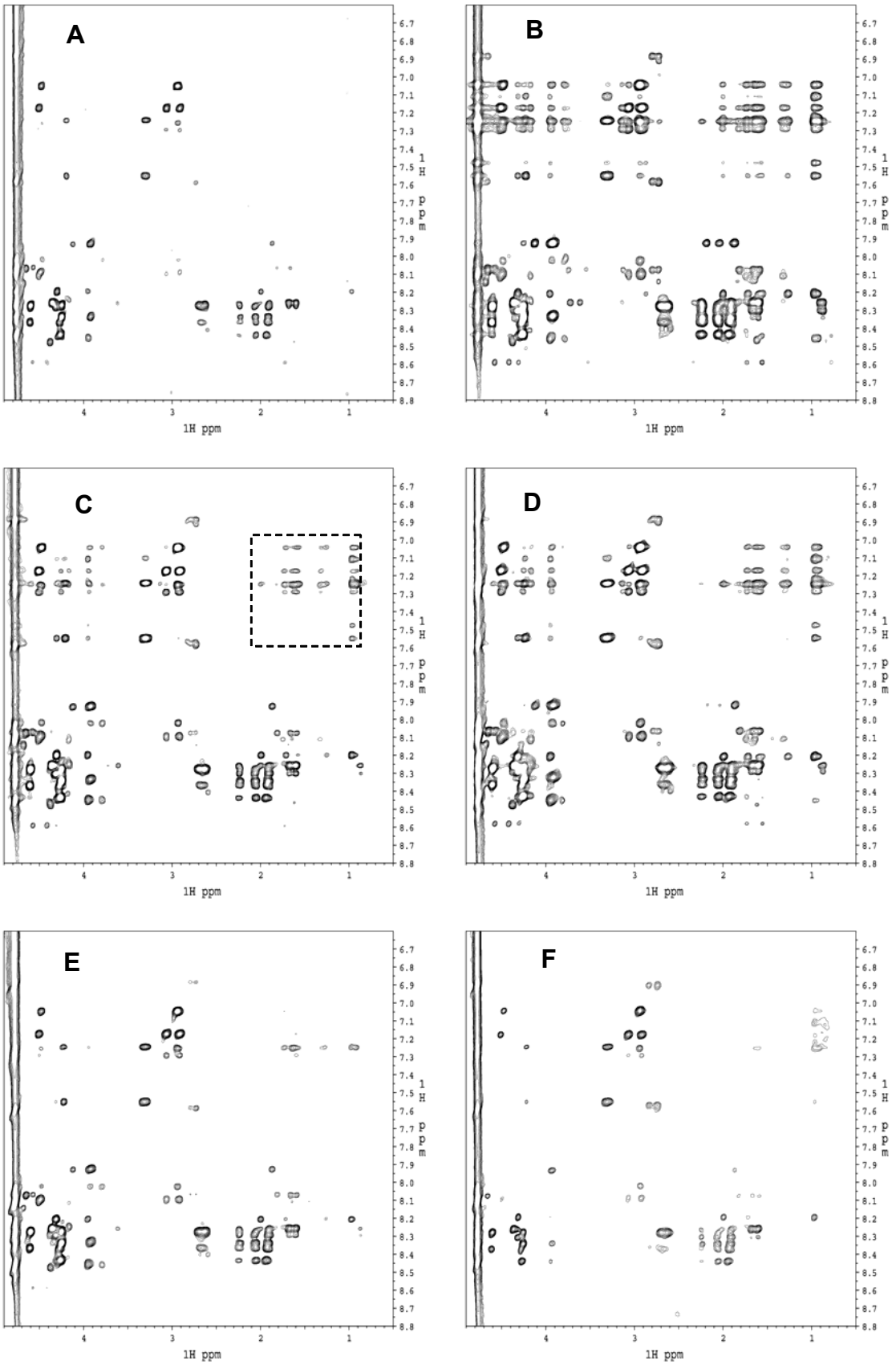
A
B
C
D
E
F
1H ppm
1H ppm

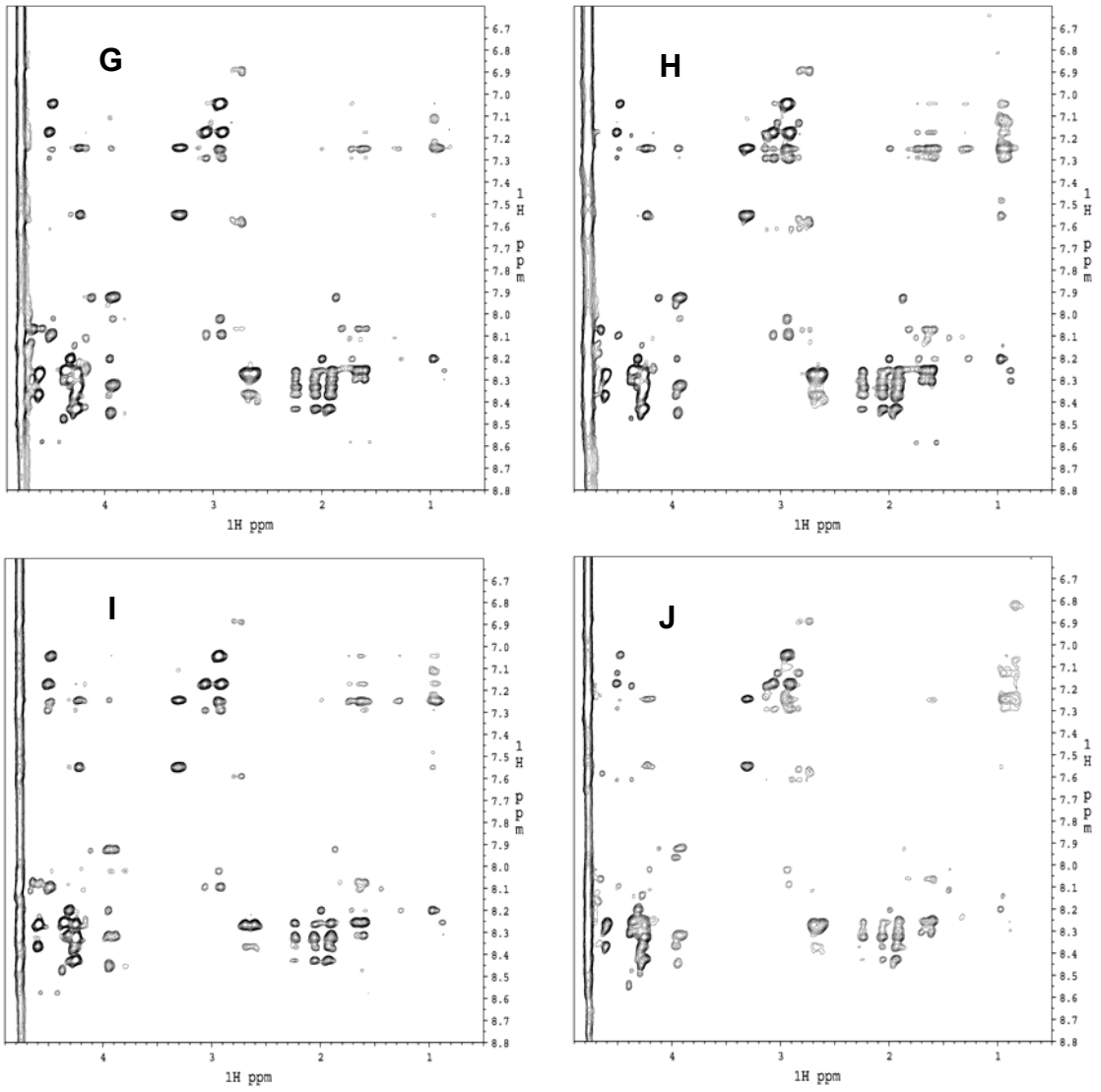
G
H
I
J
1H ppm
1H ppm

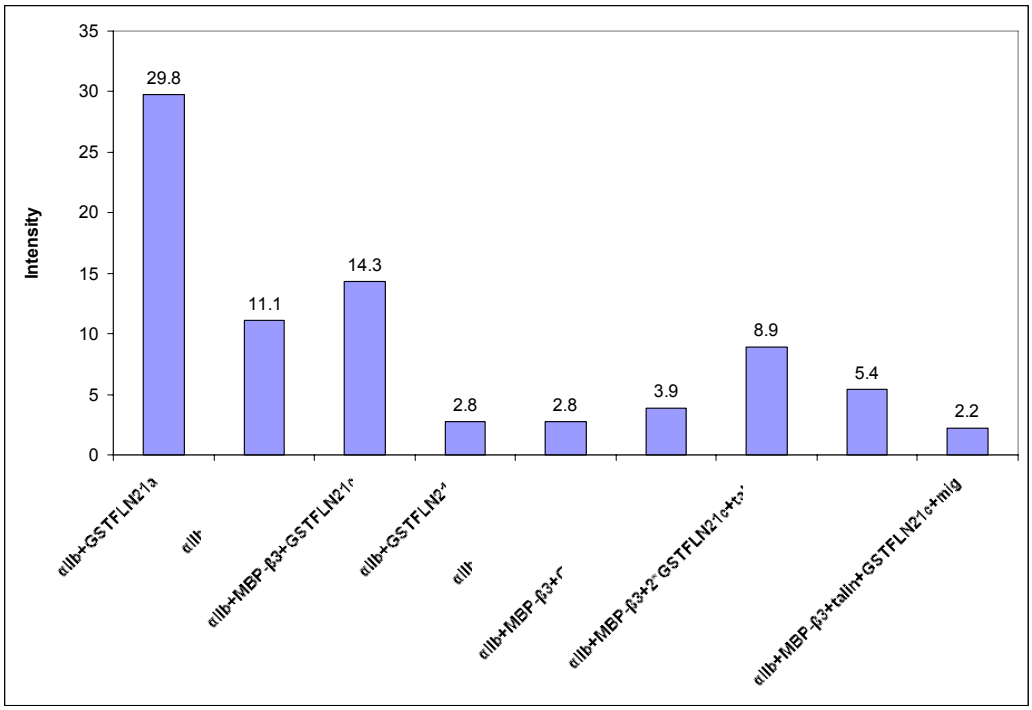

Figure 20 Filamin enhances integrin tails' interaction.
2D NOESY of 2 mM α_{IIb} in the presence of
(A). None.
(B). 2.5% GST-FLN21a.
(C). 2.5% MBP-β_3.
(D). 2.5% MBP-β_3 and 2.5% GST-FLN21c.
(E). 2.5% GST-FLN21c. F. 2.5% MBP-β_3 and 2.5% Talin head domain.
(G). 2.5% MBP-β_3 and 2.5% GST-FLN21c and 2.5% Talin head domain.
(H). 2.5% MBP-β_3 and 5% GST-FLN21c and 2.5% Talin head domain.
(I). 5% GST-FLN21c.
(J). 2.5% MBP-β_3 and 5% GST-FLN21c and 2.5% Talin head domain and 5% migfilin.
The box on C indicates the peak picking region.
The chart summarizes the peak intensity of 2D NOESY experiments B-J. Acquisition time is the same for all experiments. Peaks were picked in a region that is indicated in C. Peaks were picked on the same contour level.

3.4 Investigation of the enhancement of filamin on the interaction between α_{IIb} and β_3 by transferred NOE

Transferred NOE is a convenient experiment to study the interaction between α_{IIb} and β_3 (Figure 20 C). The interaction in this experiment can be clearly disrupted by adding talin (Vinogradova et al. 2002)(Figure 20 F). Therefore a series of transferred NOE experiments were performed to investigate the effect of filamin on the interaction between α_{IIb} and β_3. Because FLN21a induces very strong transferred NOEs (Figure 20 B) which are indistinguishable from β_3 induced ones on α_{IIb}, FLN21c, which binds α_{IIb} poorly and consequently induces only a few NOE peaks, was used in these experiments (Figure 20 E). Firstly, the addition of GST-FLNc to the mixture of α_{IIb} and MBP-β_3 does not disrupt the α_{IIb}/β_3 interaction (Figure 20 D). Instead, the intensities of transferred NOEs are increased, indicating that filamin enhances the α_{IIb}/β_3 interaction. Secondly, the addition of talin to the mixture above still can diminish the transferred NOEs, but less powerfully than it can in the absence of filamin (Figure 20 G). Furthermore, the addition of double the amount of filamin can recover more NOE signals from the disruption of talin (Figure 20 H). Thirdly, the addition of migfilin peptide ablates the effect of filamin and the NOE signals are subject to the disruption by talin again. (Figure 20 J). Thus, I conclude that: 1. Filamin can compete against talin to protect α_{IIb}/β_3 interaction. 2. At an equal ratio to filamin, talin still has an unchallengeable advantage to separate α_{IIb}/β_3. However, an excess of filamin

starts a tug-of-war with talin. Considering the fact that filamin, as a cytoskeletal protein, is often locally more abundant than talin, and that filamin's other repeats can also bind to integrin, this competition can be important to talin-dependant integrin regulation. More importantly, if filamin can protect the α_{IIb}/β_3 interaction against talin, which is probably the strongest integrin activator, filamin's protective effect on integrin could also be significant for the other integrin regulators.

3.5 The approach to the complete structural determination of FLN21a, α_{IIb} and β_3

Because β_3 cytoplasmic tail is highly insoluble and its interaction with FLN21a falls into the intermediate exchange region that reduces the NMR signal to noise ratio, the structural determination with this protein is awfully difficult. A great deal of effort was expended to overcome these problems by modifying this protein. Eventually, a LL to KK mutant (KK-β_3), which is only a small modification but which has much better solubility and signal to noise ratio upon binding, was chosen to pursue the ternary complex structure of FLN21a, α_{IIb} and β_3. (Figure 18 D) The intermolecular NOEs were obtained from ^{15}N NOESY experiments of deuterated ^{15}N-FLN21a separately mixed with αIIb and KK-β_3. This experiment is especially helpful for the current condition of comparable low solubility and signal to noise ratio since it does not require filtered pulses, which would rather sacrifice NMR sensitivity. Structural determination using XPLOR-NIH (Schwieters et al.

2003; C.D. Schwieters 2006) was performed based on a combination of NOE constraints including α_{IIb}, KK-β_3 and FLN21a, and intermolecular NOE constraints of FLN21a/α_{IIb} and FLN21a/KK-β_3 (see Table 1 for structural statistics).

3.6 Overall structural of FLN21a, α_{IIb} and KK-β_3 cytoplasmic tails

The superposition of the 20 best structures calculated is shown in Figure 22 A. The structure discloses that α_{IIb} and β_3 N-termini form a clasp defined in a previous publication (Vinogradova et al. 2002), although no intermolecular constraints between α_{IIb} and β_3 were used in the structural calculations (Figure 22 B). In other words, α_{IIb} and β_3 tails interact with each other because they both interact with filamin. This also illustrates that filamin can enhance α_{IIb}/β_3 interaction. The ternary complex is mainly stabilized by two interfaces denoted as the black and red triangles in Figure 22 B. The red triangle is formed along surfaces around FLN21a-G2269, α_{IIb}-k989 and β_3-I719, whereas the black triangle is formed along surfaces around FLN21a-I2316, α_{IIb}-R995 and β_3-D781. α_{IIb}-R995 and β_3-D781 happen to be the pair in the proposed salt bridge. The loop around FLN21a-G2269 is dragged away from forming interfaces with either α_{IIb} or β_3 N-terminus (Figure 22 C), which accounts for migfilin detaching FLN21a from α_{IIb} and β_3 N-termini. (Figure 18 A and B). In addition, compared to the free form and the migfilin-bound form, FLN21a in ternary complex opens a pocket in order to form the black triangle contact with α_{IIb} and β_3 (Figure 22 D), which again

makes FLN21a unable to bind α_{IIb} and β_3 N-termini in the presence of migfilin. The NPLY region in the β_3 structure forms a turn which is predicted but not defined in the previous publication (Vinogradova et al. 2002). The N-terminus and C-terminus of β_3 clip FLN21a in the middle, which may facilitate mechanical force transmission.

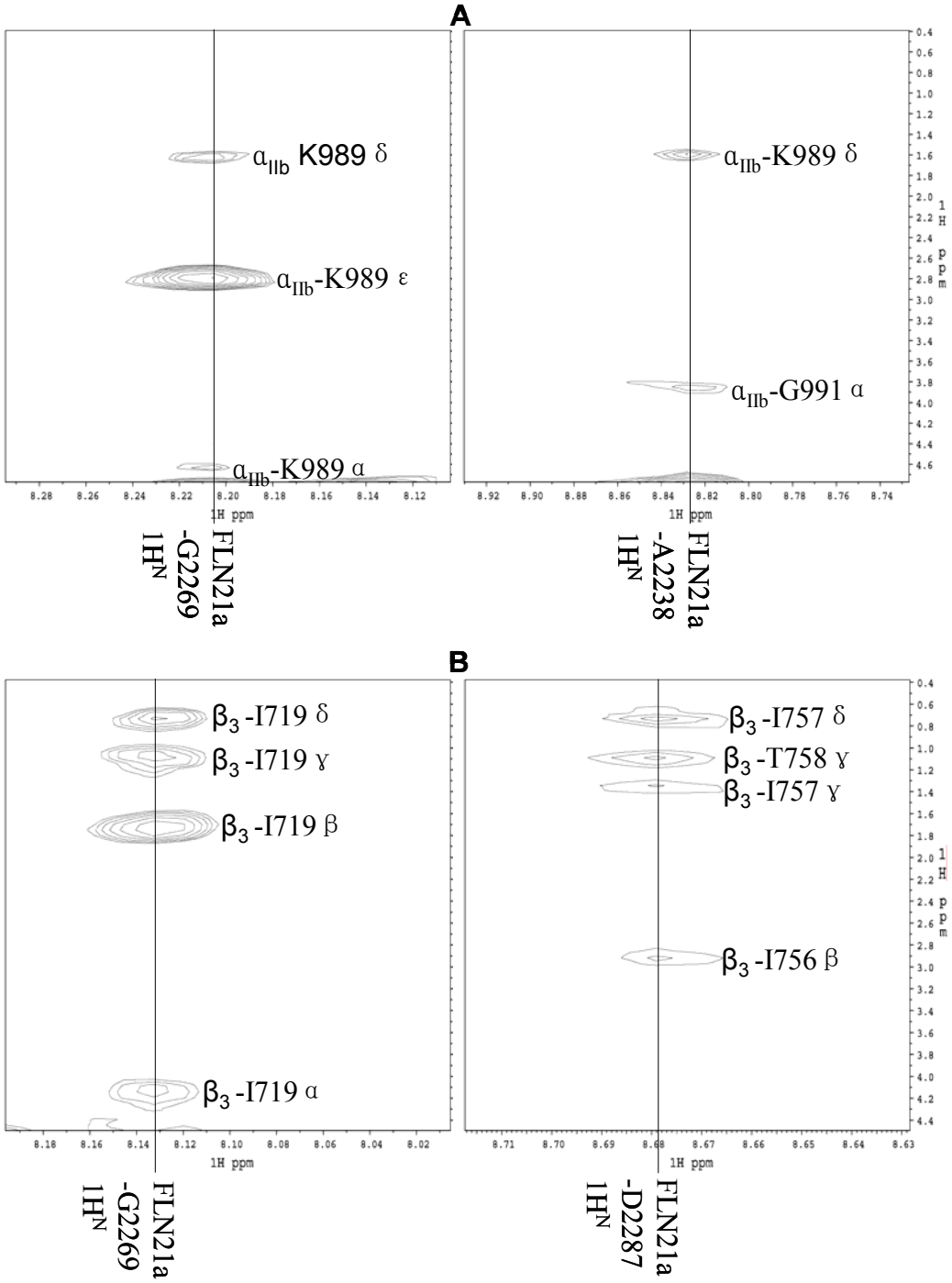

Figure 21 ^{15}N-NOESY of ^{15}N/2D FLN21a in the presence of integrin tails.
Selected regions of ^{15}N-NOESY of ^{15}N/2D FLN21a in the presence of unlabeled α_{IIb} (A) and β_3 (B) respectively.
A. Intermolecular NOE crosspeaks from α_{IIb} sidechains to FLN21a amide protons;
B. Intermolecular NOE crosspeaks from β_3 sidechains to FLN21a amide protons.

Table I Structural Statistics for FLN21a/α_{IIb}/β_3 Tail Complex

Parameter	SA Ensemble[a]
RMSD from experimental distance restraints (Å)	
All (1475)	0.082 ± 0.003
Intraresidue, i=j (380)	0.053 ± 0.006
Sequential, |i-j|=1 (557)	0.064 ± 0.005
Medium range, 1<|i-j|<5 (263)	0.089 ± 0.011
Long rang, |i-j|>4) (275)	0.094 ± 0.009
RMSD from idealized covalent geometry	
Bonds (Å)	0.005 ± 0.000
Angles (º)	0.707 ± 0.024
Impropers (º)	0.540 ± 0.017
E_{L-J} (kcal/mol)[b]	-506.39 ± 18
Ramachandran plot[c]	
Most favored regions (%)	75.5
Additional allowed rigeions (%)	24.3
Generously allowed regions (%)	0.2
Disallowed regions (%)	0
Coordinate precision[d]	
RMSD of backbone atoms to the mean (Å)	0.98
RMSDof all heavy atoms to the mean (Å)	1.61

[a]Mean ± standard error where applicable.

[b]Lennard-Jones potential energy function, calculated with CHARMM19 empirical energy parameters

[c]Residues FLN21a (2246-2262, 2269-2311, 2319-2332)/α_{IIb} (990-1000)/β_3 (719-736) which are the well-defined regions. Total 20 SA structures.

[d]Residues FLN21a (2246-2332)/α_{IIb} (990-1000)/β_3 (719-753) which are well-converged regions. Total 20 SA structures.

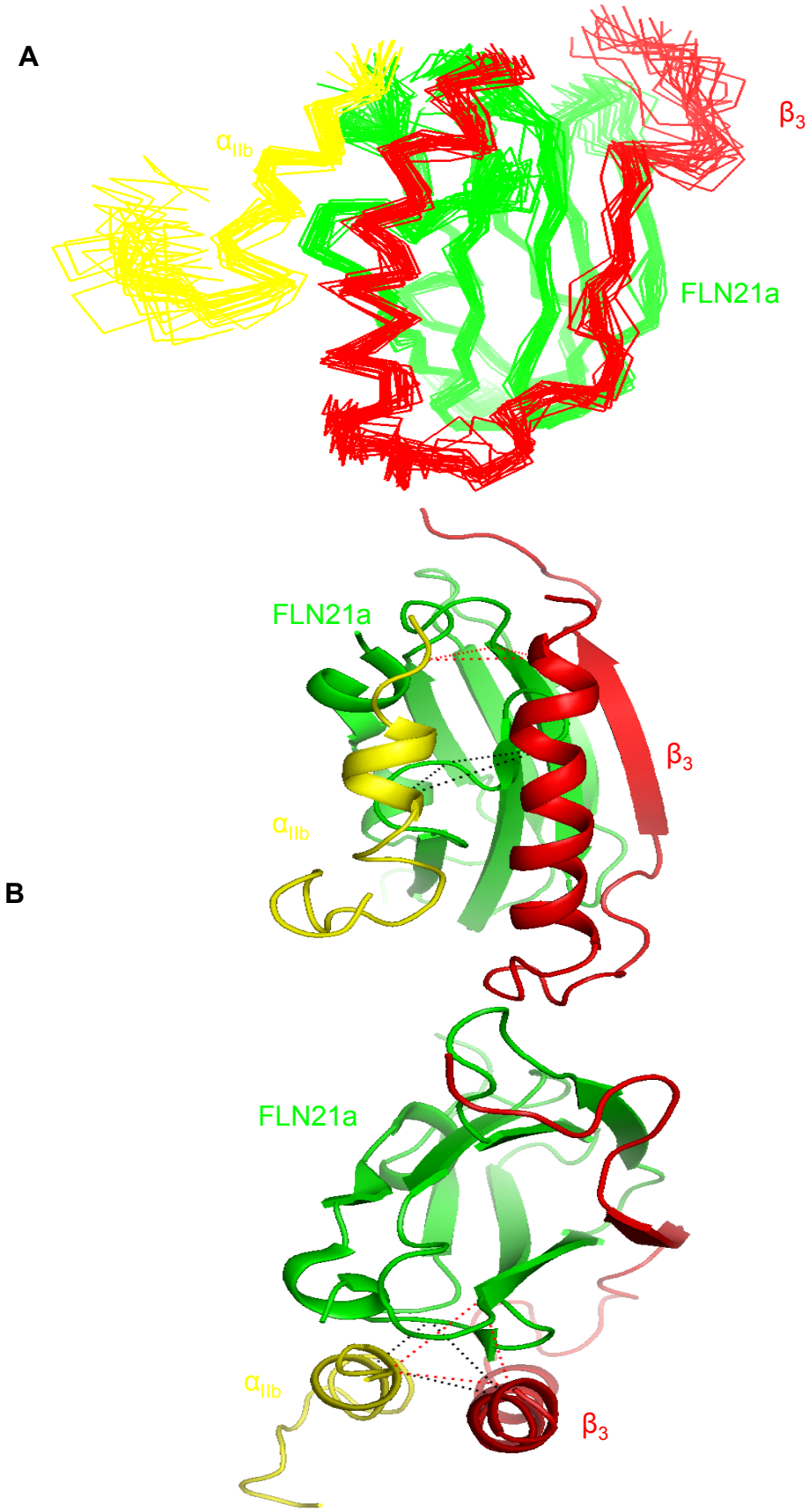
A
α_{IIb}
β_3
FLN21a
FLN21a
β_3
α_{IIb}
B
FLN21a
α_{IIb}
β_3

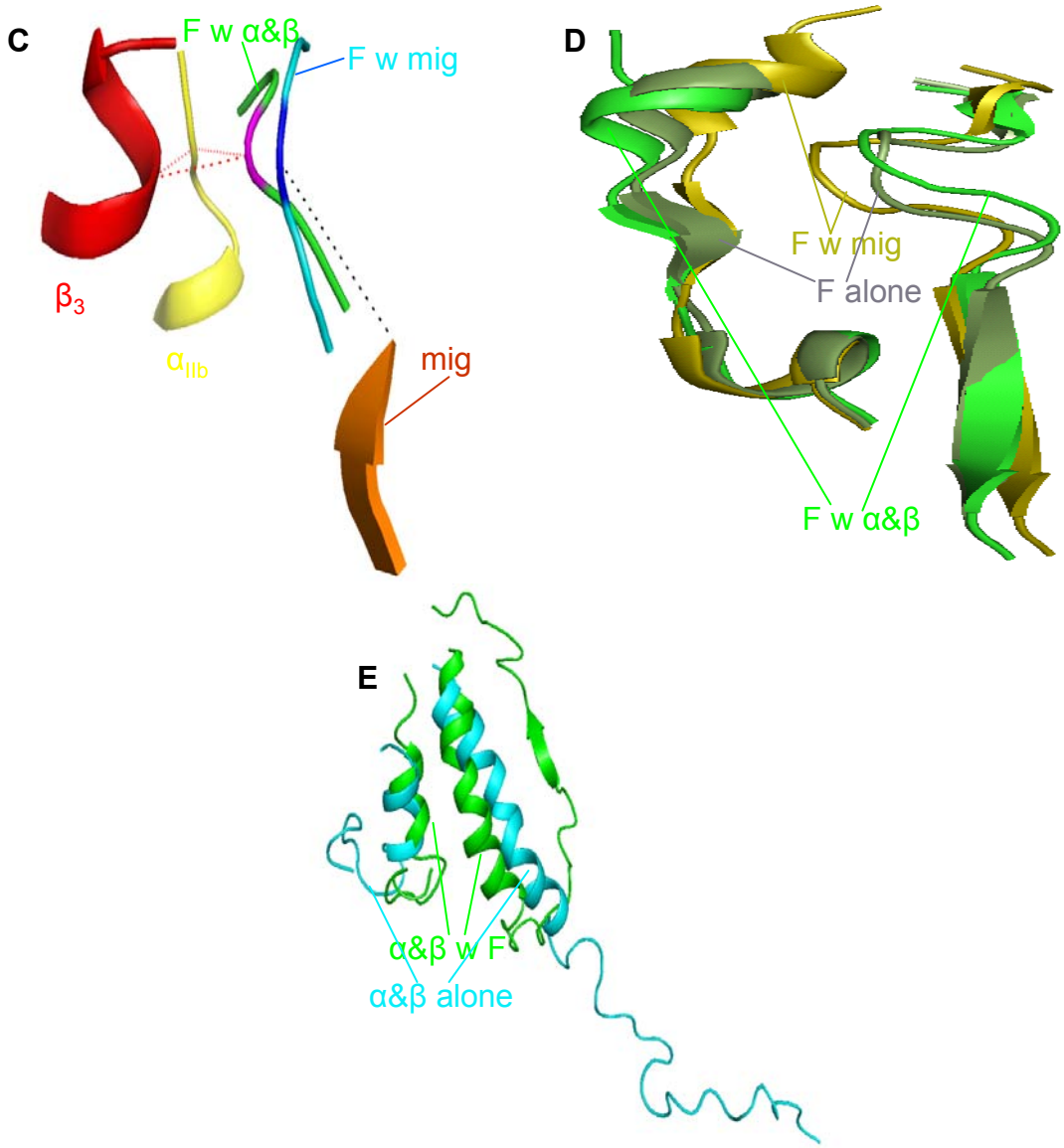

Figure 22 The calculated ternary structure of FLN21a-α_{IIb}-β_3.
(A). Backbone superposition of the 20 best structures of F21a-α_{IIb}-β_3 picked by the energy.
(B) Backbone of the single reprehensive the F21a-α_{IIb}-β_3 complex structure picked by the lowest energy. FLN21a - green, α_{IIb} - yellow, β_3 - red. The red triangle of FLN21a-G2269, α_{IIb}-k989 and β_3-I719, and the black triangle of FLN21a-I2316, α_{IIb}-R995 and β_3-D781 indicate the main interface for the ternary complex. α_{IIb}-R995 and β_3-D781 are the pair in the proposed salt bridge.
(C). Migfilin (in purple) drags the loop at FLN21a-G2269 and disrupts the red triangle in (B).

(D). Partial structural superposition of FLN21a: free form (blue), migfilin-bound form (purple)(Kiema, 2006), and α_{IIb}/β_3-bound form (green). The closed conformation in migfilin-bound FLN21a disrupts the black triangle in (B).
(E). The comparison of α_{IIb}/β_3 complex in the ternary complex with FLN21a (green) and α_{IIb}/β_3 alone (cyan) determined in Vinogradova et al. 2002.

3.7 The proposed mechanism of filamin-mediated integrin activity

Using multiple NMR techniques, I have demonstrated that filamin and integrin α & β cytoplasmic tails form a ternary complex in which the interaction between α_{IIb} and β_3 is enhanced by filamin. In this triangular relationship, the complexed structure between integrin cytoplasmic tails is stabilized by filamin, which can efficiently keep integrin in its inactive state. This provides an explanation as to why the comparably weak α/β cytoplasmic tails' interaction can have a big role in regulating integrin extracellular adhesion. For years the role of the interaction between integrin cytoplasmic tails, or even the existence of this interaction, has been quite controversial. However, the data here have strongly revealed that filamin can protect this interaction against non-specific activation. Furthermore, it can even contend with integrin's major activator, talin. Although it can not be unambiguously stated that filamin can inhibit integrin adhesion, filamin's presence is sufficient enough to raise the bar for integrin activation. Recently, it was found that overexpression of talin cannot fully activate integrin adhesion, which may be due to filamin's protection effect. This mechanism can both preserve integrin's sensitivity to respond to activation and block non-specific or accidental activation, which form the key balance for normal platelet function.

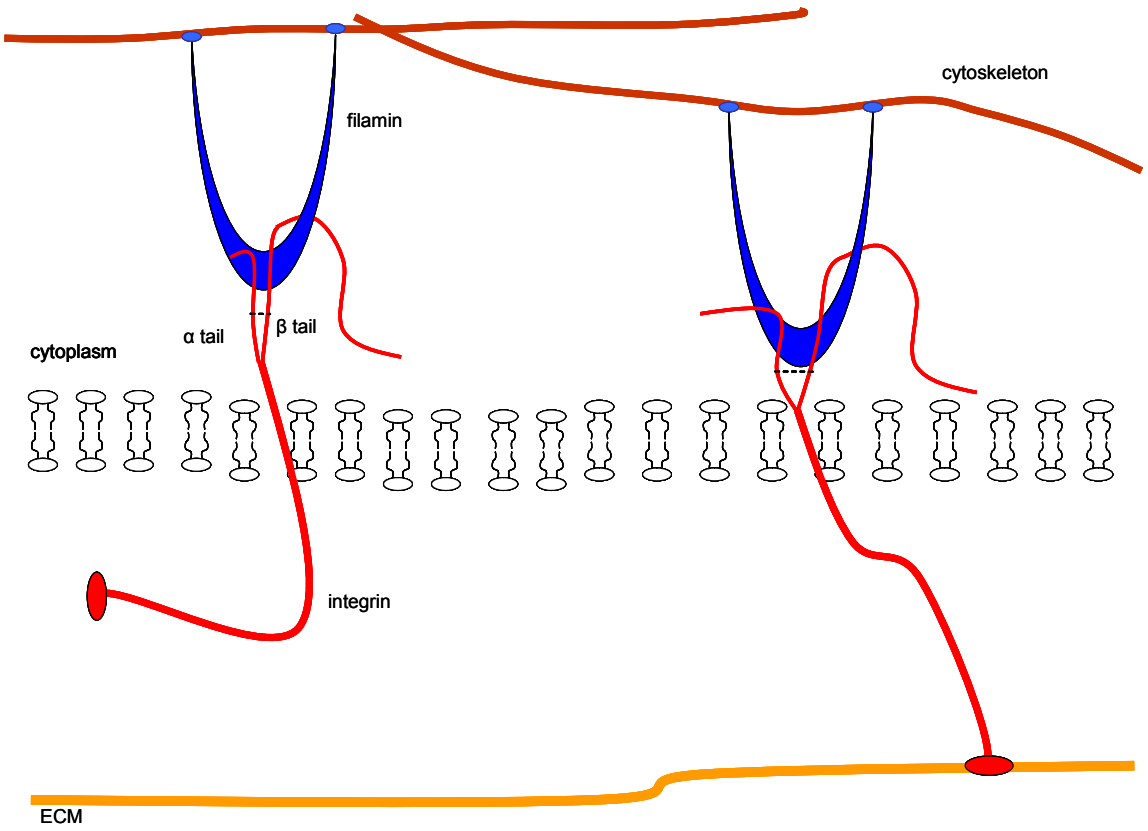

Figure 23 The integrin-filamin complex delivers the mechanical force transmitted between cytoskeleton and ECM to facilitate cell movement.

The dotted lines indicate the dynamic changes of the proximity of the cytoplasmic tails during the contraction and release of the cytoskeleton. The left represents the highly inhibitory state of the integrin, which is accomplished by the filamin interaction with the cytoplasmic tails and the energy from the cytoskeleton contraction. The right represents the state in which integrin is subject to outside-in signaling, *i.e.*, filamin releases the integrin so that integrin can be activated by ECM binding. Once the ECM-integrin connection is established the connection exerts the force on the integrin-filamin complex and triggers the cytoskeleton contraction (outside-in signaling). The contraction force is transmitted to the ECM-integrin connection through the filamin-integrin-ECM link and the cell is pulled forward. Further pulling breaks the ECM-integrin connection, which may be accompanied with the break of integrin-filamin either by ligand (Figure 24) or by mechanical force (Figure 25). Losing the connection on the both sides of the membrane, integrin can diffuse to a new site and rebuild the filamin connection so that a new cycle of cell migration may start. An alternative mechanism of cell migration is proposed in Figure 26.

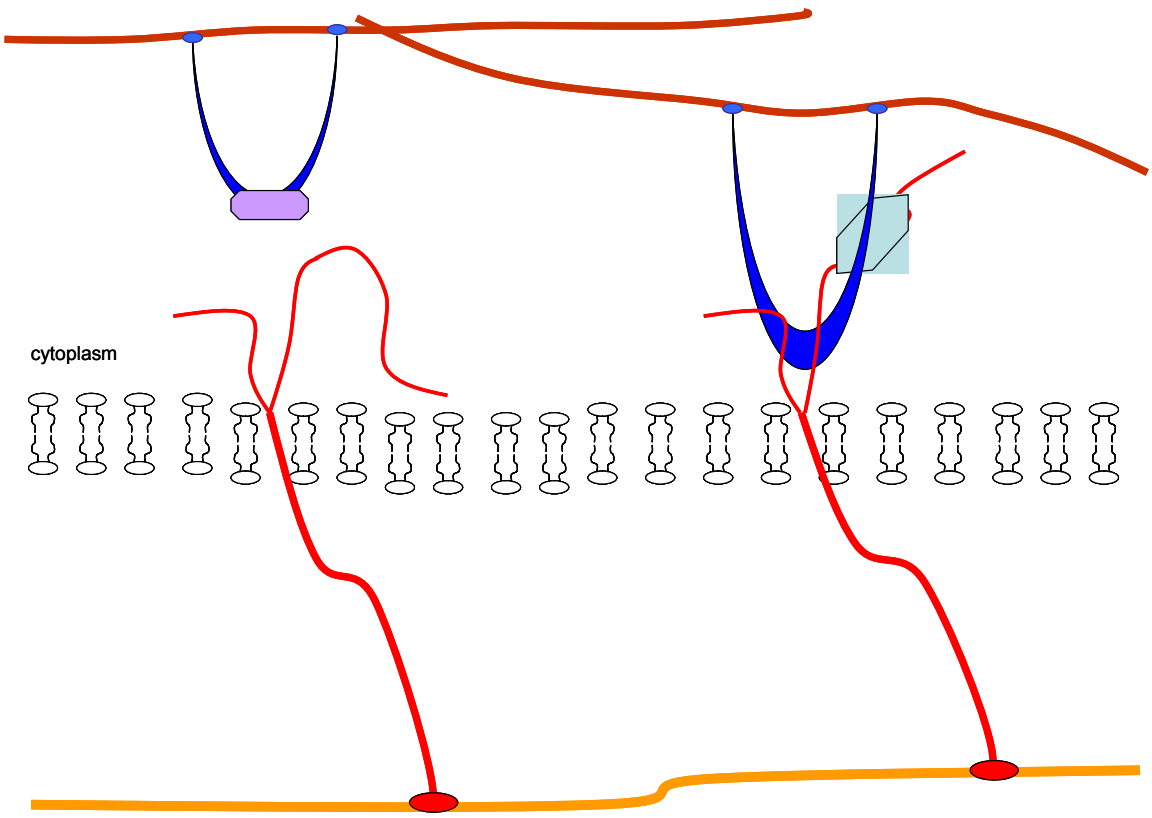

Figure 24 Two ways of ligand-disruption of the integrin-filamin connection that may happen in platelet aggregation or fixation in the front edge of cell movement.

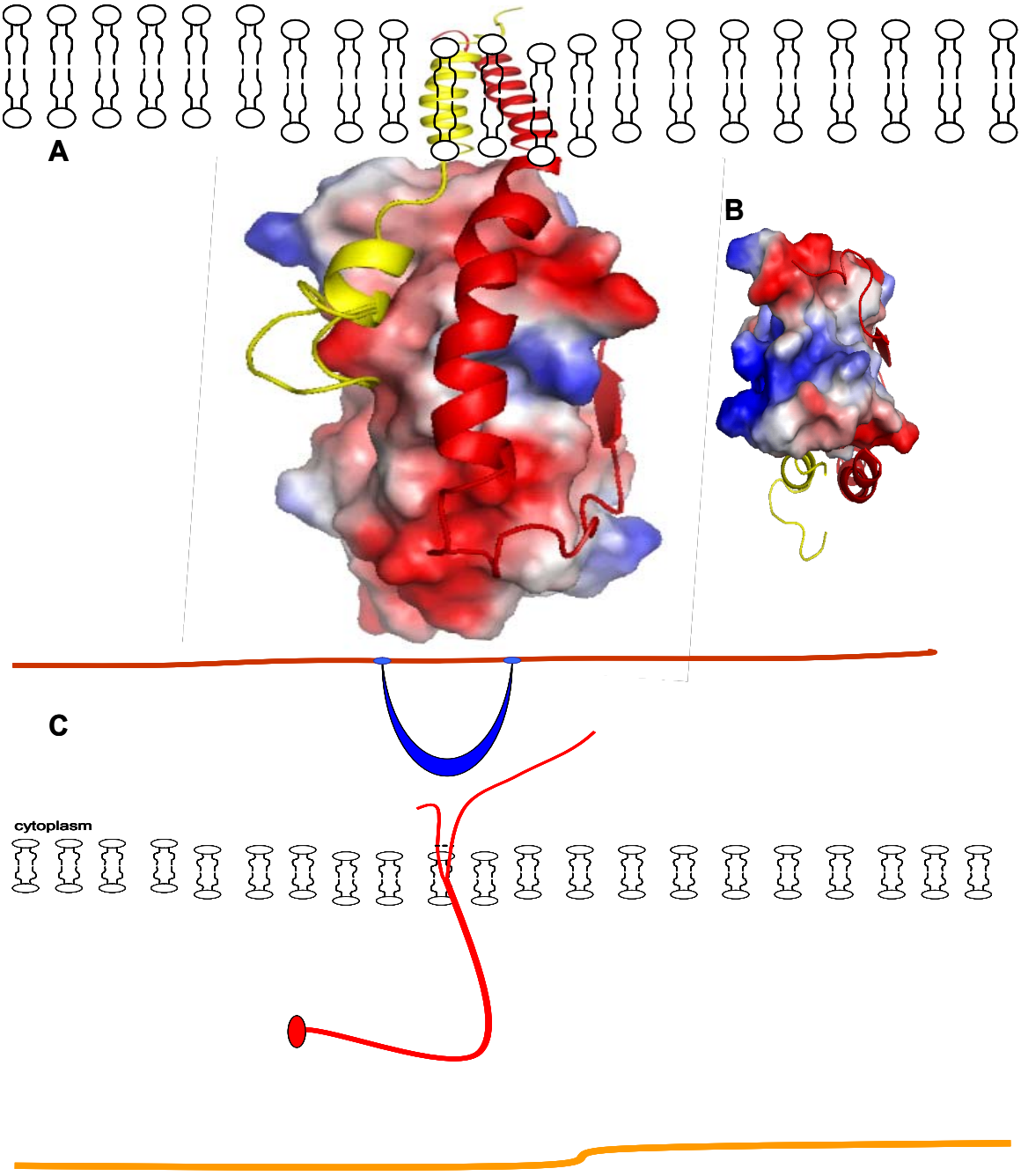

Figure 25 Mechanical disruption of the integrin-filamin connection.
(A). The complex of FLN21a-α_{IIb}-β_3 fused with the model of the integrin transmembrane domains. Filamin is displayed with electrostatics potential on the surface. The region that faces the cell membrane is shown in (B). Red - negative charge, green - positive charge, white - others.
(C). When the cell membrane moves toward the nucleus and has movement relative to filamin, several residues of the integrin cytoplasmic tails go into the membrane. The result is filamin is detached from integrin because it has lost the binding site on integrin N-terminus and it is bounced off by the membrane.

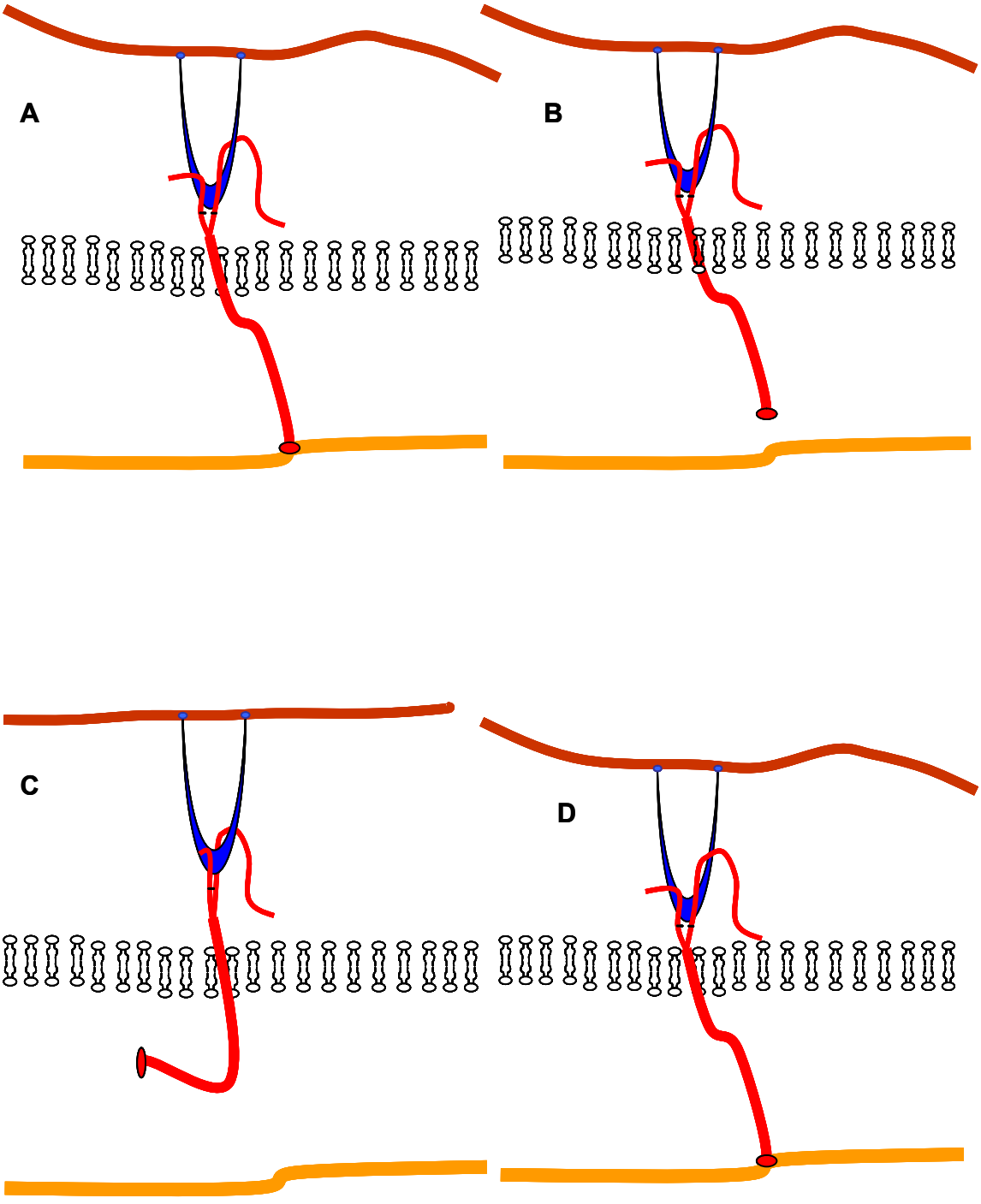
A
B
C
D

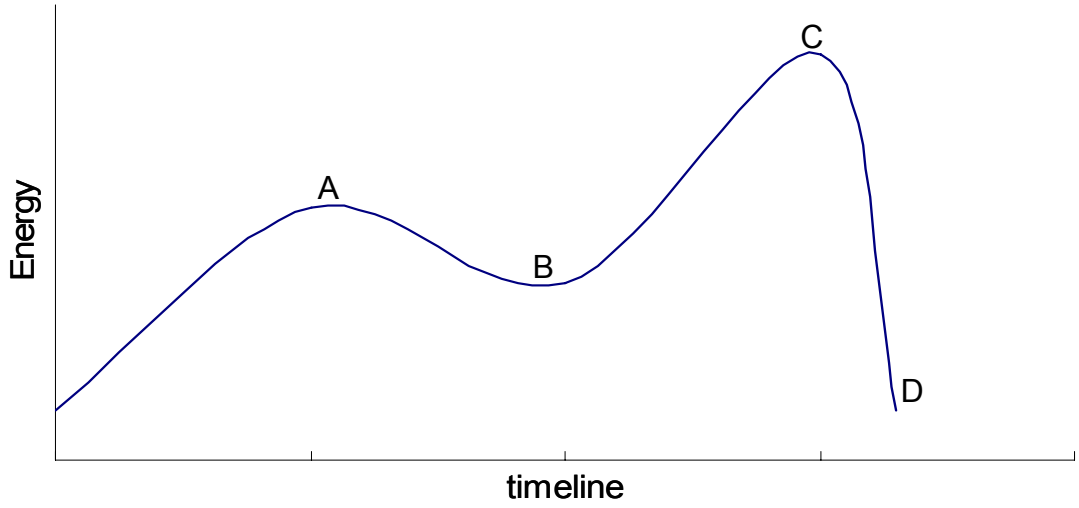

Figure 26 Four-step mechanism for cell movement.
(A), Upon cytoskeleton contraction, filamin starts to pull integrin down and a few hydrophobic residues are pulled out of the cell membrane, boosting the energy of the whole system.
(B). The pulling forces eventually overcome the association between integrin and ECM, and disassociates them. The system energy drops down a little due to the disassociation. Cells move during the first two steps.
(C). The continued pulling bends the integrin extracellular domains and more residues of integrin are pulled out of membrane. Due to this, the energy is boosted up to the maximum.
(D). Once the contraction is released, the stored energy is discharged and the hydrophobic residues return into the membrane and the extracellular domains straighten up. The association of integrin and ECM may recover at the new cell location. The system energy drops down to the original level.

Moreover, the studies here have revealed that filamin is much more intimate with integrin tails than previously suggested. It does not only bind to β C-terminus but also binds to the β N-terminus and the α tail. I propose that, other than just protecting the tails' interaction, this ternary complex plays a more principal role for integrin transmitting mechanochemical signals than has been suggested. The filamin and integrin complex may transmit the mechanical force generated by cytoskeleton contraction directly to the cell surface. This mechanical force may have two direct effects: 1. It may provide the necessary energy for integrin extracellular domain to bend over and break the link with the extracellular matrix. This pull-bend mechanism can be well illustrated by a spring tied with two strands; 2. It may provide the necessary energy for cell movement (Figure 23). The specific direction of cell movement may derive from the directional forces of cytoskeleton contraction preserved and transmitted by the filamin/integrin complex. The mechanism of filamin pulling the membrane protein upon the contraction of the cytoskeleton has been investigated by atomic force microscopy (Yamazaki M, 2002). Moreover, this force may pull several hydrophobic residues of integrin out of the cell membrane. In this way, the extra energy would be stored since those residues have the tendency to return into the membrane. When the cytoskeleton releases the filamin/integrin complex, immediately the stored energy would be discharged and those residues would return into the membrane while the extracellular domains straighten up and recover ECM

adhesion. This process may occur cyclically and in each cycle the ECM adhesion is recovered at the farther location in the direction of cell movement. A four-step mechanism of cell movement is proposed here (Figure 25). Furthermore, this complex may also sense the mechanical forces exerted on cells and transmit them to other parts of the cell.

On the other hand, logically and most likely realistically, there would be two ways of ligand-disruption of this complex: 1. A strong filamin-binding protein like migfilin may detach filamin from integrins; 2. A strong integrin-binding protein like talin may target integrin tails and disassociate integrin from filamin (Figure 24). In those situations, integrins become no longer subject to the cytoskeleton contraction and their extracellular domains may straighten and become exposed to any appropriate ligand. Different from the filamin-mediated process, integrins could no longer generate forces for cell movement due to loss of the cytoskeleton linkage, although they could still bind to ECM. This may happen at the fixation of the cell migration front or during platelet aggregation. Additionally, the separation of tails may take place, slightly, when cytoskeleton contraction is released and considerably more when the filamin/integrin complex is disrupted. The possible conformational propagation induced in this way is not a topic in this dissertation.

There is a possible way to mechanically disrupt the integrin-filamin connection. Figure 25 A and B show that filamin's surface, including the region that faces the cell membrane, is full of charges which make filamin unable to

move into the cell membrane. Once cells start to shrink the membrane moves toward the nucleus and thus has movement relative to the integrin-filamin complex. This relative movement may have two effects: 1. Several residues of the integrin cytoplasmic tails may go into the cell membrane; 2. Filamin is detached from integrin because it has lost the binding site on the N-terminal region of the integrin cytoplasmic tails, which is critical for the complex (Figure 18 C), and it is repelled by the cell membrane. After going into the membrane, interaction between the integrin cytoplasmic tails is highly facilitated by hydrophobic forces, which inhibit integrin extracellular ligand binding. With force coming from the cell's further shrinking and with the integrin tails acquiring their inhibitory conformation, the connection of integrin to the extracellular matrix is broken. At this point integrin loses both extracellular matrix and cytoskeleton connections, which allows the integrin freely to move on the cell membrane. Integrins may diffuse to a new site to rebuild the cytoskeleton and ECM linkages and start a new cycle of migration.

I proposed two mechanisms for cell migration because the integrin-mediated cell adhesions at the migration front and rear are believed to be subject to different mechanisms. Thus I propose that the mechanism in Figure 26 is used in the migration front to facilitate the continuity of movement whereas the mechanism in Figure 24 and 25 is used in the migration rear to facilitate the diffusion of integrins. On the other hand, I did not include the situation when integrins link to the cytoskeleton through other actin binding protein such as talin.

In this situation integrin will have the ECM-integrin-talin-cytoskeleton link instead of the ECM-integrin-filamin-cytoskeleton link. It is reasonable that the two different links that respectively represent the inhibitory (filamin link) and activated (talin link) states occur alternatively and cyclically to facilitate cell migration. But I think that it is less efficient for the cell to manage the cyclical break and re-establishment of two different links to accomplish cell migration which is just a basic cell function. However, as we know, cells do handle a lot of functions that are very complicated and seem less energetically efficient. Besides, there may be unknown reasons for cells to choose one mechanism over another.

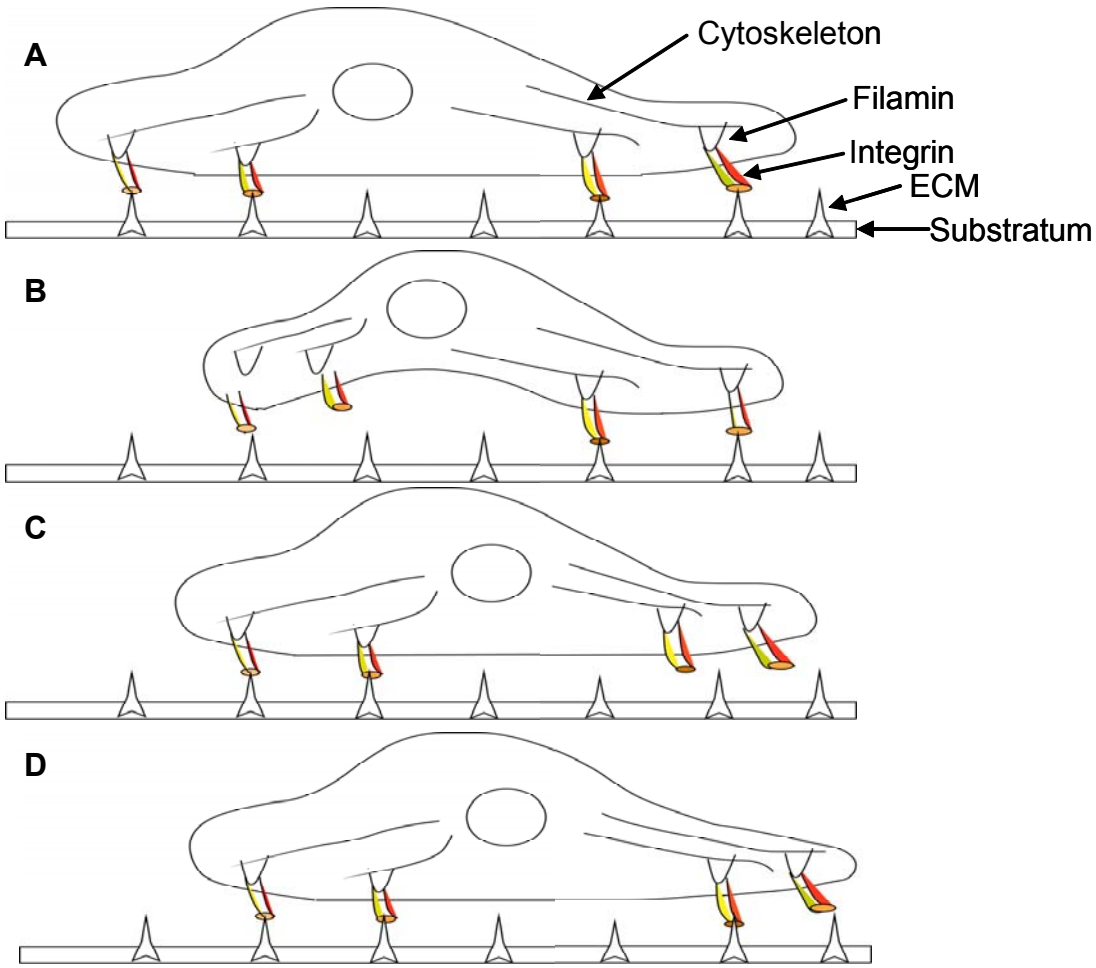

Figure 27 Proposed model of cell migration with filamin-integrin as a "transmission".

(A). Cell cytoskeleton starts to contract and pull the associated integrin-ECM and consequently pull the cell front forward as proposed in Figure 26.

(B). The whole cell starts to shrink, subsequently the cell's rear breaks integrin-ECM association by adopting one of the proposed filamin-detachment mechanisms, either by ligand in Figure 24 or by force in Figure 25. Integrins at the rear lose both ECM and cytoskeleton linkage and are free to diffuse. The cell moves forward.

(C). In the matter of cooperation, the migration front breaks the integrin-ECM associations while the rear establishes new ones.

(D). Then the cell front protrudes and establishes new associations and a new cycle starts.

3.8 The proposed model of cell migration with filamin-integrin as a "transmission".

The model in which cell migration is mediated by the filamin-integrin linkage is proposed in Figure 27. In this model, the linkage of filamin-integrin can transmit the cytoskeleton contraction forces to the integrin-ECM linkage on the cell surface, meanwhile modifying the integrin ligand binding states. Accordingly, the dynamic cooperation of the force transmission and the integrin-ECM linkage modification facilitates the cell migration process. Thus, filamin-integrin interaction incorporates the transmission of mechanical forces generated from the cytoskeleton contraction to the cyclical association and disassociation of the integrin-ECM linkage, accomplishing the central part of cell migration. The best analogue in the macroscopic world I can think is the vehicle transmission that incorporates the mechanical forces generated from the engine to the wheels.

BIBLIOGRAPHY 1

Ali, I. U. and R. O. Hynes (1977). "Effects of cytochalasin B and colchicine on attachment of a major surface protein of fibroblasts." Biochim Biophys Acta **471**(1): 16-24.

Arnaout, M. A., B. Mahalingam, et al. (2005). "Integrin structure, allostery, and bidirectional signaling." Annu Rev Cell Dev Biol **21**: 381-410.

Arno Bundi, K. W. (1979). "1H-nmr parameters of the common amino acid residues measured in aqueous solutions of the linear tetrapeptides H-Gly-Gly-X-L-Ala-OH." Biopolymers **18**: 285-297.

Balaban, N. Q., U. S. Schwarz, et al. (2001). "Force and focal adhesion assembly: a close relationship studied using elastic micropatterned substrates." Nat Cell Biol **3**(5): 466-72.

Ballestrem, C., B. Hinz, et al. (2001). "Marching at the front and dragging behind: differential alphaVbeta3-integrin turnover regulates focal adhesion behavior." J Cell Biol **155**(7): 1319-32.

Barsukov, I. L., A. Prescot, et al. (2003). "Phosphatidylinositol phosphate kinase type 1gamma and beta1-integrin cytoplasmic domain bind to the same region in the talin FERM domain." J Biol Chem **278**(33): 31202-9.

Belkin, A. M., S. F. Retta, et al. (1997). "Muscle beta1D integrin reinforces the cytoskeleton-matrix link: modulation of integrin adhesive function by alternative splicing." J Cell Biol **139**(6): 1583-95.

Beverly R. Seavey, E. A. F., William M. Westler and John L. Markley (1991). "A relational database for sequence-specific protein NMR data." J. Biomol. NMR **1**: 217-236.

Brooks, B. R., C. L. Brooks, 3rd, et al. (2009). "CHARMM: the biomolecular simulation program." J Comput Chem **30**(10): 1545-614.

Brunger, A. T. (1992). X-PLOR: version 3.1 : a system for x-ray crystallography and NMR, New Haven: Yale University Press.

Brunger, A. T., P. D. Adams, et al. (1998). "Crystallography & NMR system: A new software suite for macromolecular structure determination." Acta Crystallogr D Biol Crystallogr **54**(Pt 5): 905-21.

Burridge, K. and M. Chrzanowska-Wodnicka (1996). "Focal adhesions,

contractility, and signaling." Annu Rev Cell Dev Biol **12**: 463-518.

C.D. Schwieters, J. J. K., and G.M. Clore (2006). "Using Xplor-NIH for NMR molecular structure determination." Progr. NMR Spectroscopy **48**: 47-62

Calderwood, D. A. (2004). "Integrin activation." J Cell Sci **117**(Pt 5): 657-66.

Calderwood, D. A., A. Huttenlocher, et al. (2001). "Increased filamin binding to beta-integrin cytoplasmic domains inhibits cell migration." Nat Cell Biol **3**(12): 1060-8.

Calderwood, D. A., S. J. Shattil, et al. (2000). "Integrins and actin filaments: reciprocal regulation of cell adhesion and signaling." J Biol Chem **275**(30): 22607-10.

Calderwood, D. A., B. Yan, et al. (2002). "The phosphotyrosine binding-like domain of talin activates integrins." J Biol Chem **277**(24): 21749-58.

Calderwood, D. A., R. Zent, et al. (1999). "The Talin head domain binds to integrin beta subunit cytoplasmic tails and regulates integrin activation." J Biol Chem **274**(40): 28071-4.

Chen, Y. P., T. E. O'Toole, et al. (1994). "A point mutation in the integrin beta 3 cytoplasmic domain (S752-->P) impairs bidirectional signaling through alpha IIb beta 3 (platelet glycoprotein IIb-IIIa)." Blood **84**(6): 1857-65.

Clark, E. A. and J. S. Brugge (1995). "Integrins and signal transduction pathways: the road taken." Science **268**(5208): 233-9.

Clark, E. A. and R. O. Hynes (1997). "1997 keystone symposium on signal transduction by cell adhesion receptors." Biochim Biophys Acta **1333**(3): R9-16.

Clore, G. M., A. M. Gronenborn, et al. (1987). "Three-dimensional structure of potato carboxypeptidase inhibitor in solution. A study using nuclear magnetic resonance, distance geometry, and restrained molecular dynamics." Biochemistry **26**(24): 8012-23.

Constantin, G., M. Majeed, et al. (2000). "Chemokines trigger immediate beta2 integrin affinity and mobility changes: differential regulation and roles in lymphocyte arrest under flow." Immunity **13**(6): 759-69.

Cornilescu, G., F. Delaglio, et al. (1999). "Protein backbone angle restraints from searching a database for chemical shift and sequence homology." J Biomol

NMR **13**(3): 289-302.

Cybulsky, A. V., A. J. McTavish, et al. (1994). "Extracellular matrix modulates epidermal growth factor receptor activation in rat glomerular epithelial cells." J Clin Invest **94**(1): 68-78.

Davies, P. F. (1995). "Flow-mediated endothelial mechanotransduction." Physiol Rev **75**(3): 519-60.

Du, X., M. Gu, et al. (1993). "Long range propagation of conformational changes in integrin alpha IIb beta 3." J Biol Chem **268**(31): 23087-92.

Ernstrom, G. G. and M. Chalfie (2002). "Genetics of sensory mechanotransduction." Annu Rev Genet **36**: 411-53.

Feng, Y. and C. A. Walsh (2004). "The many faces of filamin: a versatile molecular scaffold for cell motility and signalling." Nat Cell Biol **6**(11): 1034-8.

Fox, J. W., E. D. Lamperti, et al. (1998). "Mutations in filamin 1 prevent migration of cerebral cortical neurons in human periventricular heterotopia." Neuron **21**(6): 1315-25.

Frisch, S. M. and H. Francis (1994). "Disruption of epithelial cell-matrix interactions induces apoptosis." J Cell Biol **124**(4): 619-26.

George, J. N., J. P. Caen, et al. (1990). "Glanzmann's thrombasthenia: the spectrum of clinical disease." Blood **75**(7): 1383-95.

Ginsberg, M. H., B. Yaspan, et al. (2001). "A membrane-distal segment of the integrin alpha IIb cytoplasmic domain regulates integrin activation." J Biol Chem **276**(25): 22514-21.

Glogauer, M., P. Arora, et al. (1998). "The role of actin-binding protein 280 in integrin-dependent mechanoprotection." J Biol Chem **273**(3): 1689-98.

Goldmann, W. H. (2000). "Kinetic determination of focal adhesion protein formation." Biochem Biophys Res Commun **271**(2): 553-7.

Grzesiek, S., and Bax, A (1992). "Correlating backbone amide and side chain resonances in larger proteins by multiple relayed triple resonance NMR." J. Am. Chem. Soc. **114**(16): 6291-6293.

Grzesiek, S., and Bax, A. (1992). "An efficient experiment for sequential backbone assignment of medium-sized isotopically enriched proteins." J. Magn.

Reson. **99**: 201-207.

Grzesiek, S., Anglister, J., and Bax, A. (1993a). "Correlation of backbone amide and aliphatic side-chain resonances in 13C/15N-enriched proteins by isotropic mixing of 13C magnetization." J. Magn. Reson. **101**: 114-119.

Haas, T. A. and E. F. Plow (1996). "The cytoplasmic domain of alphaIIb beta3. A ternary complex of the integrin alpha and beta subunits and a divalent cation." J Biol Chem **271**(11): 6017-26.

Harris, A. K., P. Wild, et al. (1980). "Silicone rubber substrata: a new wrinkle in the study of cell locomotion." Science **208**(4440): 177-9.

Haussinger, D., A. K. Kurz, et al. (2003). "Involvement of integrins and Src in tauroursodeoxycholate-induced and swelling-induced choleresis." Gastroenterology **124**(5): 1476-87.

Havel, T. F. (1991). "An evaluation of computational strategies for use in the determination of protein structure from distance constraints obtained by nuclear magnetic resonance." Prog Biophys Mol Biol **56**(1): 43-78.

Hibbs, M. L., S. Jakes, et al. (1991). "The cytoplasmic domain of the integrin lymphocyte function-associated antigen 1 beta subunit: sites required for binding to intercellular adhesion molecule 1 and the phorbol ester-stimulated phosphorylation site." J Exp Med **174**(5): 1227-38.

Hibbs, M. L., H. Xu, et al. (1991). "Regulation of adhesion of ICAM-1 by the cytoplasmic domain of LFA-1 integrin beta subunit." Science **251**(5001): 1611-3.

Horwitz, A. F. (1997). "Integrins and health." Sci Am **276**(5): 68-75.

Huang, S. and D. E. Ingber (1999). "The structural and mechanical complexity of cell-growth control." Nat Cell Biol **1**(5): E131-8.

Hughes, P. E., F. Diaz-Gonzalez, et al. (1996). "Breaking the integrin hinge. A defined structural constraint regulates integrin signaling." J Biol Chem **271**(12): 6571-4.

Hughes, P. E., T. E. O'Toole, et al. (1995). "The conserved membrane-proximal region of an integrin cytoplasmic domain specifies ligand binding affinity." J Biol Chem **270**(21): 12411-7.

Humphries, M. J., P. A. McEwan, et al. (2003). "Integrin structure: heady

advances in ligand binding, but activation still makes the knees wobble." Trends Biochem Sci **28**(6): 313-20.

Huttenlocher, A., M. H. Ginsberg, et al. (1996). "Modulation of cell migration by integrin-mediated cytoskeletal linkages and ligand-binding affinity." J Cell Biol **134**(6): 1551-62.

Hyberts, S. G., M. S. Goldberg, et al. (1992). "The solution structure of eglin c based on measurements of many NOEs and coupling constants and its comparison with X-ray structures." Protein Sci **1**(6): 736-51.

Hynes, R. O. (1987). "Integrins: a family of cell surface receptors." Cell **48**(4): 549-54.

Hynes, R. O. (2002). "Integrins: bidirectional, allosteric signaling machines." Cell **110**(6): 673-87.

Jones, P. L., J. Crack, et al. (1997). "Regulation of tenascin-C, a vascular smooth muscle cell survival factor that interacts with the alpha v beta 3 integrin to promote epidermal growth factor receptor phosphorylation and growth." J Cell Biol **139**(1): 279-93.

Kawasaki, J., G. E. Davis, et al. (2004). "Regulation of Ca2+-dependent K+ current by alphavbeta3 integrin engagement in vascular endothelium." J Biol Chem **279**(13): 12959-66.

Kiema, T., Y. Lad, et al. (2006). "The molecular basis of filamin binding to integrins and competition with talin." Mol Cell **21**(3): 337-47.

Kim, M., C. V. Carman, et al. (2003). "Bidirectional transmembrane signaling by cytoplasmic domain separation in integrins." Science **301**(5640): 1720-5.

Lad, Y., P. Jiang, et al. (2008). "Structural basis of the migfilin-filamin interaction and competition with integrin beta tails." J Biol Chem **283**(50): 35154-63.

Laskowski, R. A., D. S. Moss, et al. (1993). "Main-chain bond lengths and bond angles in protein structures." J Mol Biol **231**(4): 1049-67.

Lefkovits, J., E. F. Plow, et al. (1995). "Platelet glycoprotein IIb/IIIa receptors in cardiovascular medicine." N Engl J Med **332**(23): 1553-9.

Lehoux, S. and A. Tedgui (2003). "Cellular mechanics and gene expression in blood vessels." J Biomech **36**(5): 631-43.

Leisner, T. M., J. D. Wencel-Drake, et al. (1999). "Bidirectional transmembrane modulation of integrin alphaIIbbeta3 conformations." J Biol Chem **274**(18): 12945-9.

Liddington, R. C. and M. H. Ginsberg (2002). "Integrin activation takes shape." J Cell Biol **158**(5): 833-9.

Ling, K., R. L. Doughman, et al. (2003). "Tyrosine phosphorylation of type Igamma phosphatidylinositol phosphate kinase by Src regulates an integrin-talin switch." J Cell Biol **163**(6): 1339-49.

Liu, S., D. A. Calderwood, et al. (2000). "Integrin cytoplasmic domain-binding proteins." J Cell Sci **113 (Pt 20)**: 3563-71.

Lollo, B. A., K. W. Chan, et al. (1993). "Direct evidence for two affinity states for lymphocyte function-associated antigen 1 on activated T cells." J Biol Chem **268**(29): 21693-700.

Lu, C., J. Takagi, et al. (2001). "Association of the membrane proximal regions of the alpha and beta subunit cytoplasmic domains constrains an integrin in the inactive state." J Biol Chem **276**(18): 14642-8.

Luginbuhl, P., P. Guntert, et al. (1996). "The new program OPAL for molecular dynamics simulations and energy refinements of biological macromolecules." J Biomol NMR **8**(2): 136-46.

Maniotis, A. J., C. S. Chen, et al. (1997). "Demonstration of mechanical connections between integrins, cytoskeletal filaments, and nucleoplasm that stabilize nuclear structure." Proc Natl Acad Sci U S A **94**(3): 849-54.

Meredith, J. E., Jr., B. Fazeli, et al. (1993). "The extracellular matrix as a cell survival factor." Mol Biol Cell **4**(9): 953-61.

Metzler, W. J., D. R. Hare, et al. (1989). "Limited sampling of conformational space by the distance geometry algorithm: implications for structures generated from NMR data." Biochemistry **28**(17): 7045-52.

Musil, D., D. Zucic, et al. (1991). "The refined 2.15 A X-ray crystal structure of human liver cathepsin B: the structural basis for its specificity." Embo J **10**(9): 2321-30.

Nilges, M., G. M. Clore, et al. (1988). "Determination of three-dimensional structures of proteins from interproton distance data by dynamical simulated annealing from a random array of atoms. Circumventing

problems associated with folding." FEBS Lett **239**(1): 129-36.

O'Toole, T. E., Y. Katagiri, et al. (1994). "Integrin cytoplasmic domains mediate inside-out signal transduction." J Cell Biol **124**(6): 1047-59.

O'Toole, T. E., D. Mandelman, et al. (1991). "Modulation of the affinity of integrin alpha IIb beta 3 (GPIIb-IIIa) by the cytoplasmic domain of alpha IIb." Science **254**(5033): 845-7.

O'Toole, T. E., J. Ylanne, et al. (1995). "Regulation of integrin affinity states through an NPXY motif in the beta subunit cytoplasmic domain." J Biol Chem **270**(15): 8553-8.

Pelham, R. J., Jr. and Y. Wang (1997). "Cell locomotion and focal adhesions are regulated by substrate flexibility." Proc Natl Acad Sci U S A **94**(25): 13661-5.

Pelham, R. J., Jr. and Y. Wang (1999). "High resolution detection of mechanical forces exerted by locomoting fibroblasts on the substrate." Mol Biol Cell **10**(4): 935-45.

Peter, K. and C. Bode (1996). "A deletion in the alpha subunit locks platelet integrin alpha IIb beta 3 into a high affinity state." Blood Coagul Fibrinolysis **7**(2): 233-6.

Pfaff, M., S. Liu, et al. (1998). "Integrin beta cytoplasmic domains differentially bind to cytoskeletal proteins." J Biol Chem **273**(11): 6104-9.

Pudas, R., T. R. Kiema, et al. (2005). "Structural basis for vertebrate filamin dimerization." Structure **13**(1): 111-9.

Ramachandran, G. N., C. Ramakrishnan, et al. (1963). "Stereochemistry of polypeptide chain configurations." J Mol Biol **7**: 95-9.

Reszka, A. A., Y. Hayashi, et al. (1992). "Identification of amino acid sequences in the integrin beta 1 cytoplasmic domain implicated in cytoskeletal association." J Cell Biol **117**(6): 1321-30.

Rieping, W., M. Habeck, et al. (2005). "Inferential structure determination." Science **309**(5732): 303-6.

Riveline, D., E. Zamir, et al. (2001). "Focal contacts as mechanosensors: externally applied local mechanical force induces growth of focal contacts by an mDia1-dependent and ROCK-independent mechanism." J Cell Biol

153(6): 1175-86.

Robertson, S. P., S. R. Twigg, et al. (2003). "Localized mutations in the gene encoding the cytoskeletal protein filamin A cause diverse malformations in humans." Nat Genet **33**(4): 487-91.

Ruoslahti, E. and M. D. Pierschbacher (1987). "New perspectives in cell adhesion: RGD and integrins." Science **238**(4826): 491-7.

Schlaepfer, D. D. and T. Hunter (1998). "Integrin signalling and tyrosine phosphorylation: just the FAKs?" Trends Cell Biol **8**(4): 151-7.

Schlueter, J. A., J. Y. Lin, et al. (2007). "Gene duplication and paleopolyploidy in soybean and the implications for whole genome sequencing." BMC Genomics **8**: 330.

Schoenwaelder, S. M. and K. Burridge (1999). "Bidirectional signaling between the cytoskeleton and integrins." Curr Opin Cell Biol **11**(2): 274-86.

Schwartz, M. A. and R. K. Assoian (2001). "Integrins and cell proliferation: regulation of cyclin-dependent kinases via cytoplasmic signaling pathways." J Cell Sci **114**(Pt 14): 2553-60.

Schwartz, M. A. and D. E. Ingber (1994). "Integrating with integrins." Mol Biol Cell **5**(4): 389-93.

Schwarzinger, S., G. J. Kroon, et al. (2001). "Sequence-dependent correction of random coil NMR chemical shifts." J Am Chem Soc **123**(13): 2970-8.

Schwarzinger, S., G. J. Kroon, et al. (2000). "Random coil chemical shifts in acidic 8 M urea: implementation of random coil shift data in NMRView." J Biomol NMR **18**(1): 43-8.

Schwieters, C. D., J. J. Kuszewski, et al. (2003). "The Xplor-NIH NMR molecular structure determination package." J Magn Reson **160**(1): 65-73.

Sheen, V. L., P. H. Dixon, et al. (2001). "Mutations in the X-linked filamin 1 gene cause periventricular nodular heterotopia in males as well as in females." Hum Mol Genet **10**(17): 1775-83.

Sheetz, M. P., D. P. Felsenfeld, et al. (1998). "Cell migration: regulation of force on extracellular-matrix-integrin complexes." Trends Cell Biol **8**(2): 51-4.

Sheffield, P. G., Sarah; Derewenda, Zygmunt (1999). "Overcoming Expression

and Purification Problems of RhoGDI Using a Family of “Parallel” Expression Vectors." Protein Expr Purif. **15**(1): 34-35.

Shimaoka, M., J. Takagi, et al. (2002). "Conformational regulation of integrin structure and function." Annu Rev Biophys Biomol Struct **31**: 485-516.

Stefanova, M., P. Meinecke, et al. (2005). "A novel 9 bp deletion in the filamin a gene causes an otopalatodigital-spectrum disorder with a variable, intermediate phenotype." Am J Med Genet A **132**(4): 386-90.

Stefansson, A., A. Armulik, et al. (2004). "Determination of N- and C-terminal borders of the transmembrane domain of integrin subunits." J Biol Chem **279**(20): 21200-5.

Stossel, T. P., J. Condeelis, et al. (2001). "Filamins as integrators of cell mechanics and signalling." Nat Rev Mol Cell Biol **2**(2): 138-45.

Travis, M. A., A. van der Flier, et al. (2004). "Interaction of filamin A with the integrin beta 7 cytoplasmic domain: role of alternative splicing and phosphorylation." FEBS Lett **569**(1-3): 185-90.

Tu, Y., S. Wu, et al. (2003). "Migfilin and Mig-2 link focal adhesions to filamin and the actin cytoskeleton and function in cell shape modulation." Cell **113**(1): 37-47.

Ulmer, T. S., B. Yaspan, et al. (2001). "NMR analysis of structure and dynamics of the cytosolic tails of integrin alpha IIb beta 3 in aqueous solution." Biochemistry **40**(25): 7498-508.

Vallar, L., C. Melchior, et al. (1999). "Divalent cations differentially regulate integrin alphaIIb cytoplasmic tail binding to beta3 and to calcium- and integrin-binding protein." J Biol Chem **274**(24): 17257-66.

van der Flier, A. and A. Sonnenberg (2001). "Structural and functional aspects of filamins." Biochim Biophys Acta **1538**(2-3): 99-117.

Vinogradova, O., T. Haas, et al. (2000). "A structural basis for integrin activation by the cytoplasmic tail of the alpha IIb-subunit." Proc Natl Acad Sci U S A **97**(4): 1450-5.

Vinogradova, O., A. Velyvis, et al. (2002). "A structural mechanism of integrin alpha(IIb)beta(3) "inside-out" activation as regulated by its cytoplasmic face." Cell **110**(5): 587-97.

Vuori, K. and E. Ruoslahti (1994). "Association of insulin receptor substrate-1 with integrins." Science **266**(5190): 1576-8.

Wagner, G., W. Braun, et al. (1987). "Protein structures in solution by nuclear magnetic resonance and distance geometry. The polypeptide fold of the basic pancreatic trypsin inhibitor determined using two different algorithms, DISGEO and DISMAN." J Mol Biol **196**(3): 611-39.

Wagner, G. W., K. (1982). "Amide proton exchange and surface conformation of the basic pancreantic trypsin inhibitor in solution." J. Mol. Biol **60**: 343-361.

Wang, R., S. J. Shattil, et al. (1997). "Truncation of the cytoplasmic domain of beta3 in a variant form of Glanzmann thrombasthenia abrogates signaling through the integrin alpha(IIb)beta3 complex." J Clin Invest **100**(9): 2393-403.

Wary, K. K., F. Mainiero, et al. (1996). "The adaptor protein Shc couples a class of integrins to the control of cell cycle progression." Cell **87**(4): 733-43.

Wary, K. K., A. Mariotti, et al. (1998). "A requirement for caveolin-1 and associated kinase Fyn in integrin signaling and anchorage-dependent cell growth." Cell **94**(5): 625-34.

Weisel, J. W., C. Nagaswami, et al. (1992). "Examination of the platelet membrane glycoprotein IIb-IIIa complex and its interaction with fibrinogen and other ligands by electron microscopy." J Biol Chem **267**(23): 16637-43.

Weljie, A. M., P. M. Hwang, et al. (2002). "Solution structures of the cytoplasmic tail complex from platelet integrin alpha IIb- and beta 3-subunits." Proc Natl Acad Sci U S A **99**(9): 5878-83.

Williams, M. J., P. E. Hughes, et al. (1994). "The inner world of cell adhesion: integrin cytoplasmic domains." Trends Cell Biol **4**(4): 109-12.

Williamson, M. P., T. F. Havel, et al. (1985). "Solution conformation of proteinase inhibitor IIA from bull seminal plasma by 1H nuclear magnetic resonance and distance geometry." J Mol Biol **182**(2): 295-315.

Wu, C., V. M. Keivens, et al. (1995). "Integrin activation and cytoskeletal interaction are essential for the assembly of a fibronectin matrix." Cell **83**(5): 715-24.

Wuthrich, K. (1986). NMR of Proteins and Nucleic Acids. New York, Wiley.

Wuthrich, K., M. Billeter, et al. (1983). "Pseudo-structures for the 20 common amino acids for use in studies of protein conformations by measurements of intramolecular proton-proton distance constraints with nuclear magnetic resonance." J Mol Biol **169**(4): 949-61.

Xiong, J. P., T. Stehle, et al. (2001). "Crystal structure of the extracellular segment of integrin alpha Vbeta3." Science **294**(5541): 339-45.

Yamazaki, M., S. Furuike, et al. (2002). "Mechanical response of single filamin A (ABP-280) molecules and its role in the actin cytoskeleton." J Muscle Res Cell Motil **23**(5-6): 525-34.

Zaidel-Bar, R., M. Cohen, et al. (2004). "Hierarchical assembly of cell-matrix adhesion complexes." Biochem Soc Trans **32**(Pt3): 416-20.

Zamir, E. and B. Geiger (2001). "Molecular complexity and dynamics of cell-matrix adhesions." J Cell Sci **114**(Pt 20): 3583-90.

Zhao, R., A. S. Pathak, et al. (2004). "beta(3)-Integrin cytoplasmic binding proteins." Arch Immunol Ther Exp (Warsz) **52**(5): 348-55.

Zwartz, G. J., A. Chigaev, et al. (2004). "Real-time analysis of very late antigen-4 affinity modulation by shear." J Biol Chem **279**(37): 38277-86.